DEVELOPMENT OF SELF-TUNED INDOOR THERMAL ENVIRONMENTS

by

Seungjae Lee

A Dissertation

Submitted to the Faculty of Purdue University

In Partial Fulfillment of the Requirements for the degree of

Doctor of Philosophy

Lyles School of Civil Engineering

West Lafayette, Indiana

December 2019

THE PURDUE UNIVERSITY GRADUATE SCHOOL
STATEMENT OF COMMITTEE APPROVAL

Dr. Athanasios Tzempelikos
Lyles School of Civil Engineering

Dr. Panagiota Karava
Lyles School of Civil Engineering

Dr. Ilias Bilionis
School of Mechanical Engineering

Dr. Jianghai Hu
School of Electrical and Computer Engineering

Dr. Brandon E. Boor
Lyles School of Civil Engineering

Approved by:
Dr. Dulcy M. Abraham

For my parents and my wife.

ACKNOWLEDGMENTS

I would like to express my sincere gratitude and appreciation to my advisors, Professor Athanasios Tzempelikos and Professor Panagiota Karava. Undertaking this Ph.D. would not be possible without their support, encouragement, insight, and guidance. They provided priceless advice and helped me gain broad and in-depth knowledge and experience. It was fortunate that I started my Ph.D. at Purdue and worked with them.

I would like to thank Professor Ilias Bilionis for helping me learn and explore methodologies for my research. He spent a lot of his time and energy to help me build a solid background and develop skills. Also, his great insight and intuition significantly helped my Ph.D. studies.

I would like to thank Professor Jianghai Hu and Professor Brandon Boor for their invaluable comments. Also, I would like to thank all faculty and staff members at Herrick Laboratories for building and providing wonderful research environments and organizing and holding professional events.

I gratefully acknowledge the support from the National Science Foundation and the Center for High Performance Buildings at Purdue University.

I am indebted to all my friends and colleagues at Purdue and in Korea. My Ph.D. was not a lonely journey, thanks to them. I would like to thank my father and mothers for always supporting and encouraging me to follow my dreams. Also, I would like to thank my father and mother in law for their encouragement. Finally, I would like to thank my wife, Yaejin, who has always been by my side during my Ph.D. and dealt with this picky person, for her unparalleled support and endless love.

TABLE OF CONTENTS

LIST OF TABLES

LIST OF FIGURES

ABSTRACT

Operation of typical heating, ventilation, and air conditioning (HVAC) systems has been based on general thermal comfort models. However, because of individual differences in thermal comfort, typical HVAC systems have not been able to achieve high levels of occupants' satisfaction. Moreover, conservative control settings designed for "widely acceptable" conditions have resulted in a high chance of energy waste.

To resolve these issues, HVAC systems have been proposed that can (i) learn their occupants' thermal preferences; (ii) be self-tuned to provide customized indoor thermal environments. This Thesis presents approaches and algorithms for the realization of self-tuned indoor thermal environments and demonstrates their experimental and simulation implementations.

First, this Thesis presents a new data-driven method for learning individual occupants' thermal preferences developed by combining classification and inference problems, without developing different models for each occupant. The approach is fully Bayesian, and it is based on the premise that the thermal preference is mainly governed by (i) an overall thermal stress, represented using physical process equations with relatively few parameters along with prior knowledge of the parameters, and (ii) the personal thermal preference characteristic, which is modeled as a hidden random variable. The concept of clustering occupants based on this hidden variable, i.e., similar thermal preference characteristic, is introduced. The algorithm also incorporates hidden parameters and informative priors to account for the uncertainty associated with variables that are noisy or difficult to measure (unobserved) in real buildings (for example, the metabolic rate, air speed and occupants' clothing level). Experimental results show that the algorithm provides accurate predictions for personalized thermal preference profiles and it is efficient as it only requires a relatively small dataset collected from each occupant.

Second, this Thesis presents a self-tuned HVAC controller that provides customized thermal conditions to satisfy occupant preferences (i.e., online learning) while minimizing energy consumption. The evolution of personalized thermal preference models and the delivery of thermal conditions with model predictive control (MPC) form a closed-loop. To integrate these two parts, a new method that always provides a set of lower and upper indoor temperature bounds is proposed. Experimental and simulation results show that the self-tuned controller can (i) significantly

decrease the level of occupant dissatisfaction compared to a baseline MPC controller; (ii) automatically adjust the system based on comfort-energy trade-off tuning.

Finally, this Thesis presents a Bayesian modeling approach which allows incorporating voluntary feedback data (comfort-related responses), collected via participatory interfaces, along with requested feedback data, into the thermal preference learning framework. The incorporation is done by explicitly considering occupants' participation –a type of behavior –in the model. The approach is evaluated with data from real occupants and a smart feedback request algorithm is developed, which determines whether to request feedback at any given time based on the quantified value of the request. Simulation results show that effective -but less-intrusive- user-interfaces can be developed, utilizing the developed models and algorithms for smart and human-centered HVAC operation.

1. INTRODUCTION

1.1 Background and motivation

One of the major purposes of heating, ventilation, and air conditioning (HVAC) is to provide comfortable thermal conditions to building occupants [3]. Toward this goal, extensive research has been conducted on human thermal comfort in addition to the development of various building and HVAC systems. To understand and predict human thermal comfort, researchers have focused on developing empirical models with data collected from large populations through climate chamber experiments and field studies [1,4–6]. The models succeeded in predicting the average comfort-related responses of large populations, were adopted in international standards, and used to design and control typical HVAC systems in office buildings [7–9].

However, numerous studies have shown that there are differences between individuals in their thermally comfortable conditions and such models cannot accurately predict thermal comfort of individual occupants [1,10–12]. As a result, typical HVAC systems operating based on thermal comfort standards have not been able to achieve high levels of occupants' satisfaction. Moreover, because of the conservative control settings designed for "widely acceptable" conditions, there is a high chance of energy waste [13–16].

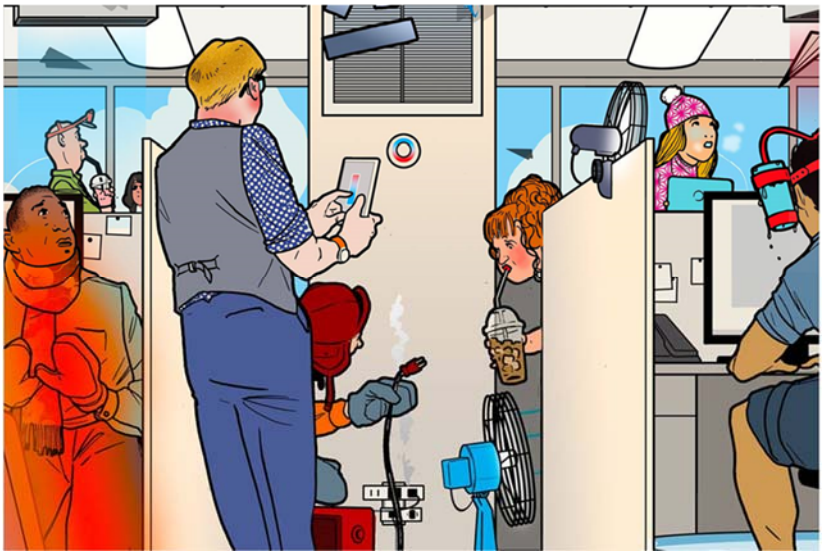

Figure 1.1. Occupants' contradicting thermal preferences in an office space [17].

Researchers have recognized these issues and suggested solutions that incorporate building occupants in sensing and control frameworks (a.k.a., human-in-the-loop) and systems tuning based on personal preferences to achieve customized indoor environments. With the rapid development of wireless sensor network, mobile devices, data-driven modeling (machine learning), and ubiquitous computing over the last decade, initial studies have been conducted to verify the feasibility of this concept. The results have shown that HVAC systems tuned based on individuals' preferences have the potential to increase occupants' satisfaction and reduce energy consumption [18–23]. However, despite of the successful demonstration of early studies, major components necessary for the robust implementation of self-tuned environments, i.e., learning occupant preferences, and incorporating their feedback into HVAC controls, are still quite anecdotal [24].

1.2 Objectives

Realization of self-tuned indoor thermal environments is the final goal of this research. In this thesis, the focus is on learning individual occupants' thermal comfort and developing a control algorithm that enables customized thermal environments in modern office buildings. To enable this approach, we explicitly encode our main hypothesis: "Different people prefer different thermal conditions" in the general model. Figure 1.2 shows the overall process for learning the thermal preference of an individual occupant.

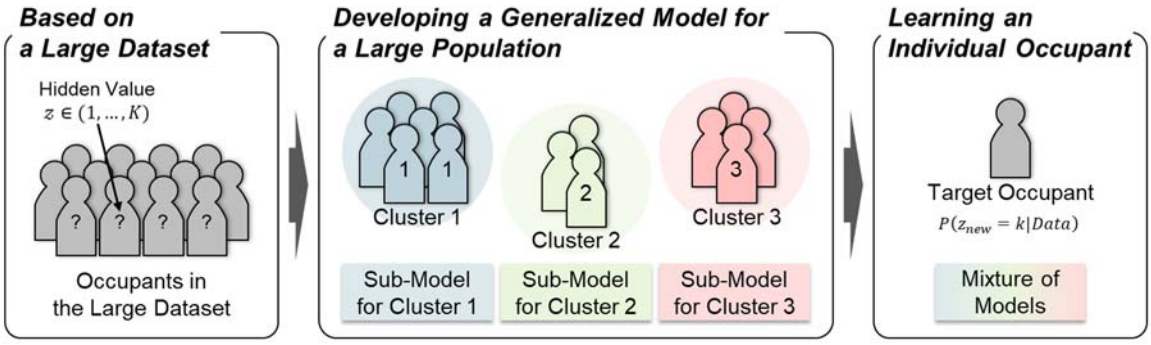

Figure 1.2. Overall process for learning the thermal preference of an individual occupant.

The main objectives of this thesis are:

1. To develop a data-driven modeling algorithm for learning individual occupants' thermal preferences, which provides reliable predictions (effectiveness) and requires less data to be trained (efficiency).

2. To develop smart occupant feedback request algorithms and efficient modeling approaches for less-intrusive user interfaces towards human-centered HVAC operation.
3. To develop and demonstrate a self-tuned HVAC a controller that uses personalized models to achieve occupants' satisfaction while minimizing energy consumption.

The work proposed in this research is based on a Bayesian modeling approach. The rationale behind this modeling choice, is related to its inherent advantages: it allows encoding and testing our prior knowledge and beliefs about the relationships between the different variables; it can easily account for hidden (unobserved) variables; and it can seamlessly combine data from heterogeneous sources as they become available [24]. Although this study only focuses on occupants' thermal comfort, the proposed modeling approaches are applicable to other occupant-related problems, e.g., visual environment preferences, occupancy and behavior.

1.3 Document overview

Chapter 2 contains a literature review with focus on conventional models predicting occupants' thermal comfort, individual differences in thermal comfort, personalized thermal comfort modeling, and control based on personalized models.

Chapter 3 presents a Bayesian approach for probabilistic classification and inference of occupant thermal preferences in office buildings. A Bayesian mixture model is developed based on prior knowledge on the heat balance around the human body to achieve the goal. A subset of ASHRAE RP-884 database is used to validate the approach.

Chapter 4 presents a Bayesian approach for learning personalized comfort models in real buildings where clothing level, metabolic rate and air speed cannot be measured. Hidden variables are introduced in the models to deal with the unobserved parameters. Data collected from 9 test-subjects are used to validate the approach.

Chapter 5 presents a self-tuned HVAC controller in which the evolution of personalized thermal preference models (online-learning) and the delivery of thermal conditions with model predictive control (MPC-based HVAC operation) form a closed-loop. The controller was implemented in an open-plan office. The experimental results with the self-tuned controller evaluate the dissatisfaction level and energy consumption during the implementation period by comparing those with a baseline controller.

Chapter 6 presents a Bayesian modeling approach for smart and less-intrusive user interfaces towards human-centered HVAC operation. The modeling approach allows incorporating voluntary feedback data (comfort-related responses), collected via participatory interfaces, along with requested feedback data, into the thermal preference learning framework. Based on the approach, a smart occupant feedback request algorithm, that determines whether to request feedback at each moment based on the quantified value of the request, is proposed.

Chapter 7 includes ideas for future work and potential extensions of this research.

2. LITERATURE REVIEW

The American Society of Heating, Refrigerating and Air-Conditioning Engineers (ASHRAE) defined thermal comfort as ‘‘the condition of the mind in which satisfaction is expressed with the thermal environment’’ [7]. Previous studies have shown that temperature and moisture sensations from the skin, deep body temperatures, and the level of physiological efforts required to thermoregulation are the major factors resulting in thermal comfort or discomfort besides of psychological and other processes [25]. Here, typical physiological efforts are vasodilation, vasoconstriction, sweating, and change in muscle tension (shivering).

Building thermal comfort in indoor spaces has been an active research topic for research because of its significant influence on occupants' overall satisfaction with indoor environments [26,27], but also on their productivity [27–32] and energy consumption [15,16,33,34]. Inevitably, there have been numerous studies to develop predictive empirical models predicting occupants' thermal comfort [35–37]. There are two main models which are widely accepted and used: the predicted mean vote (PMV) model and adaptive models.

The PMV model was developed based on prior research on heat balance of the human body and data collected through extensive laboratory experiments by Fanger [1], which became the basis for standards such as ASHRAE 55 [7] and ISO 7730 [8]. The PMV model calculates the thermal load on the body in steady-state conditions, defined as the difference between internal heat production and heat loss to the actual environment for a person hypothetically kept at comfort values of mean skin temperature and sweat rate at the actual activity level. In the PMV model, the comfort values of mean skin temperature ($T_{\text{skin, comfort}}$ in Kelvin) and sweat rate ($h_{\text{sweat, comfort}}$ in W/m^2) are estimated by equations developed based on data of Rohles and Nevins [38]:

$$T_{\text{skin, comfort}} = 308.7 - 0.0275 \cdot (M - W) \tag{2-1}$$

$$h_{\text{sweat, comfort}} = 0.42 \cdot (M - W - 58.15) \tag{2-2}$$

where M is the metabolic rate (W/m^2) and W is the external work (W/m^2, usually 0 in office environments). Then, the heat loss (h_{loss} in W/m^2) is calculated via empirical equations representing physical heat transfer mechanisms, which were examined in previous research [39], as follows:

$$h_{\text{loss}} = h_{\text{radiation}} + h_{\text{convection}} + h_{\text{evaporation}} + h_{\text{respiration}} + h_{\text{sweat, comfort}} \tag{2-3}$$

where

$$h_{\text{radiation}} = 3.96 \times 10^{-8} \cdot f_{cl} \cdot (T_{cl}^4 - MRT^4) \quad (2\text{-}4)$$

$$h_{\text{convection}} = f_{cl} \cdot h_c \cdot (T_{cl} - T_{\text{air}}) \quad (2\text{-}5)$$

$$h_{\text{evaporation}} = 3.05 \cdot (5.73 - 0.007 \cdot (M - W) - p_a) \quad (2\text{-}6)$$

$$h_{\text{respiration}} = 0.0014 \cdot M \cdot \big(34 - (T_{air} - 273)\big) + 0.0173 \cdot M \cdot (5.87 - p_a) \quad (2\text{-}7)$$

where T_{air} is air temperature in Kelvin, MRT is mean radiant temperature in Kelvin, h_c is convective heat transfer coefficient ($\text{W/m}^2\text{K}$), f_{cl} is clothing area factor, p_a is water vapor pressure in Pascal, and T_{cl} is clothing temperature in Kelvin. For the values of h_c, f_{cl}, and p_a, Fanger used the following relationships:

$$h_c = \max\big(2.38 \cdot (T_{cl} - T_{\text{air}})^{0.25}, 12.1 \cdot \sqrt{Vel}\big) \quad (2\text{-}8)$$

$$f_{cl} = \begin{cases} 1.0 + 0.2 \cdot I_{cl}, & I_{cl} < 0.5 \text{ clo} \\ 1.05 + 0.1 \cdot I_{cl}, & otherwise \end{cases} \quad (2\text{-}9)$$

$$p_a = RH \cdot 10 \cdot e^{-((16.6536 - 4030.183)/(T_{\text{air}} - 273 + 235))} \quad (2\text{-}10)$$

where Vel is air velocity (m/s), I_{cl} is clothing insulation (clo), and RH is relative humidity (%). As part of the calculation, clothing temperature T_{cl} is estimated by solving the following equation:

$$T_{cl} = T_{\text{skin, comfort}} - 0.155 \cdot I_{cl} \cdot (h_{\text{radiation}} + h_{\text{convection}}) \quad (2\text{-}11)$$

Finally, the thermal load is calculated by:

$$L = (M - W) - h_{\text{loss}} \quad (2\text{-}12)$$

Then, the thermal load is mapped to the thermal sensation vote by:

$$PMV = (0.303 \cdot e^{(-0.036M)} + 0.028) \cdot L \quad (2\text{-}13)$$

In contrast, adaptive models consider people's inherent ability to adapt to variable environment conditions (psychological, behavioral, and physiological adaptation) in nsaturally-conditioned buildings [5]. Adaptive models are linear regression models developed based on global field data, which represent a linear relationship between a comfortable indoor temperature and the prevailing outdoor temperature. There are two widely used adaptive models: the ASHRAE 55 adaptive model developed by de Dear and Brager [5] and the EN 15251 adaptive model developed by Nicol and Humphreys [6]. For example, in ASHRAE 55 adaptive model (Figure 2.1), the upper and lower acceptable indoor operative temperatures with 80% acceptability limits are calculated by:

$$t_{o,upper} = 0.31 \cdot \overline{t_{pma(out)}} + 21.3, \quad (2\text{-}14)$$

$$t_{o,lower} = 0.31 \cdot \overline{t_{pma(out)}} + 14.3, \quad (2\text{-}15)$$

where $\overline{t_{pma(out)}}$ is a simple arithmetic mean of all of the mean daily outdoor air temperature.

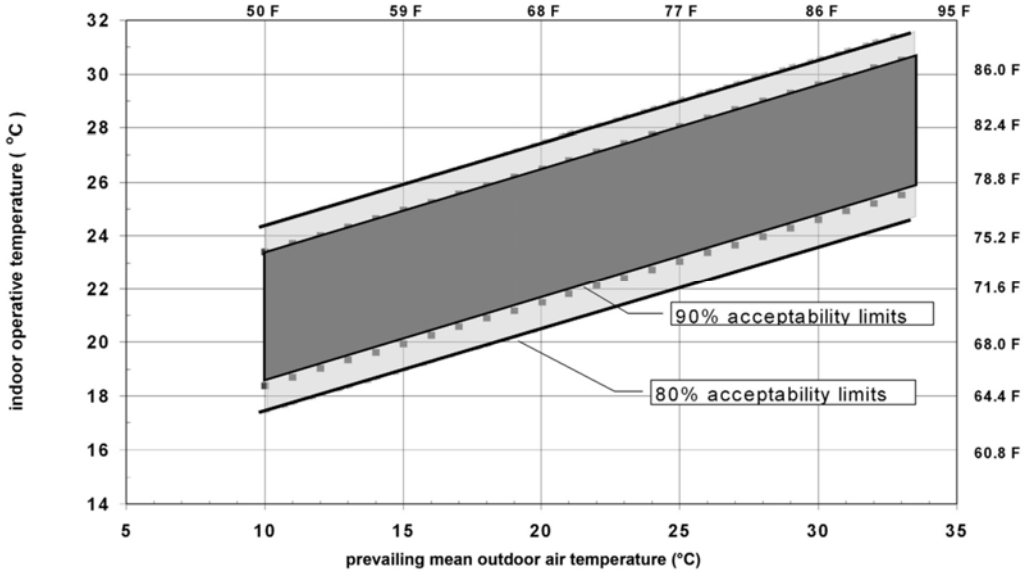

Figure 2.1. ASHRAE 55 adaptive model by de Dear and Brager [5]

These models succeeded in predicting the average comfort related responses of large populations and were adopted in international standards for HVAC systems control in typical office buildings [7–9].

2.1 Individual difference in thermal comfort

Individual differences in thermal comfort have been observed and studied through climate chamber experiments and field studies [2,37]. As a result, conventional thermal comfort models, i.e., the PMV model and adaptive models, cannot accurately predict thermal comfort of individual occupants [1,10–12]. To address this issue, studies have been conducted to identify causal factors for these differences: gender, age, etc. However, a literature review by Wang et. al. [2] showed that there were no clear and consistent conclusions as to the significance and size of inter-group differences over previous studies. For example, among 36 studies on the significance of gender difference, 11 studies found that the difference was significant while 14 studies did not. Some studies argued that individual differences in thermal comfort are not directly caused by the

aforementioned factors but by differences in physiological characteristics which relate to heat gain and heat loss of the human body [40–44]. Unfortunately, there have been no thermal comfort model which can consider all the physiological characteristics. Moreover, it may be impossible to measure the characteristics of each individual in real buildings.

To deal with thermal comfort differences of individual occupants, a shift from using one model predicting the average response of large populations to thermal environment control based on personalized thermal comfort models (i.e., self-tuned HVAC systems learning their occupants) is required. This concept is supported by today's advanced technologies [2,24]: wireless sensor networks, mobile devices, data-driven modeling (machine-learning) techniques, and ubiquitous computing. This new paradigm consists of two major components: 1) learning individual occupants' thermal comfort; 2) control based on the personalized models.

2.2 Personalized thermal comfort modeling

The authors in [45], one of the early studies for learning individuals' thermal comfort, proposed training a neural network model to predict one's thermal sensation. In the study, the authors exposed each subject to 20-40 conditions, which are different combinations of air temperature and velocity, and asked their thermal sensation. Neural network models having 5 hidden layers were trained with occupants' responses and measured air temperature, mean radiant temperature, humidity, and air speed. The trained models showed high prediction performance (accuracy of 80 %) with 20 training data points. However, unreported data distribution and lack of clarity of the validation process degrades the reliability of the results.

In [19], the authors demonstrated a personalized HVAC control system learning occupants' sensation with their participatory votes. Unlike [45], the controller did not intentionally expose the occupants to different conditions for the learning purpose. A linear discriminant algorithm with air temperature and humidity as inputs was used. To accommodate the adaptation of the comfort algorithm, only nine data points, which took 2~3 weeks to collect, were used in creating the decision boundary, with new points replacing the old. However, the predictive performance of the models was not evaluated.

In [46], the authors trained univariate multinomial logistic regression models to predict occupants' thermal sensation using the air temperature as an input variable . The authors collected data for the subjects' thermal sensation up to 4 times a day. 22 synthetic data points were included

in the training dataset which formed a starting profile to boost the learning process and to allow the control to work from the beginning. Different models were developed for different subjects but their prediction performance was not evaluated. A remarkable point was that the models required around 90 data points to be converged, which might take more than three months under normal office conditions. The authors also suggested removing data points older than 30 days in the vicinity of Ta±0.25 °C with new data entry to adapt to long term changes in individuals' thermal comfort.

In [20], the authors estimated time-varying air temperature correction factors for specific groups of occupants by comparing computed PMV values and actual sensation votes from them. The correction factors were used to adjust the setpoint temperature. Occupants' thermal sensation responses were collected through a participatory voting interface. It was assumed that no vote from occupants during a period implied they were in neutral (comfortable) since occupants would seldom participated to the system under comfortable conditions but would be eager to participate under uncomfortable conditions.

In [21,22], the authors proposed to use a linear regression model trained with data from a target occupant to correct the discrepancy between computed PMV values and the occupant's actual thermal sensation votes. Although the prediction performance of a developed model was promising (RMSE 0.5377 with 12 training data points), since the study was conducted with only one subject, further validation is required.

In [47], the authors collected more than 60 thermal preference votes over 3 weeks from each of the 4 test-subjects relying on their participations. To ensure each subject has been exposed to different ranges of air temperature, it was a set between 18 and 29°C on different days. In addition, to encourage subjects' participation, the average of responses was considered in adjusting the room temperature. With the data, the authors trained personalized models with the Wang-Mendel fuzzy rule extraction algorithm. The results showed that the method required about 40 -50 data points to train a converged model.

In [48], the authors proposed a model structure derived based on heat balance of human body. The inputs were air temperature, mean radiant temperature, and humidity and the output was thermal sensation. A personalized comfort model was developed by estimating four parameters in the model structure with data from each occupant with the recursive least-square (RLS) method. The forgetting factor in RLS helped adaptation of a model to long-term variation in one's thermal

comfort. The method was evaluated with data collected from 9 test-subjects. The thermal sensation was requested by the participants every one hour. Personalized models showed lower mean square error and bias over the testing data compare to PMV model.

In [49], the authors developed personalized models using a Bayesian network in which the observed variables are the operative temperature, humidity, outside temperature, the current day of the year, and the thermal sensation . A subset of ASHRAE RP-884 database was used to validate the method. The trained models showed 17.5-23.5 % higher performance in terms of RMSE compared to the PMV model and the adaptive model described in [11]. Also, the RMSE converged after 10 observations.

In [50], unlike other studies, the authors proposed a method for developing personalized dynamic thermal comfort models with a state-space Wiener model structure with a logistic output function. The authors conducted an experiment in which 13 subjects experienced significant temperature changes. During the experiment, the test-subjects' thermal sensation was recorded. Personalized models were developed with the measured air temperature and the subjects' responses. The trained models showed better results in terms of R-square compared to the PMV model and a model proposed in [51]. To adapt the model prediction to environmental and/or occupant variability, the authors proposed using the Extended Kalman Filter to update the offset parameter in models. Since this method is not updating the dynamics of the model but a parallel translation of the output, its reliability is questionable.

In [52], the authors developed a learning method using a Bayesian network with the air temperature and the thermal sensation as variables. Data from each occupant were used to estimate the probability threshold as well as model parameters to convert the probability to a prediction. To detect long-term comfort variation and to update models accordingly, the Kolmogorov-Smirnov test was introduced in the method. To validate the method, the thermal sensation of 33 test-subjects was collected through their participatory votes. The validation results showed that the model prediction performance was higher than that of alternative methods. The authors claimed that the improvement was due to utilization of the Kolmogorov-Smirnov test.

In [53], the authors proposed a classification algorithm they developed. The algorithm was evaluated with synthetic data they generated. Although the algorithm worked as expected, however, the authors did not discuss the necessity of using the proposed algorithm compared to other approaches.

In [54], the authors used a C-support Vector Classification algorithm to develop personalized comfort models. Model inputs were the air temperature, mean radiant temperature, humidity, air speed, clothing level, and metabolic rate, and the output was the thermal sensation. To collect data to evaluate the method, 20 subjects were exposed to different conditions and their thermal sensation was collected every 10 minutes. The developed models showed very high prediction performances (accuracy of 89.8%). However, the testing conditions and distribution of responses were not reported.

In [55], the authors modeled individuals' thermal comfort with a Gaussian formulation, i.e., estimation of mean and variance of a Gaussian form for each occupant. Although the authors implemented the method in their controller, they did not evaluate it analytically.

In [56], the authors demonstrated the use of Random Forest algorithm. Different variables, i.e., clothing level, heart rate, skin temperature, activity level, air temperature, humidity, CO2 level, window state, outdoor temperature, and outdoor humidity, were tested as model inputs. The model output was the thermal preference. To collect the preference votes, a participatory voting interface was developed. To obtain data in the natural ventilation mode, subjects were asked to open the window (also set back HVAC system) twice per day when the outdoor temperatures were deemed acceptable. Similarly with [20], the authors in [56] assumed that if no reports were received from an occupant, he/she was considered as comfortable in that period. The results showed that incorporating human physiological and behavioral data was important to increase models' prediction performance (accuracy of 70-80%).

In [57], to eliminate the necessity of occupants' actual responses in the learning process, the authors used hidden Markov model with face skin temperature as the observed variable. Estimated hidden states were expected to reflect occupants' thermal preferences. To measure the face skin temperature, an eyeglasses frame on which four infrared sensors were installed was used. Although the results were promising, i.e., overall specificity of 82.8% over 10 subjects, there are two unclear points that make the reliability of the results doubtful: 1) hyper-parameters in the algorithm were selected arbitrary; 2) the metric specificity was not enough to show the validity.

The authors of [58] tested six machine-learning algorithms and different variables with data collected 3 times daily from 38 occupants. All the personalized models developed showed higher prediction performances compared to PMV model and the adaptive model in [7]. The authors claimed that 1) the algorithms required over 60 survey responses in order to produce a model with

stable predictions; 2) the algorithms required data of all the three classes, i.e., 'want warmer', 'no change', 'want cooler'; 3) considering occupants' behaviors as model inputs increases the prediction performance significantly.

2.2.1 Feedback collection

There has been a lack of discussion regarding methods of collecting the feedback responses in real buildings, e.g., how feasible or intrusive a method is, how effective a method is in collecting sufficient data, how reliable data can be collected with a method, how reliable a machine learning algorithm is in developing a personalized model with data collected with a method, etc.

Thermal comfort is defined as the condition of mind [7] and thus the only way we can measure it is surveying individual occupants [59] assuming that their responses are reliable. In this context, in terms of minimizing the risk of sampling bias and subsequently developing unbiased personalized comfort models, requesting occupants' responses randomly or regularly would be preferred [45,46,48–50,54,58]. However, frequent response requests are intrusive and thus not feasible in real buildings especially if continuous data collection is required for online model update. On the contrary, if we decrease the feedback frequency, it would take a long time to collect enough data to train personalized comfort models. To resolve the practicality issue, in [19,20,47,56], the authors proposed using participatory user-interfaces with which occupants can voluntarily report their state of thermal comfort. Although this alternative method seems practical for real-world applications, occupants' participation, a type of behavior, could be affected by multiple factors; consequently, there is a high risk of sampling bias. For example, people would actively participate and provide their feedback if they are uncomfortable believing that the feedback could improve the thermal conditions. On the contrary, if they are satisfied with the conditions, they would not be as responsive. If we train a predictive model with the biased data without any treatment, because of the lack of satisfaction/comfort/neutral responses, the predictive probability (or corresponding score) of satisfaction/comfort/neutral will keep decreasing as we feed data, i.e., more data do not guarantee better model. In [20,56], researchers assumed that occupants were satisfied/comfortable if there was no participation for a while and added hypothetical data points in their training dataset. However, it is possible that occupants may not (or forget to) participate even though they are not satisfied because of their workload [56]. Also, there are other factors, e.g., the ease of interface use, the level of expectation that the system will

adapt to their response, making it difficult to develop generalizable heuristic rules for participatory data collection [47]. Moreover, the proposed rules cannot distinguish effects of one's thermal preference and the level of one's activeness in using the participatory interface on the data distribution. Hence, if we operate an HVAC system serving a shared space, e.g., open-plan office, with personalized comfort models based on one of the rules, the thermal condition will be biased towards the thermal preference of active occupants, which may not be fair. In addition, using a participatory interface does not guarantee that we can collect enough data to learn one's thermal preference.

2.2.2 Selection of input variables (predictors)

It is well known that the input variables should be selected by their importance in making accurate predictions, i.e., prediction power as predictors, and the cost of collecting the data [56,58]. In [56–58], occupants' physiological (e.g., skin temperature, heart rate) and behavioral data (e.g., window operation, PCS behaviors) were used to increase the prediction performance. In [19,20,46,47,50,55,57], only one or two (i.e., air temperature, humidity) variables were used to minimize the data collection cost. However, another important point has not been studied yet: can we know (e.g., control or predict) values of a variable for future moments to determine future thermal conditions? For example, let's suppose that fan on/off behavior is one of input variables in a model. Since the behavior is directly related with one's thermal comfort, the prediction performance of the model would be very high. However, since it is a cause of one's thermal comfort, we cannot know whether the occupant would act or not at a future moment. Therefore, the prediction power gained by having the variable will be lost if the model is used for future predictions.

2.2.3 Prediction performance evaluation

Different metrics have been used to evaluate the prediction performances of models. Metrics designed for classification problems (e.g., accuracy, specificity, precision, recall, and area under the Receiving Operating Characteristics (ROC) curve) were used in [45,54,56–58], and metrics considering the magnitude of errors (e.g., root-mean-square error, mean absolute error) were used in [22,47–49]. In [50], a statistical measure, R^2, was used. However, none of the metric is ideal

since there are two issues with using general metrics in this problem. First, it is highly probable that the test dataset distribution will be imbalanced (e.g., more than half of votes can be "no change"), which will negatively affect the reliability of most of metrics. Second, costs for different misclassification cases are different (i.e., different costs to different cases in the confusion matrix), but general metrics do not consider the differences. Therefore, a new general metric for the problem should be developed based on suture studies.

Another issue is that there is no metric can guarantee whether the model is good or not by itself since a value of a metric is affected by not only the goodness of the model but also various characteristics of data. Therefore, a comparative evaluation with alternative models or methods will be needed to draw correct conclusions as in [49,50,52,58].

2.2.4 Data efficiency

Training a reliable model requires data with sufficient quantity and quality. Daum et al. [46] showed that their model required around 90 data points converge. Li et al. [56] reported that their comfort models achieved an acceptable accuracy with approximately 50 training data points. Kim et al. [58] reported that individual subjects needed to supply over 60 responses to train a model with stable predictions. The required number of reliable data can vary with conditions that occupants experience to some extent; in real buildings, this process could take a few months [46,60,61].

The long-term data collection often translates into long times required for developing functionally advanced controls, which is usually the objective of learning occupant preferences. If a model needs to be updated continuously to maintain a certain level of accuracy [23,46,48,52], but the amount of data collected in a certain period of time is not adequate, the model may not be able to make reliable predictions or continuously converge. Therefore, the efficiency of a learning method in terms of required quantity and quality of data should be re-examined.

2.3 Control based on personalized models

Some of the aforementioned studies actually demonstrated self-tuned HVAC systems and achieved the goals: increasing occupants' satisfaction and reducing energy consumption. Feldmeier and Paradiso [19] tested their system based on personalized thermal comfort models

and actual occupancy in real offices and reported 24% savings in HVAC energy consumption (compared to standard HVAC control) and improved thermal comfort. Erickson and Cerpa [20] controlled a space based on thermal comfort models that used occupant feedback and reported that occupants were fully satisfied with the thermal conditions while 10.1% energy savings were achieved. Gao and Keshav [21,22] developed a controller by integrating the learning method with clothing level estimation, occupancy detection and model predictive techniques, and implemented the controller in an office room, with resulting energy savings up to 60%. Jazizadeh et al. [23] implemented a HVAC system learned their occupants with the method in [47] and showed that 39% of HVAC energy was reduced while occupant comfort was improved. However, the energy saving was achieved by not only considering personalized thermal comfort but also improving a limitation of the existing HVAC system. Ghahramani et al. [62] demonstrated an optimal controller performing based on personalized comfort models and simple room energy models. The personalized comfort models were developed with the method in [47]. The result showed that the cooling energy consumption was reduced by 12.08 %. Sarkar et al. [55] showed that a heuristic rule-based controller with personalized profiles, which were Normal distribution density functions fitted to feedback from occupants, reduced HVAC energy consumption by 39%. Li et al. [56] showed that, on average, the total number of uncomfortable reports was reduced by 54% after implementing a controller which adjusted the room set point temperature with personalized comfort models developed based on Random Forest algorithm.

2.3.1 Considering a single condition vs. a range of conditions

Personalized comfort models used in most of previous studies return a "score" (e.g., predictive probability with logistic regression) for a person being comfortable/satisfied with a given set of inputs. This value usually corresponds to the level of certainty in the prediction. In [20,23,47], the authors controlled the HVAC system to provide a single condition (i.e., a certain room air temperature) maximizing the score for comfortable class (i.e., maximize the possibility of the occupants being comfortable). This strategy is good for ensuring occupants' thermal comfort, however, it could be too conservative and reduce the potential of energy saving [62]. Therefore, in other studies [21,22,55,56,62], the authors considered a range of conditions in which occupants would be comfortable by setting a threshold for the score. However, this approach does not guarantee that this range always exists. For example, the maximum score of a personalized model

could be lower than a threshold which a user sets in advance [52]. Although this could be solved by re-scaling the score or by simply picking the maximum point, another issue arises: how to define a control range for multiple occupants, e.g., in an open-plan office. In [63], the authors posed a multi-objective optimization problem, considering occupant comfort and energy use, to resolve this issue. However, non-convex optimization algorithms are required when including both complex personalized comfort models and building models, which could be computationally costly for real-time control.

2.3.2 Aggregation of different occupants' different preferences

In many cases, spaces of multiple occupants are conditioned by a couple of shared HVAC systems. In such spaces, aggregation of different occupants' different preferences is an important issue to increase the group's satisfaction. In [20], the authors proposed simply training a single model for a group of occupants by using all the data collected from them. However, there is a problem that if occupants' responses are collected via a participatory vote scheme, the model will bias to responses of occupants who actively participate [47]. The authors of [47,55,56] suggested learning individuals separately and aggregating them later. Jazizadeh et. al. [47] calculated a single point with which the sum of deviations from occupants' preferred temperatures. Sarkar et. al. [55] set a threshold for the score to gain occupants' comfort ranges and simply used the overlapped range. Li et. al. [56] used a heuristic rule to determine the setpoint based on personalized models. However, there have been no studies which investigated pros and cons of different aggregation methods.

2.3.3 Integration with advanced building controls

There have been a few studies which attempted to integrate advanced building controls, such as model predictive control (MPC), into the human-in-the-loop framework to maximize the system performance. MPC solves a constrained optimization problem that minimizes the HVAC energy consumption over a prediction horizon, using a data-driven building model along with weather forecast and prediction of other disturbances, such as occupancy schedule, internal heat gains, etc. Previous studies showed significant benefits in terms of minimizing HVAC energy consumption while maintaining occupant thermal comfort [64–69]. With regards to personalized thermal

environments, Gao and Keshav [21,22] developed a controller by integrating a learning method (which adjusted the PMV model with a personalized linear equation) with clothing level estimation, occupancy detection and a model predictive control technique for space heating. The controller was implemented in an office room with resulting energy savings up to 60% compared to a fixed-temperature setpoint control. However, the experiment was conducted with only one occupant, so results cannot be generalized. Majumdar et al. [70] and Zhao et al. [71] used simulation to show that MPC, considering individual differences in thermal comfort, can save energy while improving the comfort level. Chen et al. [72] conducted 3-hour long chamber experiments to test their MPC controller with a dynamic thermal sensation model using occupant feedback. Although the above studies are useful, none of them was conducted with real occupants in their natural office work environment. This paper presents the first self-tuned HVAC controller that integrates model predictive control and personalized thermal preference models, and its successful implementation in a real occupied office space.

3. A BAYESIAN APPROACH FOR PROBABILISTIC CLASSIFICATION AND INFERENCE OF OCCUPANT THERMAL PREFERENCES IN OFFICE BUILDINGS

3.1 Overview

This chapter presents a novel Bayesian modeling approach for learning individual occupants' thermal preferences, with improved efficiency and accuracy, even if the model structure is complex and the amount of data collected from each occupant is relatively limited. The approach includes (i) developing a general model structure to explain the thermal preferences for a population of occupants (Section 3.2); verification with a synthetic dataset collected in various office buildings, finding the optimal number of clusters, and presentation of results based on a subset of the large ASHRAE RP-884 database [5] (Section 3.3); (ii) using the general model to infer the personalized thermal preference profile of an individual occupant and prediction results for personalized thermal preference profiles (Section 3.4). The prediction performance of the overall method along with limitations and recommendations for future work is discussed in Section 3.5.

3.2 The general model: discovering clusters of occupants with similar thermal preference characteristics

3.2.1 Modeling methodology

An important starting point for developing a probabilistic model is drawing relationships between variables. Figure 3.1 is a simplified version of the graph representing connections between thermal preference and related factors (i.e., environmental, human, hidden features, and occupant behavior) drawn based on our knowledge and beliefs. Solid and void (white) nodes correspond to observed and latent variables, respectively. The arrows in the graph represent conditional probabilistic relationships between the nodes. The 'personal thermal preference characteristic' is included in the graph, which is an unobserved variable, induced by our main hypothesis. In this study, it is assumed that thermal preference is mainly governed by the overall thermal stress and the personal thermal preference characteristic, while other potential factors are neglected, for simplicity.

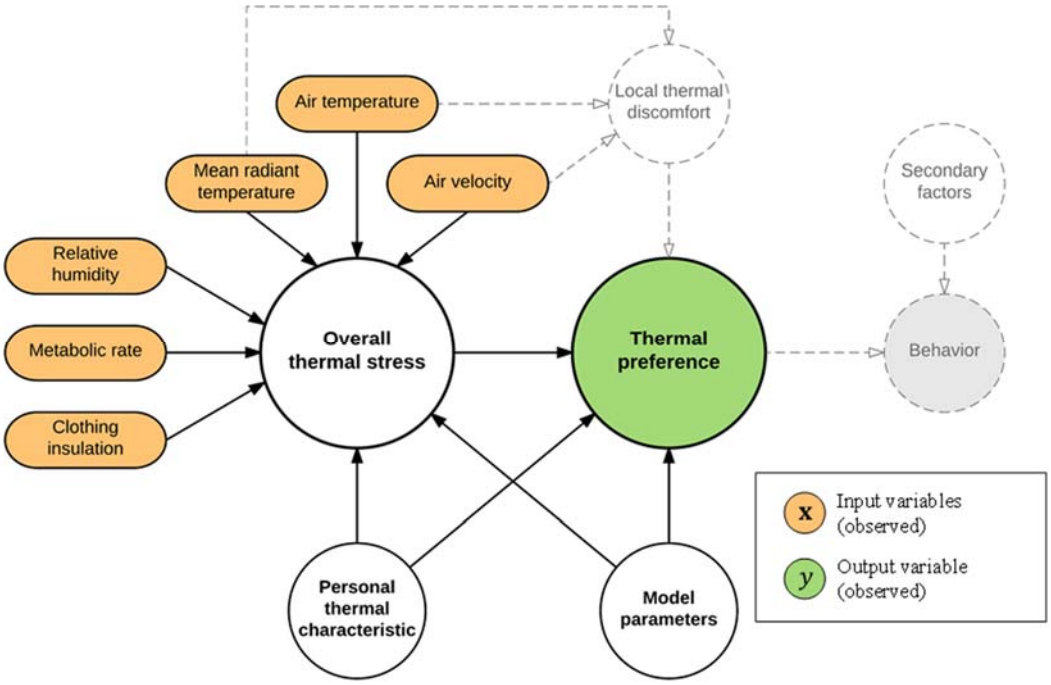

Figure 3.1. A graph representing our knowledge and beliefs regarding occupants' thermal preference

Based on the above, the joint probability of all the random variables is decomposed as follows:

$$P(y, E, z, \mathbf{x}, \boldsymbol{\theta}) = P(E|z, \mathbf{x}, \boldsymbol{\theta}) \cdot P(y|E, z, \boldsymbol{\theta}) \cdot P(z) \cdot P(\mathbf{x}) \cdot P(\boldsymbol{\theta}) \quad (3\text{-}1)$$

where y is the occupant's thermal preference, E is the overall thermal stress, z is the thermal preference characteristic of an individual occupant, $\mathbf{x} = (x_1, x_2, \dots, x_6)$ are the input variables (i.e., air temperature, mean radiant temperature, air velocity, relative humidity, clothing insulation, and metabolic rate), and $\boldsymbol{\theta}$ collects all the model parameters. In this study, the thermal preference, y, is discretized to take only three values: "want warmer", "no change", and "want cooler". Also, by assuming that there is an unknown number K of possible clusters of people who have similar z, i.e., the thermal preference characteristic, z is discretized to take K values. Based on this assumption, developing the general model becomes a clustering problem, i.e., discovering clusters of people based on a large dataset and developing sub-models for them. Accordingly, z becomes a hidden variable indicating a cluster to which an occupant belongs. The model is developed with a fully Bayesian approach. Eq. (3-1) represents that the general model requires two subparts, $P(E|z, \mathbf{x}, \boldsymbol{\theta})$ and $P(y|E, z, \boldsymbol{\theta})$.

The first subpart, $P(E|z,\mathbf{x},\boldsymbol{\theta})$, predicts the overall thermal stress level with the input variables and the personal thermal characteristic. If we modeled this subpart with a general regression method from scratch, it would require a very large dataset, which is difficult to collect, since heat transfer processes are highly non-linear, and consequently we need to estimate many parameters on which we don't have prior knowledge. This problem can be resolved by designing a model structure, in which we can introduce our prior knowledge (e.g., physical knowledge, results of previous studies), and estimating parameters with the prior knowledge. In this study, we introduce equations of the PMV model developed by Fanger [1] for the model structure. The details of the PMV model equations are listed in Chapter 2, with important parameters that are re-estimated in the present study as described below. The equations in Fanger's model aggregate the effect of different factors and turn it into a single value (i.e., the thermal load, L) using physics-based equations, assumptions and outcomes of previous studies. These equations are adopted in our work based on the assumption that the thermal load represents the overall thermal stress. However, related studies have shown that the original PMV model, developed based on a laboratory study to predict occupants' thermal sensation, cannot explain occupants' thermal preference in real buildings [73–76].

To overcome this limitation, five new parameters are added in the equations. First, to adjust the coefficients of the radiative and convective heat transfer in the equations, we add three parameters, ξ_1, ξ_2, and ξ_3, in the original equations ((2-4) and (2-8)):

$$h_{\text{radiation}} = (1+\xi_1)\cdot 3.96\times 10^{-8}\cdot f_{cl}\cdot (T_{cl}^4 - MRT^4) \tag{3-2}$$

$$h_c = \max\left((1+\xi_2)\cdot 2.38\cdot (T_{cl}-T_{\text{air}})^{0.25}, (1+\xi_3)\cdot 12.1\cdot\sqrt{Vel}\right) \tag{3-3}$$

Second, to incorporate the evaporation at the clothing surface, a term, $h_{\text{adj.}cl}$, is added in the clothing temperature calculation that was originally developed to consider only radiative and convective heat losses. Additionally, since the comfort value of mean skin temperature may be different from the original estimation based on laboratory measurements, a term, $T_{\text{adj.}cl}$, is added in the same equation. Then, by assuming that $h_{\text{adj.}cl}$ is inversely proportional to I_{cl}, the two terms are aggregated in a parameter, ξ_4 as follows:

$$\begin{aligned} T_{cl} &= T_{\text{skin, comfort}} + T_{\text{adj.}cl} - 0.155\cdot I_{cl}\cdot\left(h_{\text{radiation}} + h_{\text{convection}} + h_{\text{adj.}cl}\right) \\ &= T_{\text{skin, comfort}} - 0.155\cdot I_{cl}\cdot(h_{\text{radiation}} + h_{\text{convection}}) + \xi_4 \end{aligned} \tag{3-4}$$

where

$$\xi_4 = T_{\text{adj.}cl} - 0.155 \cdot I_{cl} \cdot h_{\text{adj.}cl} \quad (3\text{-}5)$$

The parameter ξ_4 is also expected to improve assumptions in Fanger's model related to the clothing temperature.

Finally, the total heat loss is adjusted since the equations for estimating the heat loss components may not be sufficiently accurate or important heat loss components may have been omitted. A term, $h_{\text{adj.loss}}$, which has a linear relationship with the internal heat production is designed by adopting the form of Eq. (2-2) since the amount of heat loss caused by evaporation, sweating, and respiration tends to be proportional to the internal heat production. Then, the adjustment term in Eq. (2-3) is added as follows:

$$h_{\text{loss}} = h_{\text{radiation}} + h_{\text{convection}} + h_{\text{evaporation}} + h_{\text{respiration}} + h_{\text{sweat, comfort}} + h_{\text{adj.loss}} \quad (3\text{-}6)$$

where

$$h_{\text{adj.loss}} = \xi_5 \cdot (M - W - 58.15) \quad (3\text{-}7)$$

The five new parameters (ξ_1, ξ_2, ξ_3, ξ_4, and ξ_5) are estimated based on data in the inference (model training) stage. Since two of the three parameters (ξ_4, and ξ_5) may relate to the personal characteristic z, we design the model to allow each cluster have its own values for these two parameters (i.e., $\xi_{z,4}$ and $\xi_{z,5}$, where $z = 1, \dots, K$). Therefore, $P(E|z, \mathbf{x}, \boldsymbol{\theta})$ is modeled as:

$$P(E|z, \mathbf{x}, \boldsymbol{\theta}) = \delta(E - L(\mathbf{x}; \boldsymbol{\xi}_z)/10) \quad (3\text{-}8)$$

where δ is the Dirac δ-function and $\boldsymbol{\xi}_z = \left(\xi_1, \xi_2, \xi_3, \xi_{z,4}, \xi_{z,5}\right)$. Note that the thermal load is divided by 10 to scale the size of the values for numerical stability. Since this subpart is modeled with the Dirac δ-function, it may appear that the probability is oversimplified. However, adopting the Dirac δ-function here is actually equivalent to adopting a Gaussian distribution in terms of the overall model. The reason is that the second modeling subpart of Eq. (3-1), discussed in the next paragraph, has Gaussian formulation. In other words, instead of modeling this subpart, i.e. (Eq. (3-8)), with a Gaussian distribution explicitly, by integrating the variance of the Gaussian into the second modeling subpart of Eq. (3-1), we can model this subpart (Eq. (3-8)) with the Dirac delta function and reduce the computational load.

The second subpart of Eq. (3-1), $P(y|E, z, \boldsymbol{\theta})$, is used for mapping the thermal stress to thermal preference. Since y is a discrete variable, we use linear discriminant analysis (LDA) which is equivalent to multinomial logistic regression [77]. The general form of LDA is:

$$P(y = c|E, \boldsymbol{\mu}, \sigma) = \frac{\exp\left(-\frac{1}{2\sigma^2}(E - \mu_c)^2\right)}{\sum_{c'=1}^{C} \exp\left(-\frac{1}{2\sigma^2}(E - \mu_{c'})^2\right)}, \qquad c = 1, \dots, C \tag{3-9}$$

where E is an input variable of which dimension is 1, y is an output variable, and $\boldsymbol{\mu} = (\mu_1, \mu_2, \dots, \mu_C)$ and σ are coefficients in LDA. Note that LDA assumes that $P(E|y = c)$ follows a normal distribution, $\mathcal{N}(\mu_c, \sigma^2)$.

If we define:

$$\beta_c = \frac{\mu_c}{\sigma^2} \tag{3-10}$$

$$\gamma_c = -\frac{\mu_c^2}{\sigma^2} \tag{3-11}$$

then the model becomes equivalent to the multinomial logistic regression:

$$P(y = c|E, \boldsymbol{\beta}, \boldsymbol{\gamma}) = \frac{\exp(\beta_c E + \gamma_c)}{\sum_{c'=1}^{C} \exp(\beta_c E + \gamma_{c'})}, \qquad c = 1, \dots, C \tag{3-12}$$

where $\boldsymbol{\beta} = (\beta_1, \beta_2, \dots, \beta_C)$ and $\boldsymbol{\gamma} = (\gamma_1, \gamma_2, \dots, \gamma_C)$ are vectors of coefficients in the multinomial logistic regression. Although LDA is equivalent to multinomial logistic regression, there is a remarkable difference between them in terms of training. In the case of multinomial logistic regression, its parameters (i.e., β and γ) do not have a clear intuitive meaning, and this makes it difficult to introduce prior knowledge in the model. However, parameters in LDA formulation, i.e., $\boldsymbol{\mu} = \left(\mu_{\text{prefer warmer}}, \mu_{\text{no change}}, \mu_{\text{prefer cooler}}\right)$ and σ, have intuitive meanings. For example, μ_c can be interpreted as the center of values on the domain of input E at which a specific class c is more likely than others. Since we believe that thermal stress for "prefer cooler" class would be greater than that for "no change" class, and thermal stress for "no change" would be greater than that for "want warmer" class, we impose prior information in the model. By introducing this information, less data is required for developing the model: $\mu_{\text{prefer warmer}} < \mu_{\text{no change}} < \mu_{\text{prefer cooler}}$.

Since parameters in LDA may relate to the personal characteristic z, we design the model to allow each cluster to have its values for these parameters (i.e., $\boldsymbol{\mu}_z = \left(\mu_{z,\text{prefer warmer}}, \mu_{z,\text{no change}}, \mu_{z,\text{prefer cooler}}\right)$ and σ_z, where $z = 1, \dots, K$). Thus, $P(y|E, z, \boldsymbol{\theta})$ is modeled as:

$$P(y=c|E,z,\boldsymbol{\theta})=\frac{\exp\left(-\frac{1}{2\sigma_z^2}\left(E-\mu_{z,c}\right)^2\right)}{\sum_{c'=1}^{C}\exp\left(-\frac{1}{2\sigma_z^2}\left(E-\mu_{z,c'}\right)^2\right)},\qquad c=1,2,3 \tag{3-13}$$

where $c=1,2,3$ represents "prefer warmer", "no change", and "prefer cooler", respectively.

3.2.2 Bayesian inference

Subsequently, we assemble all model subparts and we estimate parameters and the hidden cluster value z of each occupant in the dataset. Let $\mathbf{y}_{1:D}=\{\mathbf{y}_1,\mathbf{y}_2,\dots,\mathbf{y}_D\}$ and $\mathbf{X}_{1:D}=\{\mathbf{X}_1,\mathbf{X}_2,\dots,\mathbf{X}_D\}$, where $\mathbf{y}_d=\left(y_{d,1},y_{d,2},\dots,y_{d,n_d}\right)$ and $\mathbf{X}_d=\left\{\mathbf{x}_{d,1},\mathbf{x}_{d,2},\dots,\mathbf{x}_{d,n_d}\right\}$ are the observed thermal preferences and input variables from occupant d, respectively. Assuming that the sets of measurements from different occupants are conditionally independent given the features, the likelihood of the observed data is:

$$\begin{aligned}P(\mathbf{y}_{1:D}|\mathbf{X}_{1:D},z_{1:D},\boldsymbol{\mu}_{1:K},\sigma_{1:K},\boldsymbol{\xi}_{1:K})&=\prod_{d=1}^{D}P\left(\mathbf{y}_d\middle|\mathbf{X}_d,z_d,\boldsymbol{\mu}_{z_d},\sigma_{z_d},\boldsymbol{\xi}_{z_d}\right)\\&=\prod_{d=1}^{D}\prod_{i=1}^{n_d}P\left(y_{d,i}\middle|\mathbf{x}_{d,i},z_d,\boldsymbol{\mu}_{z_d},\sigma_{z_d},\boldsymbol{\xi}_{z_d}\right)\end{aligned} \tag{3-14}$$

where

$$\begin{aligned}&P\left(y_{d,i}=c\middle|\mathbf{x}_{d,i},z_d,\boldsymbol{\mu}_{z_d},\sigma_{z_d},\boldsymbol{\xi}_{z_d}\right)\\&=\int P\left(y_{d,i}=c\middle|\mathbf{x}_{d,i},E_{d,i},z_d,\boldsymbol{\mu}_{z_d},\sigma_{z_d},\boldsymbol{\xi}_{z_d}\right)P\left(E_{d,i}\middle|\mathbf{x}_{d,i},z_d,\boldsymbol{\mu}_{z_d},\sigma_{z_d},\boldsymbol{\xi}_{z_d}\right)dE_{d,i}\\&=\int P\left(y_{d,i}=c\middle|E_{d,i},z_d,\boldsymbol{\mu}_{z_d},\sigma_{z_d}\right)P\left(E_{d,i}\middle|\mathbf{x}_{d,i},z_d,\boldsymbol{\xi}_{z_d}\right)dE_{d,i}\\&=\frac{\exp\left(-\frac{1}{2\sigma_{z_d}^2}\left(L\left(\mathbf{x}_{d,i};\boldsymbol{\xi}_{z_d}\right)/10-\mu_{z_d,c}\right)^2\right)}{\sum_{c'=1}^{C}\exp\left(-\frac{1}{2\sigma_{z_d}^2}\left(L\left(\mathbf{x}_{d,i};\boldsymbol{\xi}_{z_d}\right)/10-\mu_{z_d,c'}\right)^2\right)},\qquad c=1,\dots,C\end{aligned} \tag{3-15}$$

where D is the total number of people, K is the number of clusters in the model, $z\in(1,\dots,K)$ is the hidden cluster value, $z_{1:D}=(z_1,\dots,z_D)$, $\boldsymbol{\xi}_{1:K}=\{\boldsymbol{\xi}_1,\dots,\boldsymbol{\xi}_K\}$, $\boldsymbol{\mu}_{1:K}=\{\boldsymbol{\mu}_1,\dots,\boldsymbol{\mu}_K\}$, $\sigma_{1:K}=(\sigma_1,\dots,\sigma_K)$ since we assume that $P(y|E,z,\boldsymbol{\theta})$ and $P(E|z,\mathbf{x},\boldsymbol{\theta})$ follows Eq. (3-8) and (3-13), respectively.

To proceed, we specify our prior state of knowledge about the coefficients and the hidden cluster value, i.e., $\boldsymbol{\xi}$, $\boldsymbol{\mu}$, σ, and z. By assuming that the original heat transfer coefficients may have small errors, we assign to ξ_3, ξ_4, and ξ_5 a zero mean Gaussian,

$$P(\xi_1, \xi_2, \xi_3|\lambda_1) = \mathcal{N}(\xi_1, \xi_2, \xi_3|0, \lambda_1\mathbf{I}) \tag{3-16}$$

where $\mathcal{N}(\cdot\,|\boldsymbol{\mu}, \boldsymbol{\Sigma})$ is the PDF of a multivariate Gaussian distribution with mean $\boldsymbol{\mu}$ and covariance matrix $\boldsymbol{\Sigma}$, $\mathbf{I}$ is the 3-dimensional unit matrix, and λ_1 is 0.01. To assign a prior to ξ_4, we need to consider two components, $T_{\text{adj.}cl}$ and $h_{\text{adj.}cl}$, in Eq. (3-4). Since the measured mean skin temperatures under comfort conditions are distributed around 32-36 °C [38,78], and the comfort value estimated by the original PMV model is 33.9 °C with M = 63.97 (1.1 met), we assume,

$$P\left(T_{\text{adj.}cl}\middle|\alpha_T\right) = \mathcal{N}\left(T_{\text{adj.}cl}\middle|0, \alpha_T^{-1}\right) \tag{3-17}$$

In addition to this, since we believe that there are omitted heat loss components in Eq. (3-4), we assume,

$$P\left(h_{\text{adj.cl}}\middle|\alpha_{h1}, \alpha_{h2}\right) = \mathcal{N}\left(h_{\text{adj.cl}}\middle|\alpha_{h1}, \alpha_{h2}^{-1}\right) \tag{3-18}$$

By aggregating the two equations, Eq. (3-17) and Eq. (3-18), we assign the following prior to ξ_4:

$$P\left(\xi_{z,4}|\alpha_1, \alpha_2\right) = \mathcal{N}\left(\xi_{z,4}\middle|\alpha_1, \alpha_2^{-1}\right) \tag{3-19}$$

where α_1 and α_2 are the a priori mean and precision, respectively. Although we expect that ξ_4 would be around 0-6, since we do not have strong prior information about it, we employed a hierarchical Bayesian approach and assign the following prior to α_1 and α_2:

$$P(\alpha_1|\lambda_2) = \mathcal{E}(\alpha_1|\lambda_2) \tag{3-20}$$

$$P(\alpha_2|\lambda_2) = \mathcal{E}(\alpha_2|\lambda_2) \tag{3-21}$$

where $\mathcal{E}(\cdot\,|\lambda)$ is the PDF of an exponential distribution with rate parameter λ, and λ_2 is 1. Since we believe that the original equations are reliable overall, we assign to ξ_5 a zero mean Gaussian prior,

$$P\left(\xi_{z,5}|\alpha_3\right) = \mathcal{N}\left(\xi_{z,5}\middle|0, \alpha_3^{-1}\right) \tag{3-22}$$

where α_3 is an a priori precision. Since we do not have much prior information about how much the heat loss should be adjusted by Eq. (3-6), we assign the following prior to α_3:

$$P(\alpha_3|\lambda_3) = \mathcal{E}(\alpha_3|\lambda_3) \tag{3-23}$$

Here, we set $\lambda_3 = 1$ since we do not expect that ξ_5 becomes very high, reflecting the fact that we trust the reliability of the original equations.

Figure 3.2 shows the relationship between the PMV value and the thermal load calculated by the original equations. Note that the PMV value of 0 means "neutral" and ±2 mean "warm/cool". We assign the following priors to $\boldsymbol{\mu}$ and σ:

$$P(\boldsymbol{\mu}_z|\boldsymbol{\lambda}_{\text{mean}}, \boldsymbol{\Lambda}_{\text{var}}) = \begin{cases} \mathcal{N}(\boldsymbol{\mu}_z|\boldsymbol{\lambda}_{\text{mean}}, \boldsymbol{\Lambda}_{\text{var}}), & \mu_{z,1} < \mu_{z,2} < \mu_{z,3} \\ 0, & \text{otherwise} \end{cases} \tag{3-24}$$

$$P(\sigma_z|\lambda_{10}, \lambda_{11}) = \text{Inv-Gamma}(\sigma_z|\lambda_{10}, \lambda_{11}) \tag{3-25}$$

where

$$\boldsymbol{\lambda}_{\text{mean}} = \begin{bmatrix} \lambda_4 \\ \lambda_5 \\ \lambda_6 \end{bmatrix} \tag{3-26}$$

$$\boldsymbol{\Lambda}_{\text{var}} = \begin{bmatrix} \lambda_7 & 0 & 0 \\ 0 & \lambda_8 & 0 \\ 0 & 0 & \lambda_9 \end{bmatrix} \tag{3-27}$$

and Inv-Gamma$(\cdot\,|\alpha, \beta)$ is a PDF of an inverse gamma distribution with shape parameter α and scale parameter β. Since the corresponding thermal loads to the PMV value of -2, 0, and 2 are around -35, 0, and 35, respectively, we set $\lambda_4 = -3.5$, $\lambda_5 = 0$, and $\lambda_6 = 3.5$. Since in our definition the thermal load represents the overall thermal stress, the thermal load should be close to 0 when an occupant is satisfied with the thermal conditions. Therefore, we set $\lambda_8 = 0.01$ so that μ_2 cannot be far from 0. On the contrary, we use wider priors for the others, i.e., $\lambda_7 = 1, \lambda_9 = 1, \lambda_{10} = 1, \lambda_{11} = 0.5$, as we do not have more specific knowledge about μ_1 and μ_3.

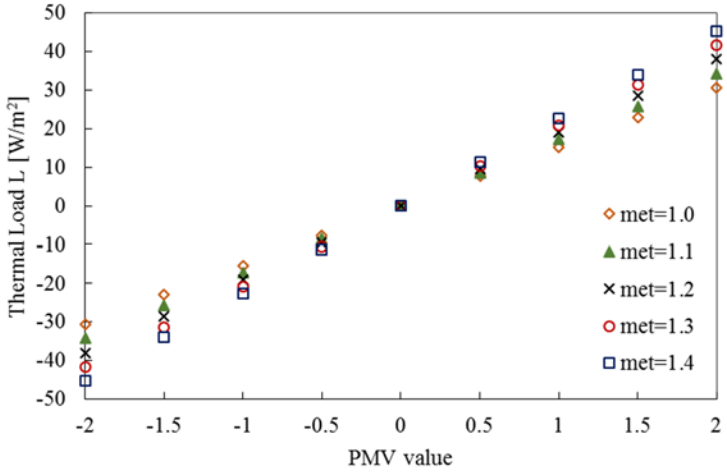

Figure 3.2. Relationship between the PMV value and the thermal load calculated by the original PMV equations

Finally, since we do not have any information about the hidden cluster value z, we assign to z a discrete uniform prior,

$$P(z_d|K) = \mathcal{U}\{z_d|1, K\} \tag{3-28}$$

where $\mathcal{U}$ is a PDF of a uniform random variable taking values in the set {1, … , K}.

Using Bayes rule, our posterior state of knowledge about the parameters and the hidden cluster value is given by:

$$\begin{aligned} &P(z_{1:D}, \boldsymbol{\xi}_{1:K}, \boldsymbol{\mu}_{1:K}, \sigma_{1:K}, \boldsymbol{\alpha}|\mathbf{y}_{1:D}, \mathbf{X}_{1:D}, \boldsymbol{\lambda}) \\ &\propto P(\mathbf{y}_{1:D}|\mathbf{X}_{1:D}, z_{1:D}, \boldsymbol{\xi}_{1:K}, \boldsymbol{\mu}_{1:K}, \sigma_{1:K}) P(z_{1:D}|K) P(\boldsymbol{\xi}_{1:K}|\boldsymbol{\alpha}, \boldsymbol{\lambda}) P(\boldsymbol{\mu}_{1:K}, \sigma_{1:K}|\boldsymbol{\lambda}) P(\boldsymbol{\alpha}|\boldsymbol{\lambda}) \end{aligned} \tag{3-29}$$

where $\boldsymbol{\alpha} = (\alpha_1, \alpha_2, \alpha_3)$, $\boldsymbol{\lambda} = (\lambda_1, \lambda_2, \lambda_3, \lambda_4, \lambda_5, \lambda_6, \lambda_7, \lambda_8, \lambda_9)$. Figure 3.3 shows the overall model structure using standard plate notation.

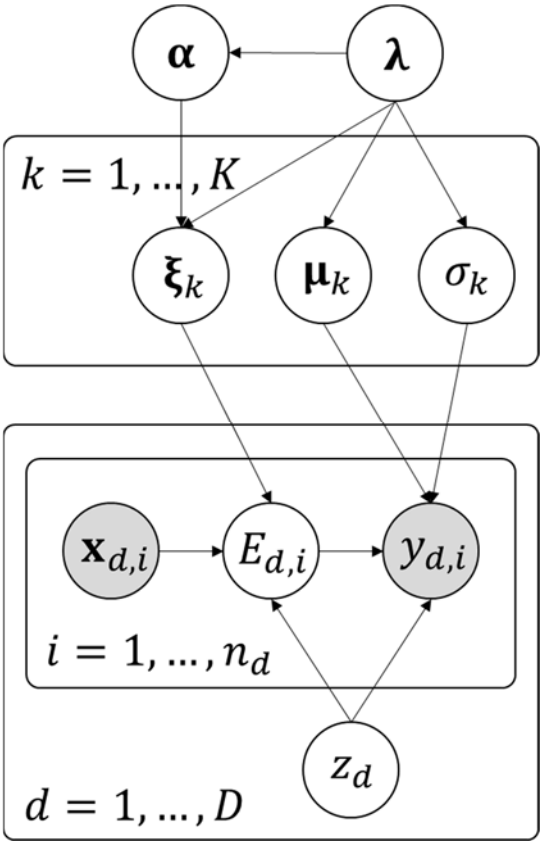

Figure 3.3. Plate notation of overall model structure

3.2.3 Training and sampling

In order to develop the model in fully Bayesian approach, the parameters and the hidden cluster values should be sampled from the posterior distribution. However, since the posterior

distribution is intractable analytically, we use sequential Monte Carlo (SMC) to sample from it, which is more efficient and effective than standard Markov chain Monte Carlo (MCMC) [79]. The addendum is that it also computes the model evidence (the normalization constant of the posterior) which can be used for Bayesian model selection (see Section 3.3.2). Moreover, SMC is parallelizable, a fact we exploit to reduce the training time by orders of magnitude. SMC approximates the posterior of the model parameters using a finite number of weighted samples (particles). This representation can be exploited to quantify the predictive uncertainty of our model induced by the limited number of observations. We implemented our model using the Python packages PySMC [80] and PyMC [81]. Table 3.1 shows SMC settings used in this study, which were selected because they provided consistent results in multiple trainings with reasonable computational cost.

Table 3.1. PySMC settings

The number of particles	3000
The number of MCMC steps per SMC step	20
The threshold of the effective sample size	0.50
The reduction of the effective sample size per SMC step	0.90
MCMC step method for continuous parameters	Random walk
MCMC step method for the hidden cluster values	Discrete random walk

3.3 Results using the general model

3.3.1 Verification with synthetic data

To verify that our methodology can indeed discover preference clusters, we first tested it on a synthetic dataset. We generated the synthetic dataset as follows. First, we assumed that there were three different clusters of people preferring cooler, middle, and warmer conditions. Second, to develop conditional probability distributions representing their preference patterns, three sets of parameter values were arbitrary defined as shown in Table 3.2. Figure 3.4 shows the probability distributions with respect to air temperature for the three clusters. To visualize the distributions in 2-D figures, the other variables were set as follows: MRT = air temperature, air velocity = 0.05 m/s, relative humidity = 50 %, met = 1.2, and clo = 0.6.

Table 3.2. Three different sets of parameters for the synthetic clusters

Parameter		Cooler cluster	Middle cluster	Warmer cluster
Cluster shared parameters	ξ_1	1	1	1
	ξ_2	1	1	1
	ξ_3	1	1	1
Cluster specific parameters	ξ_4	5	2.7	0
	ξ_5	0.2	0.3	0
	μ_1	-1.8	-1.5	-2
	μ_2	0	0	0
	μ_3	1.8	1.5	2
	σ	0.8	0.66	0.9

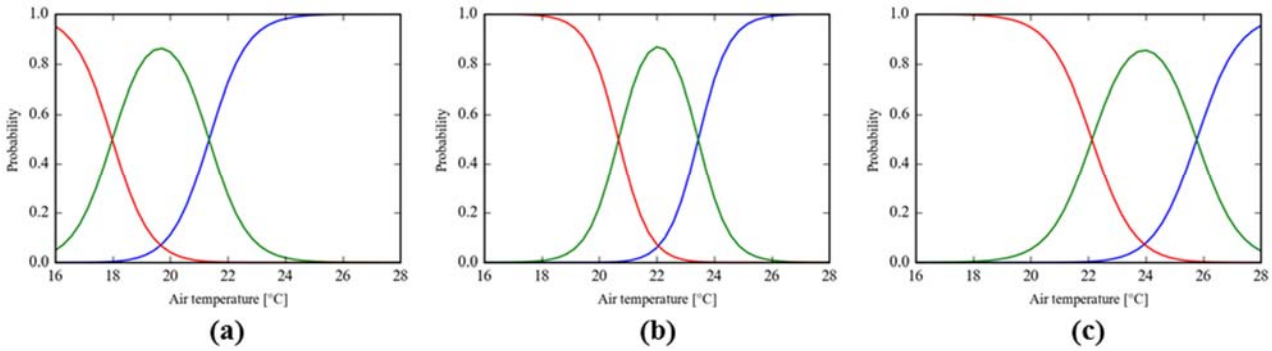

Figure 3.4. Discrete conditional probability distributions for the synthetic clusters (from left, clusters of people preferring cooler, middle, warmer conditions)

Then, 9 synthetic occupants were assigned to the clusters (i.e., three occupants per each cluster), and 900 synthetic preference votes were created with the following process:

- 900 data points were generated (sampled) from

$$P(\mathbf{x}|\boldsymbol{\beta}) = P(x_1|\boldsymbol{\beta}) \cdot P(x_2|\boldsymbol{\beta}) \cdot P(x_3|\boldsymbol{\beta}) \cdot P(x_4|\boldsymbol{\beta}) \cdot P(x_5|\boldsymbol{\beta}) \cdot P(x_6|\boldsymbol{\beta}) = \mathcal{U}(x_1|16,28) \cdot \mathcal{U}(x_2|16,28) \cdot \mathcal{U}(x_3|0.02,0.1) \cdot \mathcal{U}(x_4|20,80) \cdot \mathcal{U}(x_5|0.5,0.6) \cdot \mathcal{U}(x_6|1,1.2) \quad (3\text{-}30)$$

  where $\mathbf{x} = (x_1, x_2, \ldots, x_6)$ are the input variables (i.e., air temperature, mean radiant temperature, air velocity, relative humidity, clothing insulation, and metabolic rate).

- 100 data points were randomly assigned to each occupant.
- For each data point, a preference vote was generated (sampled) from the discrete conditional probability distribution of a cluster to which the occupant belonged (Figure 3.4).

In the model development stage, since the number of clusters in the dataset is unknown as well as the cluster value of each occupant, models having different numbers of clusters may be considered and compared. In this section, we developed and compared models having one, two, and three clusters, (i.e., $K = 1, 2, \text{and } 3$, respectively). Figure 3.5 shows the probability distribution of an occupant having each preference (i.e., "want warmer", "no change", "want cooler") with respect to air temperature. To visualize results in 2-D figures, the other variables were set as follows: MRT = air temperature, air velocity = 0.05 m/s, relative humidity = 50 %, met = 1.2, and clo = 0.6. The model uncertainty was quantified and visualized in the figure. Solid lines represent the median value of the probability (i.e., median model), and shaded areas represent the associated 95% credible intervals (i.e., 2.5- and 97.5-quantiles of the predictive distribution). Since we created the dataset with the probability distributions shown in Figure 3.4, the probability for "no change" class of this single cluster model is maximized around 22 °C. The maximum probability for "no change" class is only around 0.6 and the output probability distribution is quite flat, which are improper characteristics in terms of making concise preference predictions.

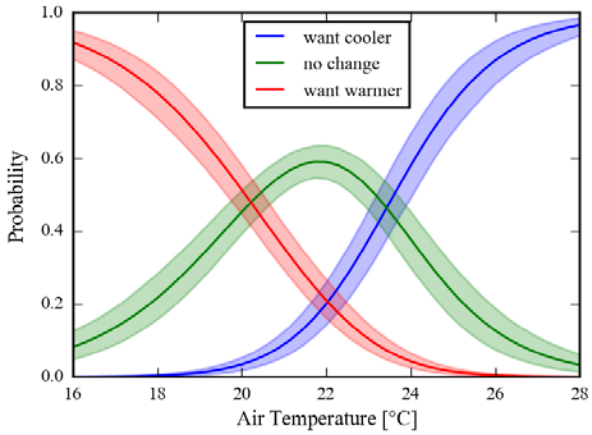

Figure 3.5. The probability distribution of an occupant's thermal preference with respect to air temperature calculated by the single-cluster model

Figure 3.6 shows the probability distributions calculated by the model having 2 clusters (i.e., K=2). Each figure represents a sub-model for each cluster. In order to visualize the results, a label switching problem was resolved before drawing figures, which arises when solving a clustering problem using mixture models in Bayesian approach caused by non-indefinability [82,83]. Details are discussed in Appendix A. Occupants having the first probability distribution in Figure 3.4(a) were grouped into one cluster, and the rest were grouped into another cluster, automatically.

Therefore, Figure 3.6(a) is similar to Figure 3.4(a), and Figure 3.6(b) looks like a mixture of Figure 3.4(b) and Figure 3.4(c). Figure 3.7 shows SMC samples for the parameters. The green histogram and dots are samples for the first cluster and the blue ones for the second cluster –as shown in the figure, they are clearly distinguished. This provides evidence that there is a high probability that there are two or more clusters of thermal preference for the people in the dataset.

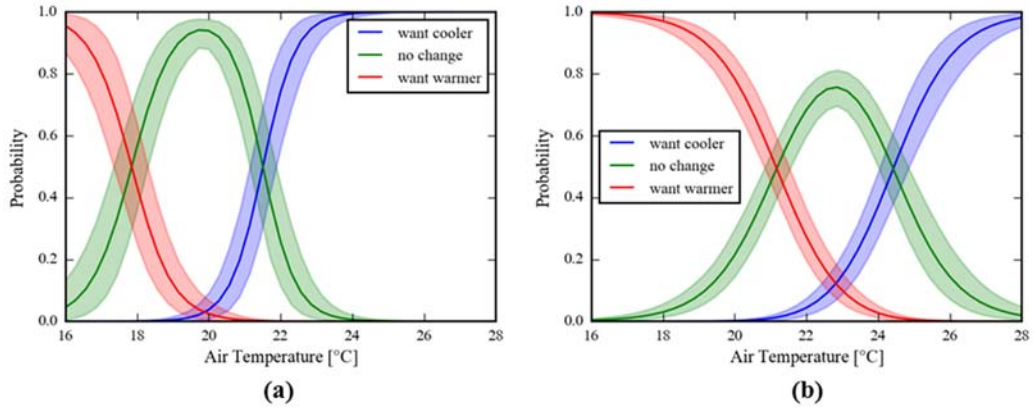

Figure 3.6. The probability distributions of an occupant's thermal preference with respect to air temperature calculated by the model having two clusters

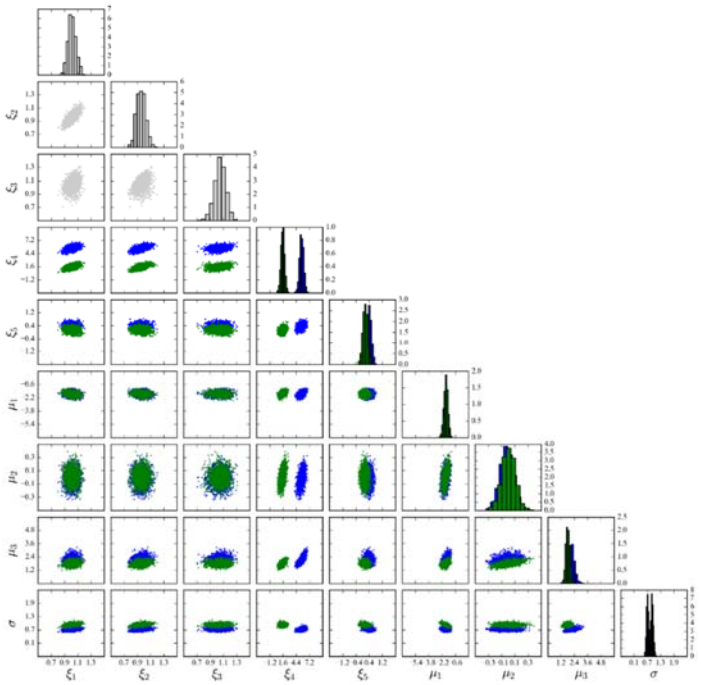

Figure 3.7. SMC samples for parameters in case of the model having two clusters

Figure 3.8 shows the probability distributions calculated by the model having 3 clusters (i.e., $K = 3$). Note that the dotted lines are the original probability distributions shown in Figure 3.4. The model discovered all the 3 clusters in the synthetic dataset, and the calculated probability distributions are also close to the originals. The samples (Figure 3.9) show that the model found 3 distinctive clusters of people. The samples are very close to the original parameters (Table 3.2) marked as triangles in the figure. If the number of data points goes to infinity, the model uncertainty shown in Figure 3.8 will be collapsed and the samples in Figure 3.9 will be concentrated at the triangles.

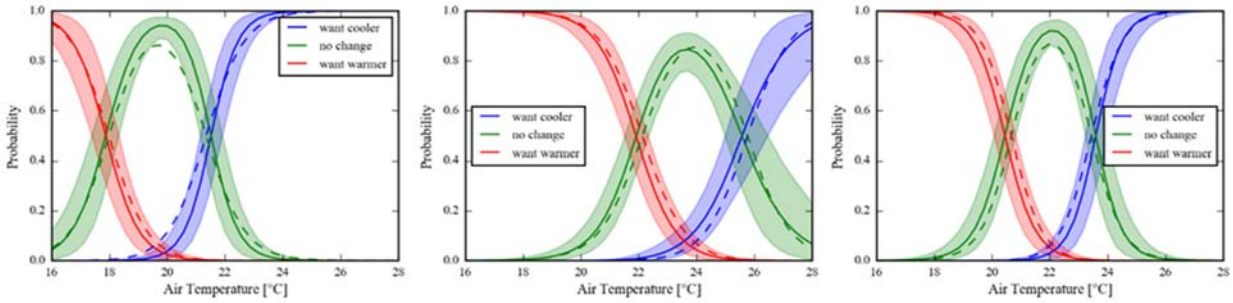

Figure 3.8. The probability distributions of an occupant's thermal preference with respect to air temperature calculated by the model having three clusters

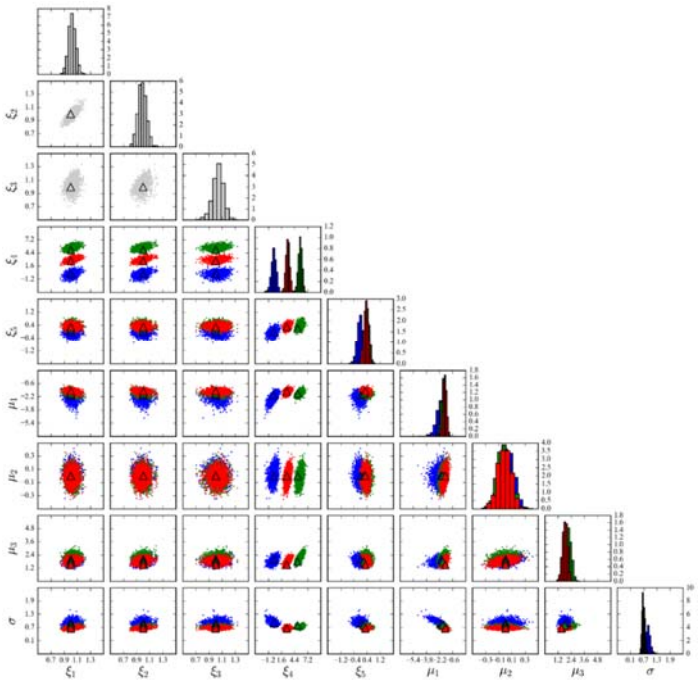

Figure 3.9. SMC samples for parameters in case of the model having three clusters

Figure 3.10 shows the probability of each occupant being in cluster k (i.e., $P(z_d = k|\mathbf{y}_{1:D}, \mathbf{X}_{1:D}, \boldsymbol{\xi}_{1:K}, \boldsymbol{\mu}_{1:K}, \sigma_{1:K}),\ k = 1, 2, 3$). The color of each circle corresponds to the probability, i.e., dark red denotes high probability and dark blue means low probability. The probabilities were close to either 0 or 1, which means that each occupant is clearly classified into one of the clusters, in this synthetic case. The model correctly found the cluster values originally assigned to the occupants when we generated the dataset.

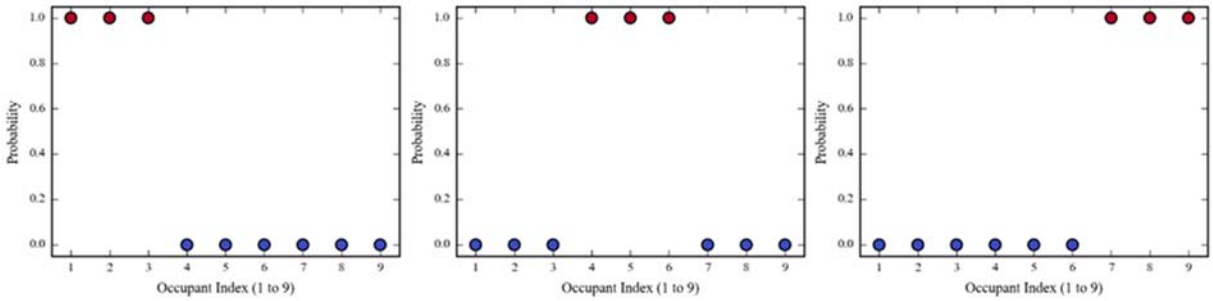

Figure 3.10. The probability of each occupant belonging to cluster k
(i.e., $P(z_d = k|\mathbf{y}_{1:D}, \mathbf{X}_{1:D}, \boldsymbol{\xi}_{1:K}, \boldsymbol{\mu}_{1:K}, \sigma_{1:K}), k = 1,2,3$))

3.3.2 The optimal number of clusters

The optimal number of clusters (K) is not known a priori. To identify it, we follow two different approaches. The first one is based on Bayesian model selection [77], which includes training all possible k-cluster models and subsequently comparing their model evidence to each other. The second one involves augmenting the model by assigning a Dirichlet process (DP) prior [84,85] over the prior probability measures on the parameter space. The DP induces a posterior probability on each cluster being active (theoretically allowing for an infinite number of possible clusters) and low probability clusters are neglected. Bayesian model selection is easy to implement when the posterior is sampled by SMC, but it is computationally expensive because of the need to train all k-cluster models. Even though the DP-based method is harder to understand, it is easy to implement as a natural extension of our methodology and it runs at a fraction of the time. See Appendix B for the details of the methods.

To test that the two methods do discover the right number of clusters, we applied them to the synthetic case. Figure 3.11(a) shows the logarithm of the model evidence with respect to the number of clusters in a model. The figure represents that the optimal number of clusters is 3 since the Bayes factor between the models having 2 and 3 clusters is greater than 100, which can be

interpreted as the 3-cluster model is decisively better than the 2-cluster model. The figure also shows that models having more than 3 clusters are not better than the 3-cluster model since the models have unnecessary parameters. Figure 3.11(b) shows that the optimal number of clusters based on the Dirichlet process is also 3. Only three clusters have significantly high π_k's (which can be interpreted as the probability of cluster k being active) compared to others. Since the synthetic data was generated from the three different probability distributions, it can be concluded that both methods accurately predict the optimal number of clusters.

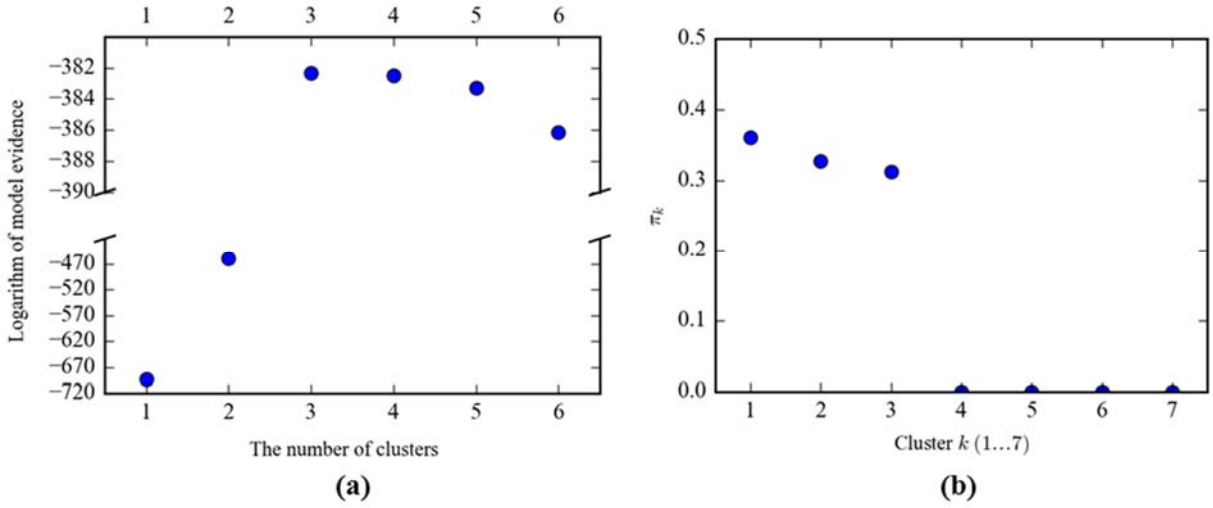

Figure 3.11. Results showing the optimal number of clusters. (a) The logarithm of the model evidence with respect to the number of clusters in a model; (b) π_k's inferred by Dirichlet process.

3.3.3 Modeling results with a large dataset

In order to develop the general model based on real world data, we used a subset of the ASHRAE RP-884 database [5], which was collected from HVAC conditioned office buildings in North America. Only people who voted more than 3 times were included in our training dataset. The number of observations in the training dataset is 1712, and the number of people is 259. Figure 3.12 shows distributions of input variables, and Figure 3.13 shows the distribution of the output variable with respect to air temperature in the training dataset. Since the data was collected from conditioned office buildings, variations in the data are limited, complicating the process of developing models which cover a wide range of conditions or having complex model structures – this is discussed later in Section 3.5.

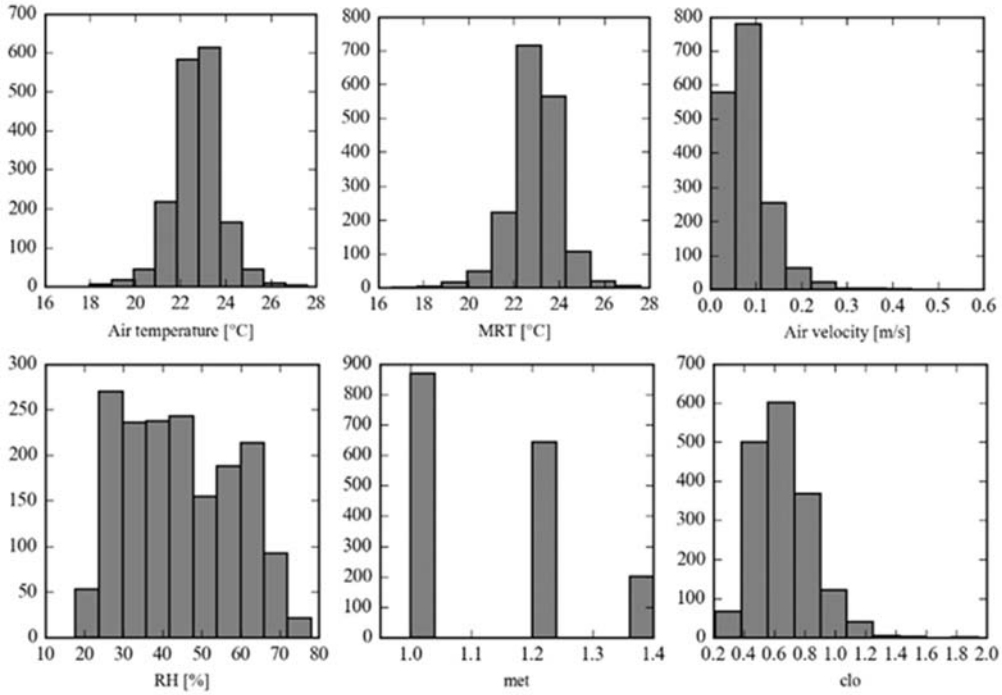

Figure 3.12. Distribution of input variables in the training dataset

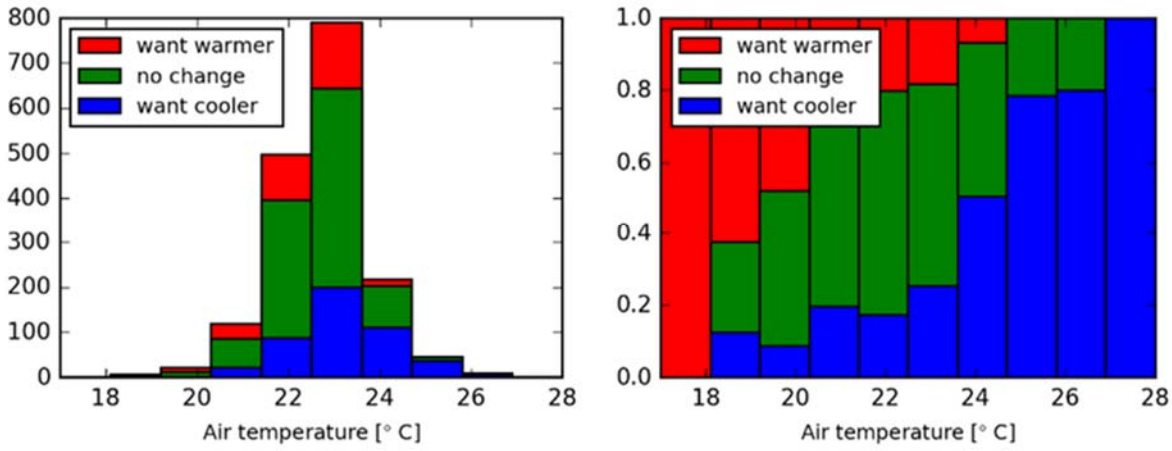

Figure 3.13. Distribution of output variable in the training dataset with respect to air temperature (left: normalized stacked histogram; right: 100% stacked bar chart)

Figure 3.14 shows the optimal number of clusters in the training dataset with the general model structure. According to the model evidence comparison (Figure 3.14(a)), the model having 5 clusters is decisively better than the model having 4 clusters. Again, according to the π_k's inferred by Dirichlet process, since only five clusters have meaningful π_k's, it could be concluded that the optimal number of clusters is five.

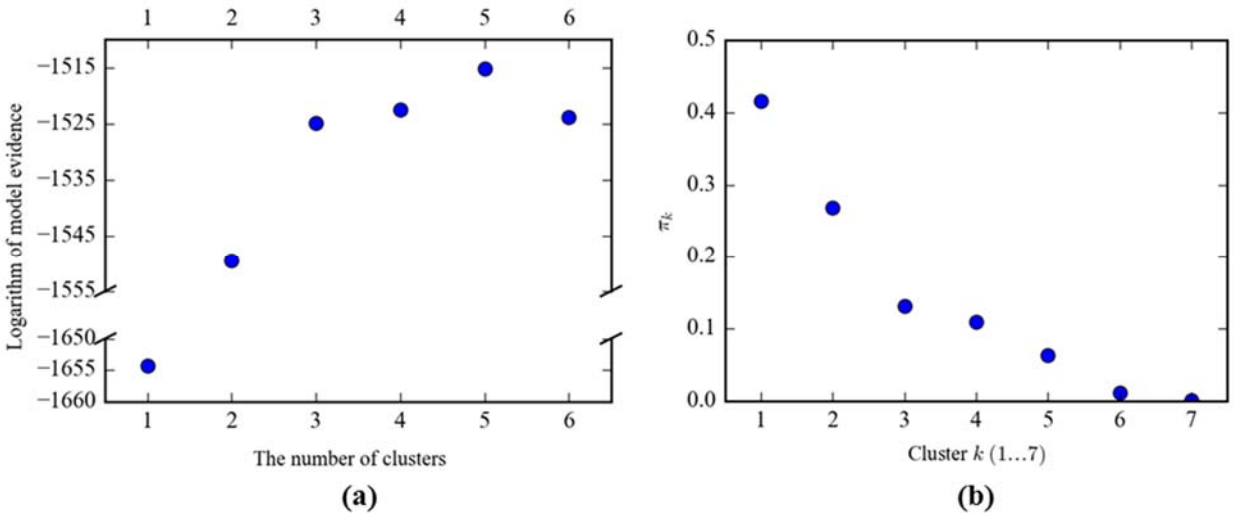

Figure 3.14. Results showing the optimal number of clusters. (a) The logarithm of the model evidence with respect to the number of clusters in a model. (b) π_k's inferred by Dirichlet process.

Figure 3.15(a) shows the probability distributions with respect to air temperature, calculated with sub-models for the 5 clusters. Note that we used the model structure explained in section 3.2.1. In order to visualize results in 2-D figures, the other variables were set as follows: MRT = air temperature, air velocity = 0.05 m/s, relative humidity = 50 %, met = 1.2, and clo = 0.6.

Clusters 1 and 3 can be interpreted as groups of people who preferred cooler and warmer conditions, respectively. Cluster 5 would be a group of people who were satisfied with a wider range of thermal conditions and less sensitive to thermal variations. Cluster 2 can be interpreted as a group of people with two characteristics: (i) preferred cooler conditions and (ii) answered both "want cooler" and "no change" votes (i.e., contradicting votes) under similar conditions. The small differences between the green and blue lines over the whole range represent the second characteristic. The contradicting votes might be caused by occupants' variability. However, it is plausible that conditions perceived as similar were actually quite different. There would be two possible reasons regarding this issue. First, because of inaccurate measurement of input values, actually different conditions might be recorded as similar conditions. For example, the metabolic rate in the training dataset has only three values (Figure 3.12) determined by a table in ASHRAE Standard 55 [7]. In other words, many different metabolic rates were recorded as the same value, and consequently, it looks as if occupants made contradicting votes with similar conditions. Another reason could be that unmeasured factors (e.g., time of the day, occupancy dynamics) might have significantly affected the occupants, resulting in contradicting votes. At this point, our

model cannot take into account the parameters discussed in these two cases -this is further elaborated in Section 3.5. Cluster 4 is the opposite case of cluster 2.

Figure 3.15 (b) shows the probability of each occupant belonging to each cluster. As mentioned earlier, each circle represents the probability for each occupant, i.e., there are 259 circles in each figure. Therefore, if the probabilities for one occupant in each figure are summed up, the total should be 1. Although some occupants were clearly classified into one cluster, i.e., significantly high probability in one figure and low probabilities in other figures, unlike the synthetic data case, some occupants were not clearly classified. The reasons could be that: (i) an occupant may be in between multiple clusters and (ii) data from an occupant may not be adequate for the classification. Their thermal preference can be explained by mixture of multiple sub-models. The figure shows that every cluster includes a portion of the population with non-negligible probability, meaning that all the sub-models are important to explain the thermal preferences of the whole population.

High model uncertainty, represented as the shaded areas around solid lines in Figure 3.15 (a), is usually caused by limited data in the training dataset. For every cluster, less data in both lower and higher temperature ranges was available than respective data in middle temperature range (see Figure 3.12); therefore, the width of the shaded areas in these ranges (i.e., uncertainty) is broader. Figure 3.15 (a) also shows that the sub-model for cluster 5 has higher model uncertainty than the rest. The reason is that the number of people belonging to cluster 5 is relatively small (Figure 3.15 (b)), which means that less data was used to develop the sub-model. The model uncertainty would decrease if more data is added in the training dataset.

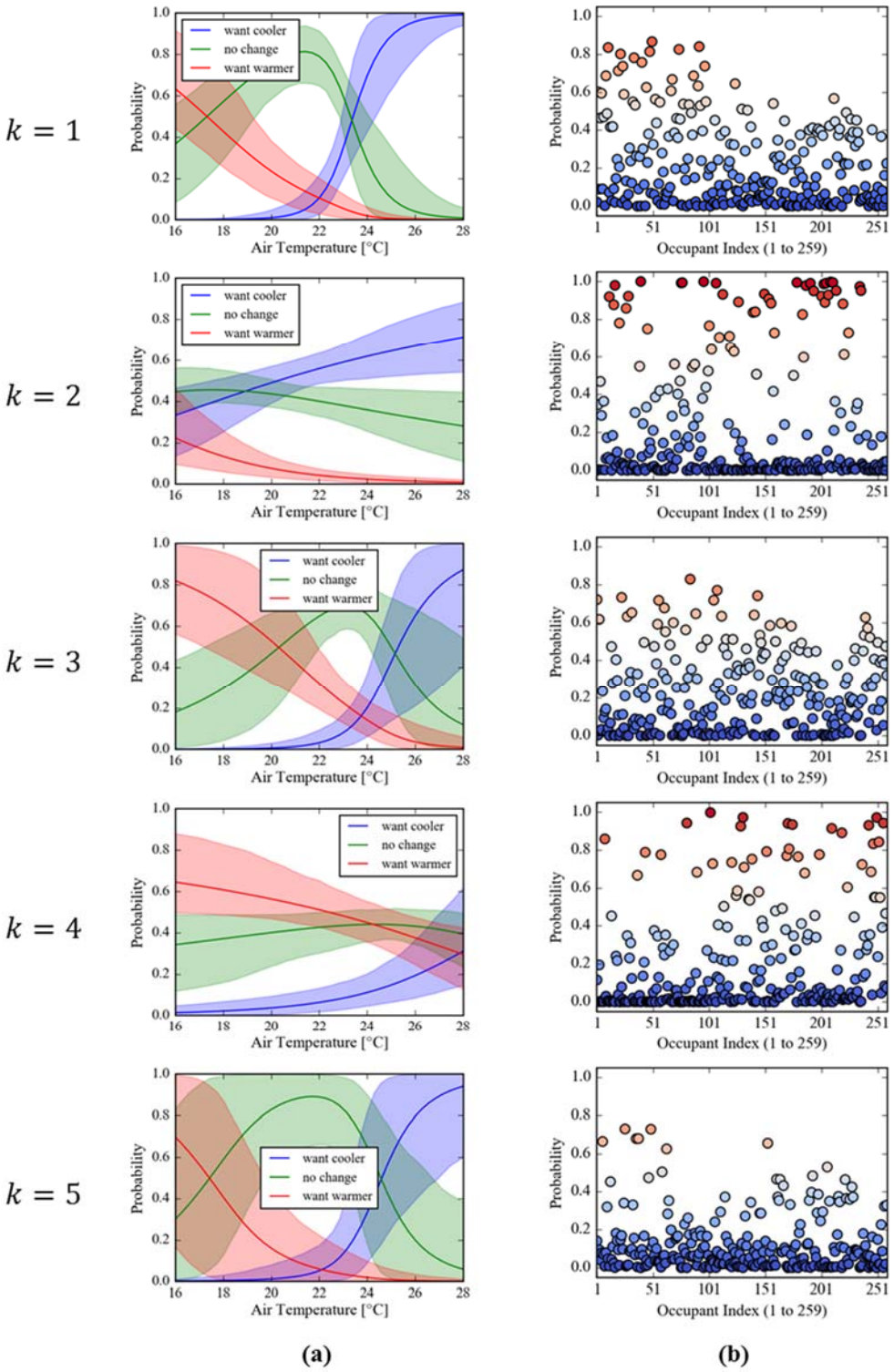

Figure 3.15. (a) The probability distributions calculated with sub-models for the 5 clusters, and (b) the probability of each occupant belongs to cluster k. The displayed probability distributions were calculated with the following settings: MRT = air temperature, air velocity = 0.05 m/s, relative humidity = 50 %, met = 1.2, and clo = 0.6.

3.4 The personal preference profiles: learning the thermal preference of individual occupants

3.4.1 Learning methodology

By using the general model for the whole population which has multiple sub-models, the thermal preference of individual occupants can be learned accurately and efficiently. Note that learning includes inferring an occupant's cluster value (i.e., personal thermal preference characteristic, z_{new}) and predicting the occupant's thermal preference under certain conditions. First, the ideal way to infer a new occupant's cluster value is re-estimating all parameters and hidden variables (i.e., $z_{\text{new}}, z_{1:D}, \boldsymbol{\mu}_{1:K}, \sigma_{1:K}, \boldsymbol{\xi}_{1:K}$) with both the old data (i.e., $\mathbf{y}_{1:D}, \mathbf{X}_{1:D}$) and new data collected from the specific occupant (i.e., $\mathbf{y}_{\text{new}}, \mathbf{X}_{\text{new}}$) as:

$$P(z_{\text{new}}|\mathbf{y}_{\text{new}}, \mathbf{X}_{\text{new}}, \mathbf{y}_{1:D}, \mathbf{X}_{1:D}) = \int \sum_{z_{1:D}} P(z_{\text{new}}, z_{1:D}, \boldsymbol{\theta}|\mathbf{y}_{\text{new}}, \mathbf{X}_{\text{new}}, \mathbf{y}_{1:D}, \mathbf{X}_{1:D})\, d\boldsymbol{\theta} \tag{3-31}$$

where $\boldsymbol{\theta} = (\boldsymbol{\mu}_{1:K}, \sigma_{1:K}, \boldsymbol{\xi}_{1:K})$. However, since this re-estimation requires heavy computational cost, this method is impractical for implementation in real buildings. Therefore, we introduce an assumption: the parameters and hidden variables for people in the old data (i.e., $z_{1:D}, \boldsymbol{\theta}$) are independent of new data (i.e., $\mathbf{y}_{\text{new}}, \mathbf{X}_{\text{new}}$), to make the inference process feasible. This is a reasonable assumption since the size of newly added data (i.e., $\mathbf{y}_{\text{new}}, \mathbf{X}_{\text{new}}$) is much smaller than the old data (i.e., $\mathbf{y}_{1:D}, \mathbf{X}_{1:D}$) and therefore, even if the parameters were re-estimated, they would not change significantly. Based on this assumption, Eq. (3-31) can be factorized as follows:

$$\begin{aligned} &\int \sum_{z_{1:D}} P(z_{\text{new}}, z_{1:D}, \boldsymbol{\theta}|\mathbf{y}_{\text{new}}, \mathbf{X}_{\text{new}}, \mathbf{y}_{1:D}, \mathbf{X}_{1:D})\, d\boldsymbol{\theta} \\ &\qquad = \frac{1}{C_1} \int \sum_{z_{1:D}} P(\mathbf{y}_{\text{new}}|\mathbf{X}_{\text{new}}, \boldsymbol{\theta}, z_{\text{new}}) P(z_{\text{new}}) P(z_{1:D}, \boldsymbol{\theta}|\mathbf{y}_{1:D}, \mathbf{X}_{1:D})\, d\boldsymbol{\theta} \end{aligned} \tag{3-32}$$

The first term, $P(\mathbf{y}_{\text{new}}|\mathbf{x}_{\text{new}}, \boldsymbol{\theta}, z_{\text{new}})$, in the right hand side is the data likelihood; the second term, $P(z_{\text{new}})$, is the prior over the occupant's cluster value z_{new}; and the last term is the parameters and hidden variables for people in the old data estimated with Eq. (3-29). Note that $P(z_{1:D}, \boldsymbol{\theta}|\mathbf{y}_{1:D}, \mathbf{X}_{1:D})$ was computed with SMC using particle approximation when developing the general model, and the particles themselves represent the probability. Therefore, with the particles, Eq. (3-32) can be efficiently computed.

Similarly, with the aforementioned assumption, predicting the thermal preference of a new occupant (i.e., y_{p}) under certain conditions (i.e., $\mathbf{x}_{\mathrm{p}}$) can be computed as:

$$
\begin{aligned}
&P\left(y_{\mathrm{p}}=j\middle|\mathbf{x}_{\mathrm{p}},\mathbf{y}_{\mathrm{new}},\mathbf{X}_{\mathrm{new}},\mathbf{y}_{1:D},\mathbf{X}_{1:D}\right), \qquad j=0,1,2\\
&=\int\sum_{z_{\mathrm{new}}}\sum_{z_{1:D}}P\left(y_{\mathrm{p}}=j\middle|\mathbf{x}_{\mathrm{p}},\mathbf{y}_{\mathrm{new}},\mathbf{X}_{\mathrm{new}},\mathbf{y}_{1:D},\mathbf{X}_{1:D},z_{1:D},z_{\mathrm{new}},\boldsymbol{\theta}\right)P(z_{1:D},z_{\mathrm{new}},\boldsymbol{\theta}|\mathbf{y}_{\mathrm{new}},\mathbf{X}_{\mathrm{new}},\mathbf{y}_{1:D},\mathbf{X}_{1:D})\,d\boldsymbol{\theta}\\
&\approx\frac{1}{C_2}\int\sum_{z_{\mathrm{new}}}\sum_{z_{1:D}}P\left(y_{\mathrm{p}}=j\middle|\mathbf{x}_{\mathrm{p}},z_{\mathrm{new}},\boldsymbol{\theta}\right)P(\mathbf{y}_{\mathrm{new}}|\mathbf{X}_{\mathrm{new}},\boldsymbol{\theta},z_{\mathrm{new}})P(z_{\mathrm{new}})P(z_{1:D},\boldsymbol{\theta}|\mathbf{y}_{1:D},\mathbf{X}_{1:D})\,d\boldsymbol{\theta}
\end{aligned}
\tag{3-33}
$$

See Appendix C for the derivation of the factorization in Eq. (3-32) and the computation of Eq. (3-32) and Eq. (3-33). In this work, we use discrete uniform prior for $P(z_{\mathrm{new}})$ to ensure consistency with Eq. (3-28). However, the Dirichlet process prior model discussed in Appendix B gave us the information, $P(z_{\mathrm{new}})$, since we estimated $P(z|\boldsymbol{\nu})$ according to Eq. (B-9). In other words, we could use the inference result from Dirichlet process prior model to assign a reasonable prior to $P(z_{\mathrm{new}})$. Since this needs further investigation, the Dirichlet process prior model is exploited only for discovering the optimal number of clusters.

3.4.2 Implementation and evaluation

11 new occupants in the ASHRAE dataset, who voted more than 10 times but were not included in the training dataset, were selected to validate our method. 8 samples of each occupant were used as new data (i.e., $\mathbf{y}_{\mathrm{new}}$, $\mathbf{X}_{\mathrm{new}}$) for learning each occupant (i.e., training dataset), and the other samples were used for validation (i.e., validation dataset) discussed consequently. Figure 3.16 shows the probability of each occupant belonging to each cluster (i.e., $P(z_{\mathrm{new}}|\mathbf{y}_{\mathrm{new}},\mathbf{X}_{\mathrm{new}},\mathbf{y}_{1:D},\mathbf{X}_{1:D})$) and the probability of their predicted preferences under various conditions (called profile in Daum [46]), inferred using the equations presented in Section 3.4.1 and the general model with 5 clusters (results for 9 occupants are shown). To visualize results in 2-D figures, the other variables were set as follows: MRT = air temperature, air velocity = 0.05 m/s, relative humidity = 50 %, met = 1.2, and clo = 0.6. Since the profiles were developed with only 8 observations, they may not represent final estimations but they are all different from each other in accordance with our hypothesis.

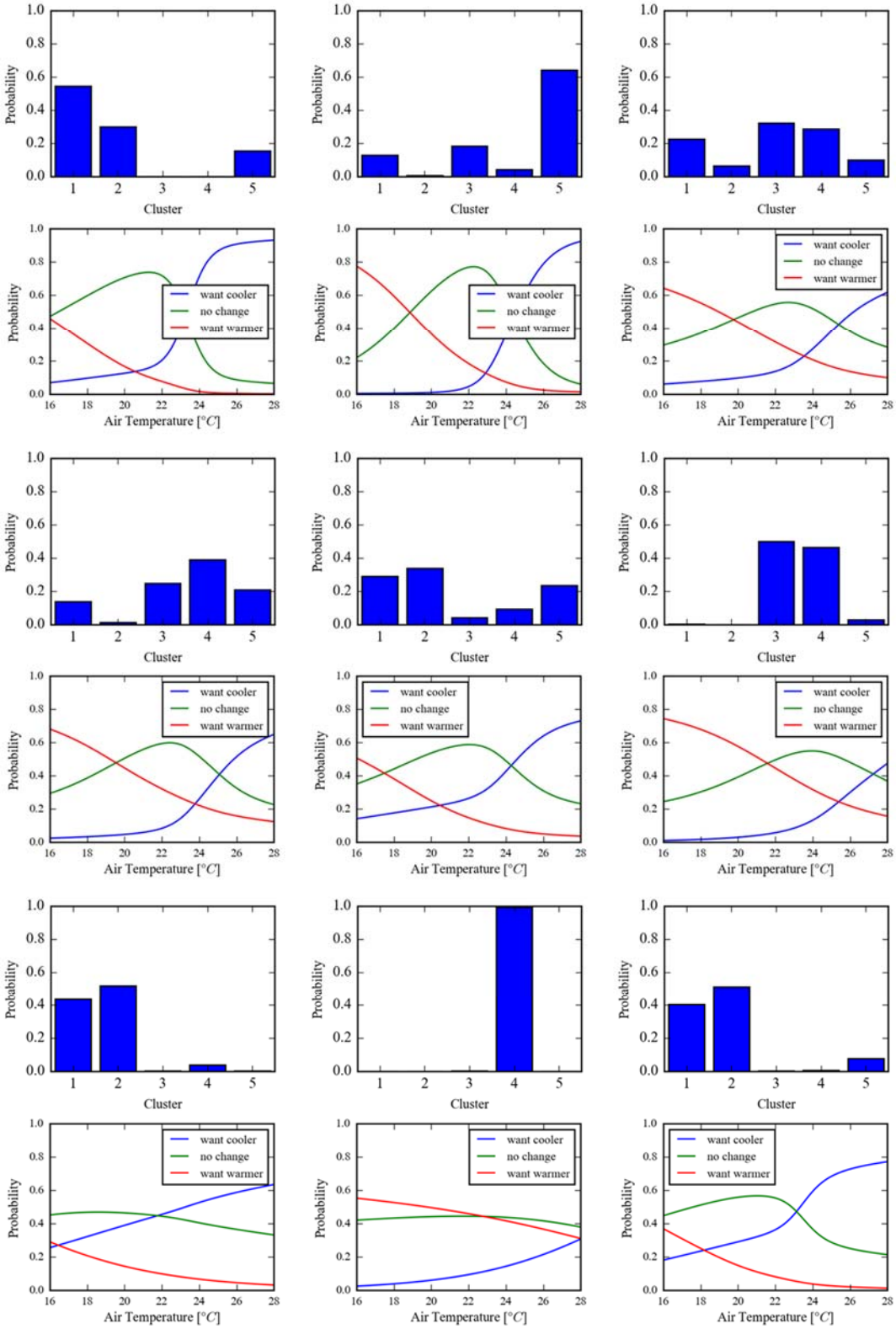

Figure 3.16. The probability of each new occupant belonging to each cluster, $P(z_{\text{new}}|\mathbf{y}_{\text{new}}, \mathbf{X}_{\text{new}}, \mathbf{y}_{1:D}, \mathbf{X}_{1:D})$ and the corresponding thermal preference profiles

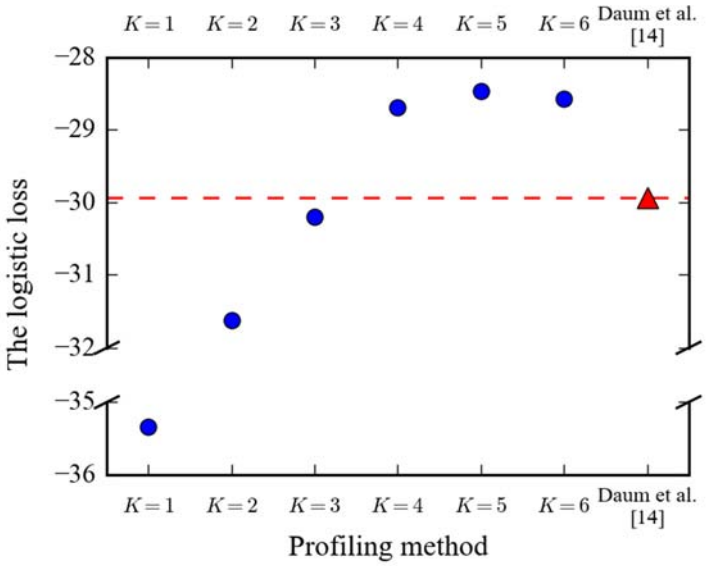

Figure 3.17. The logistic loss over the validation dataset with respect to the profiling method

Although unique personal profiles were developed, this does not guarantee the effectiveness of the overall method in this study. Thus, the prediction performance of the personal preference profiles over the validation dataset was calculated. Since profile outputs are not deterministic but probabilistic, the logistic loss ($logloss$) was used as a measure for the prediction performance:

$$logloss = \sum_{d=1}^{11} \sum_{i=1}^{n_d} \log P\left(y_{\mathrm{p},d,i} = y_{\mathrm{val},d,i} \middle| \mathbf{x}_{\mathrm{val},d,i}, \mathbf{y}_{\mathrm{new},d}, \mathbf{X}_{\mathrm{new},d}, \mathbf{y}_{1:D}, \mathbf{X}_{1:D}\right) \tag{3-34}$$

where $\mathbf{y}_{\mathrm{new},d} = \left(y_{\mathrm{new},d,1}, y_{\mathrm{new},d,2}, \dots, y_{\mathrm{new},d,8}\right)$ and $\mathbf{X}_{\mathrm{new},d} = \left\{\mathbf{x}_{\mathrm{new},d,1}, \mathbf{x}_{\mathrm{new},d,2}, \dots, \mathbf{x}_{\mathrm{new},d,8}\right\}$ are the observed thermal preferences and input variables in the training dataset from new occupant d, respectively, and $\left(y_{\mathrm{val},d,1}, y_{\mathrm{val},d,2}, \dots, y_{\mathrm{val},d,n_d}\right)$ and $\left\{\mathbf{x}_{\mathrm{val},d,1}, \mathbf{x}_{\mathrm{val},d,2}, \dots, \mathbf{x}_{\mathrm{val},d,n_d}\right\}$ are the observed thermal preferences and input variables in the validation dataset from new occupant d. However, since the logistic loss does not show whether the prediction performance is good or not by itself, the logistic loss of one model should be compared to that of another model. In this study, another set of personal profiles, based on the method presented in Daum et al. [46], i.e. with data from each individual occupant, was also developed and used for comparison. Figure 3.17 shows the logistic loss over the validation dataset with respect to each profiling method. Blue circles are the logistic losses of profiles developed with the general models having 2, 3, 4, 5, and 6 clusters, respectively. As expected, the logistic loss is maximized with the general model having the optimal number of clusters. The red triangle represents the logistic loss of profiles developed with Daum's

method [46]. Even though the general model takes into account more input variables, this result shows that the method developed in this study provides reliable preference profiles with a relatively small dataset collected from each occupant. This is a notable benefit since collecting preference feedback from occupants in real buildings is challenging.

3.5 Discussion

3.5.1 Limitations and extension of method to other data sets and dynamic conditions

In order to ensure the reliability of model predictions, it is suggested that data used for developing the model is representative of conditions for which the model would be used later. In this study, the final goal is delivering thermal comfort to occupants in real building offices. Therefore, the possible indoor conditions and HVAC control strategies which will be used with the preference profiles should be considered in this inference (model training) stage. Delivering thermal comfort to occupants who prefer different conditions only by controlling air temperature may be difficult since air temperature at one location cannot be independent from air temperature next to the location, especially in open-plan offices. A possible solution is to control other factors (e.g., local air velocity or local radiant conditions) so that every occupant can be satisfied with the thermal conditions even if air temperature cannot be controlled independently [16]. However, the current general model was developed with a subset of the ASHRAE RP-884 database collected from HVAC conditioned buildings with standard HVAC systems, and therefore, the data distributions are quite narrow as discussed in Section 3.3.3. For example, the MRT is highly correlated with the air temperature, and the air velocity is always low. Therefore, the reliability of predictions made by the model for non-standard conditions (e.g., high air velocity, big difference between air temperature and MRT) is doubtful. Experiments specifically designed to collect data for overcoming the limitations of ASHRAE database should be conducted and the general model would be updated with such data in the future.

Some output probability distributions over preference classes of both the general model and personal profiles are relatively flat under typical environmental conditions. This is not an appropriate characteristic for making reliable predictions or for optimizing the system control based on the predictions. Human nature perhaps includes high aleatoric uncertainty with respect to thermal preferences, hard to predict with distinctive probability. In that case, flat profiles are

not wrong since they properly reflect the aleatoric uncertainty [86], however, this requires further investigation. In other words, there are many factors increasing the epistemic uncertainty of models and resulting in flat probability distributions, which can be remedied. Epistemic uncertainty increases when a model does not take into account important factors affecting the system. In this study, it was assumed that occupants' thermal preference was affected by the overall thermal stress and the personal thermal preference characteristic (Figure 3.1). However, previous studies have shown that local discomfort caused by a vertical air temperature difference between the feet and the head, an asymmetric radiant field, or by local convective cooling (draft), may significantly affect thermal comfort [39]. Therefore, local discomfort may be included in the general modeling framework to decrease the epistemic uncertainty. In addition, since the developed model calculates the thermal stress based on steady-state assumptions, it does not consider the dynamic nature of human thermal comfort [4,48,50] or adaptive thermal comfort concepts under transient and variable outside conditions [46–49]. Therefore, in future work, the model structure may be modified to account for such conditions.

3.5.2 Considering inaccurate/missing data in future predictions using the developed method

The epistemic uncertainty also increases when the data used to develop a model is not sufficiently accurate. As mentioned before, it is highly probable that measured values in the ASHRAE database, especially air velocity, clo and met, were not accurate enough. This problem could be resolved by incorporating this measurement process in the model. In other words, instead of assuming that the measured values are the real values, it may be assumed that the measured values were contaminated by some disturbance or noise in the model. The aforementioned solutions may increase the model complexity, and developing a complex model from scratch requires a large dataset which is almost impossible to collect as discussed in Section 3.2.1. However, thanks to the inherent advantages of Bayesian approach and recent research activities focused on thermal comfort, developing a model based on practical data collection in buildings becomes realistic. In future work conducted by the authors, data collected from heterogeneous sources (e.g., ASHRAE database, experiments specifically designed to overcome the limitations of the ASHRAE dataset, etc.) could be combined, different model structures could be compared, and hidden variables would be embedded to deal with missing data or for unobserved features.

Finally, another important question may be raised: Can we use such a complex model which requires multiple inputs even though some of these inputs may not be easily measured in real buildings? Actually, it may be difficult to measure clo, met, and air velocity in the real world. However, this does not mean that the model cannot make reliable predictions. For example, if clo value is not measured, it can be predicted by integrating the model out over clo values as shown in Eq. (3-35). If there is no information about clo values, then a flat prior would be used for $P(\text{clo})$.

$$P(y|\text{T}_{\text{air}}, \text{MRT}, \text{RH}, \text{Vel}, \text{met}, \boldsymbol{\theta}) = \int P(y|\text{T}_{\text{air}}, \text{MRT}, \text{RH}, \text{Vel}, \text{clo}, \text{met}, \boldsymbol{\theta}) P(\text{clo})\, d\text{clo} \qquad (3\text{-}35)$$

This calculation is nothing but the Bayes' sum rule, so it is a simple probability calculation and it does not require any further assumptions. Uncertainty in the prediction increases just as much as the unknown information. On the other hand, if we have any information about the unmeasured variable, the prediction would be less uncertain than a prediction made by a model which does not take into account the variable from the beginning. In the same example, if a model predicting clo value based on outdoor air temperature is introduced, the flat prior for $P(\text{clo})$ would be replaced with a probability distribution made with the model predicting clo value, and the prediction would be less uncertain than that made with flat prior. Therefore, the high complexity would not be a barrier in terms of implementation in real buildings, but actually provides a high degree of freedom to the user to modify the model. Moreover, the evolution of sensing and information technologies enables availability of more information, and the complex model is capable of using this information to make more reliable predictions [21,22,59,87]. In future work, prediction performance without direct measure of such variables would be evaluated and possible techniques to account for the missing information would be tested.

3.6 Chapter conclusions

In this Chapter, a new method for learning personalized thermal preferences was introduced. The approach starts from developing a general model that explains the thermal preference of occupants in a large dataset collected in actual office buildings. Different from existing approaches, we developed a generalized thermal preference model using a fully Bayesian approach that also considers a thermal preference characteristic as a hidden variable. The results show that there is a high probability of classifying multiple clusters of people with respect to their thermal preference characteristic. The optimal number of clusters was determined based on two methods: comparing

different models with the Bayesian model selection process or assigning a Dirichlet process prior. Both approaches were tested with a synthetic dataset and showed consistent results. Our algorithm was also evaluated with a subset of 259 office building occupants from the ASHRAE RP-884 database and it successfully discovered clusters of thermal preference with physical interpretation. Modeling results indicate that the five-cluster model is more promising than the single cluster model for explaining the thermal preference of the occupants, therefore, it is more suitable for learning and predicting thermal preferences of individual occupants. Note that the optimal number of clusters could be different with different model structures.

Personalized thermal preference profiles were subsequently inferred by a mixture of sub-models for each cluster with a set of probabilities and particle approximation. The method was validated with a subset of 11 new occupants from the subset of the ASHRAE RP-884 database for which personalized models were developed with improved accuracy and efficiency compared to methods for training individual occupant models. The method provided reliable predictions, with a relatively small dataset collected from each occupant, which constitutes a significant benefit for implementation of personalized thermal environments in actual buildings based on occupant feedback.

The methodology presented in this chapter demonstrates the advantages of the Bayesian formalism for developing personalized thermal preference profiles based on limited data. These include the way of taking into account a hidden variable, clustering occupants based on the hidden variable, selecting the optimal number of clusters, encoding of prior knowledge in a model, and the discussion of epistemic and aleatoric uncertainty in the performance analysis.

4. INFERENCE OF THERMAL PREFERENCE PROFILES FOR PERSONALIZED THERMAL ENVIRONMENTS

4.1 Overview

This chapter presents a Bayesian modeling approach for learning personalized comfort models in real buildings where clothing level, metabolic rate and air speed cannot be measured. To achieve this goal, the generalized model presented in Chapter 3 was revised (Section 4.2); hidden variables were introduced in personalized models (Section 4.3). Limitations and recommendations for future work are discussed in Section 4.4.

4.2 A new generalized thermal preferences model

4.2.1 Model structure

The new thermal preference model considers two important issues: (1) inaccurately measured or estimated values for some variables in the training data (i.e., subset of ASHRAE RP-884 database used to train the model); (2) limited variation of thermal conditions in the training data.

In the training data, there are three measured/estimated variables of questionable accuracy: air speed, metabolic rate, and clothing insulation level. Air speed (Spd) can vary locally inside office spaces –even if measured with accurate sensors near the occupant, measured values could be quite different from the actual values very close to the occupant skin (that actually affect thermal sensation). Metabolic rate (Met) and clothing insulation level (Clo) are quite difficult to measure, therefore researchers estimated these values based on results from previous studies (e.g., tables in ASHRAE Handbook Fundamentals [7]). However, the studies showed that the estimation included non-negligible error [88–91]. Adopting potentially inaccurate values for the above parameters and training a model based on these assumptions will result in problems: the model will interpret that the target system has high aleatoric uncertainty (i.e., randomness), although the uncertainty is epistemic (i.e., is due to inaccurate values). In other words, the model will misinterpret frequent contradicting preferences under similar thermal conditions as true, although the conditions assumed as similar were actually different. The importance of proper treatment of the measurement

error (a.k.a. error-in-variables) in statistical analyses and modelling have been recognized [92–94]. Carroll et.al. [92] explained that there are "Triple Whammy of Measurement Error": 1) measurement error makes the parameter estimates biased; 2) it leads to a loss of power for detecting signals; 3) it masks important features of the data, making graphical model inspection difficult. Muff [94] showed how measurement error can be handled naturally with Bayesian approach.

To resolve this problem, the new model structure encodes that: "the true values for these three variables (Met, Clo and Spd) are uncertain" in the model. The revised structure is shown in Figure 4.1, where, for each occupant (d) and observation (i), the three colored nodes ($Spd^{obs}, Met^{obs}, Clo^{obs}$) indicate recorded values for the air speed, metabolic rate and clothing insulation level in the training data, and the three white nodes, (Spd, Met, Clo) represent the corresponding true values of which we are uncertain.

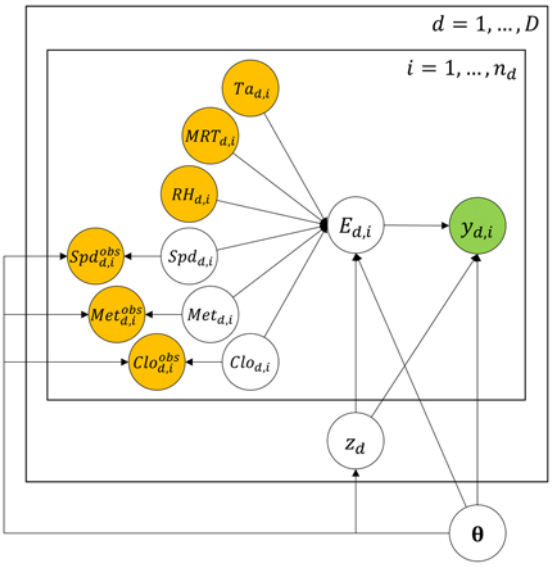

Figure 4.1. Graphical representation of the joint probability for the new generalized thermal preference model.

Following this logic, we need a prior and a likelihood function for each of these three variables. We assume that the data distributions of $Spd^{obs}, Met^{obs}, Clo^{obs}$ in the training data follow the distribution of Spd, Met, Clo to some extent. Based on the data distributions of Figure 3.12, three lognormal distributions are applied to Spd, Met, Clo as a prior, plotted in Figure 4.2:

$$p\left(Spd_{d,i}\middle|\mu_{Spd_p}, \sigma^2_{Spd_p}\right) = \text{Lognormal}\left(Spd_{d,i}\middle|\mu_{Spd_p}, \sigma^2_{Spd_p}\right) \quad (4\text{-}1)$$

$$p\left(Clo_{d,i}\middle|\mu_{Clo_p}, \sigma^2_{Clo_p}\right) = \text{Lognormal}\left(Clo_{d,i}\middle|\mu_{Clo_p}, \sigma^2_{Clo_p}\right) \quad (4\text{-}2)$$

$$p\left(Met_{d,i}\middle|\mu_{Met_p},\sigma^2_{Met_p},\omega_{Met_p}\right)=\text{Lognormal}\left(Met_{d,i}-\omega_{Met_p}\middle|\mu_{Met_p},\sigma^2_{Met_p}\right) \quad (4\text{-}3)$$

where $\text{Lognormal}(\cdot\,|\mu,\sigma^2)$ is the probability density function (PDF) of a lognormal distribution with parameters μ and σ that are the mean and standard deviation of the variable's natural logarithm, respectively: $\mu_{Spd_p}=-2.690$, $\sigma^2_{Spd_p}=0.451$, $\mu_{Met_p}=-0.871$, $\sigma^2_{Met_p}=0.111$, $\omega_{Met_p}=0.7$, $\mu_{Clo_p}=-0.431$, $\sigma^2_{Clo_p}=0.102$.

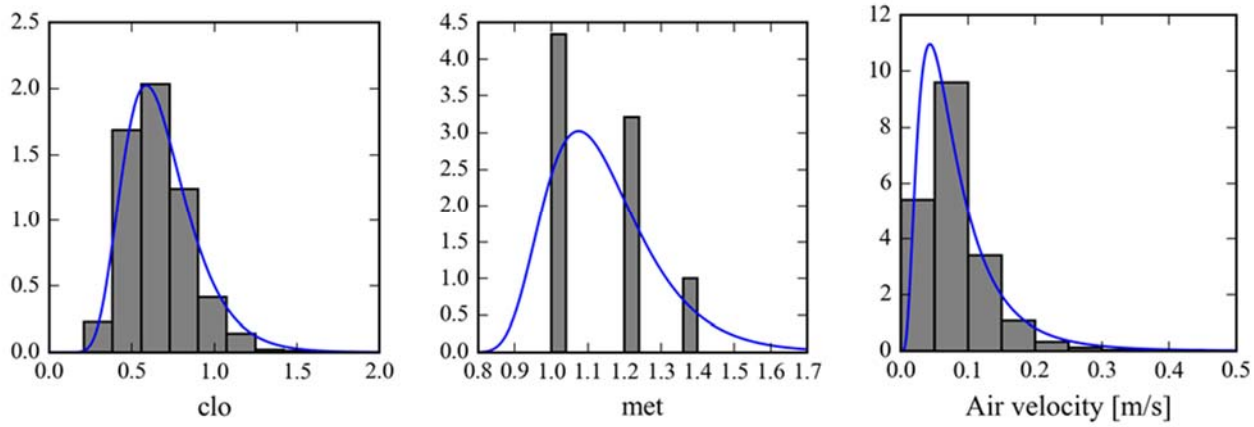

Figure 4.2. Data distributions of three variables (histograms) and probability density functions used to represent the data distributions (blue curves) for clothing insulation, metabolic rate and air speed.

For the air speed and the clothing insulation level, we assume that there were Gaussian noises in measurement and use the following likelihood:

$$p\left(Spd^{obs}_{d,i}\middle|Spd_{d,i},\sigma^2_{Spd_l}\right)=\mathcal{N}\left(Spd^{obs}_{d,i}\middle|Spd_{d,i},\sigma^2_{Spd_l}\right) \quad (4\text{-}4)$$

$$p\left(Clo^{obs}_{d,i}\middle|Clo_{d,i},\sigma^2_{Clo_l}\right)=\mathcal{N}\left(Clo^{obs}_{d,i}\middle|Clo_{d,i},\sigma^2_{Clo_l}\right) \quad (4\text{-}5)$$

where $\mathcal{N}(\cdot\,|\mu,\sigma^2)$ is the PDF of a normal distribution with mean μ and variance σ^2. Although we expect that σ_{Spd_l} and σ_{Clo_l} would be around 0.1, since we do not have strong prior information about it, we employed a hierarchical Bayesian approach and assign the following priors to $\sigma^2_{Spd_l}$ and $\sigma^2_{Clo_l}$:

$$p\left(\sigma^2_{Spd_l}\middle|\lambda_1\right)=\mathcal{E}\left(\sigma^2_{Spd_l}\middle|\lambda_1\right) \quad (4\text{-}6)$$

$$p\left(\sigma^2_{Clo_l}\middle|\lambda_1\right)=\mathcal{E}\left(\sigma^2_{Clo_l}\middle|\lambda_1\right) \quad (4\text{-}7)$$

where $\mathcal{E}(\cdot\,|\lambda)$ is the PDF of an exponential distribution with rate parameter λ, and λ_1 is equal to 100.

For the metabolic rate, since the observed values are only equal to 1.0, 1.2, and 1.4 met in the training data, we use linear discriminant analysis (LDA) formulation, which is equivalent to multinomial logistic regression for the likelihood function as follows:

$$p\left(Met_{d,i}^{obs} = c \middle| Met_{d,i}, \boldsymbol{\mu}_{Met_l}, \sigma_{Met_l}\right) = \frac{\exp\left(-\frac{1}{2\sigma_{Met_l}^2}\left(Met_{d,i} - \mu_{Met_l,c}\right)^2\right)}{\sum_{c'=1}^{3}\exp\left(-\frac{1}{2\sigma_{Met_l}^2}\left(Met_{d,i} - \mu_{Met_l,c'}\right)^2\right)}, \quad (4\text{-}8)$$

$$c = 1,2,3$$

where $\boldsymbol{\mu}_{Met_l} = \left(\mu_{Met_l,1}, \mu_{Met_l,2}, \mu_{Met_l,3}\right)$ and $c = 1,2,3$ represents 1.0, 1.2, and 1.4 met, respectively. This LDA form is more suitable to introduce prior knowledge in the model. For example, μ_c can be interpreted as the center of values on the domain of input at which a specific class c is more likely than others. We expect that $\mu_{Met_l,1}, \mu_{Met_l,2}, \mu_{Met_l,3}$ would be around 1.0, 1.2, and 1.4 met, respectively, and assign the following prior:

$$p\left(\boldsymbol{\mu}_{Met_l} \middle| \boldsymbol{\lambda}_{mean}, \lambda_2\right) = \mathcal{N}\left(\boldsymbol{\mu}_{Met_l} \middle| \boldsymbol{\lambda}_{mean}, \lambda_2^{-1}\mathbf{I}\right) \quad (4\text{-}9)$$

$$p\left(\sigma_{Met_l}^2 \middle| \lambda_1\right) = \mathcal{E}\left(\sigma_{Met_l}^2 \middle| \lambda_1\right) \quad (4\text{-}10)$$

where $\mathbf{I}$ is the 3-dimensional unit matrix, $\boldsymbol{\lambda}_{mean} = (1.0, 1.2, 1.4)^{\mathrm{T}}$, and $\lambda_2 = 400$.

Given the air temperature data of Figure 3.12, there are no observations for colder or warmer conditions (although in that case occupants would probably respond that they prefer warmer/cooler conditions respectively). So, the previous preference model did not include any prior knowledge for such conditions; it was focused on explaining well the training data collected from the middle temperature range. As a result, model predictions for higher and lower temperatures might be inaccurate. While this is fine for predicting occupants' thermal preference in spaces conditioned only within a "regular" temperature range, controlling space temperature based on this model might be problematic.

Therefore, in this study, we feed two sets of 1,000 synthetic observations to each cluster (Table 4.1) which represent occupants' expected feedback under cold and warm conditions respectively. We selected low and high ends of Ta and MRT values (i.e., 17.5 °C and 28.0 °C) considering that the maximum/minimum operative temperature of observations in the training data for which the thermal preference (y) is "no change" are 19.0 °C / 26.3 °C, respectively.

Table 4.1. Synthetic data points used to introduce our prior belief in the revised generalized thermal preference model.

Conditions	Air Temp.	MRT	RH	Air speed	Metabolic rate	Clothing level	Thermal preference
Cold condition	17.5 °C	17.5 °C	50 %	0.1 m/s	1.2 met	0.61 clo	want warmer
Warm condition	28.0 °C	28.0 °C	50 %	0.1 m/s	1.2 met	0.61 clo	want cooler

4.2.2 Model training and sampling for efficient Bayesian inference

Training the generalized model means inferring the posterior probability of the latent variables (model parameters and hidden variables) in the model. However, since the posterior distribution is intractable analytically, an approximation method is needed. Sampling methods, such as Markov Chain Monte Carlo (MCMC), are widely used since they are flexible; however, they are computationally expensive, especially for high-dimensional problems. Note that training our model is a high-dimensional problem since there are 5,454 latent variables including 59 model parameters, 259 hidden variables (preference characteristics of 259 occupants), and 5,136 hidden variables for the true air speed, metabolic rate, and clothing insulation level. In addition, a label switching problem [82] arises when solving a clustering problem using mixture models with sampling methods.

To overcome these issues, variational Bayesian methods (a.k.a., variational inference) have been being developed, which fit a variational distribution to the posterior by solving an optimization problem [83]. Unlike sampling methods, there always exists an approximation error between the fitted distribution and the true posterior. However, since they solve an optimization problem rather than drawing samples, they are computationally simpler. The major difficulty is deriving a maximization algorithm for each model structure, but there are algorithms which automate this process and consequently support the Bayesian approach in large-scale machine-learning problems. In this study, we use Automatic Differentiation Variational Inference (ADVI) [95]. ADVI transforms the support of all the parameters and hidden variables to the real coordinate space and deals with the transformed variables $\boldsymbol{\zeta}$. Thereafter, ADVI fits a mean-field Gaussian distribution to the posterior of $\boldsymbol{\zeta}$ as:

$$q(\boldsymbol{\zeta}|\boldsymbol{\phi}) = \mathcal{N}\left(\boldsymbol{\zeta}|\boldsymbol{\mu}, \mathrm{diag}(\boldsymbol{\sigma}^2)\right) = \prod_{n=1}^{N} \mathcal{N}\left(\zeta_n|\mu_n, \sigma_n^2\right) \tag{4-11}$$

where $\boldsymbol{\phi} = (\mu_1, \ldots, \mu_N, \sigma_1^2, \ldots, \sigma_N^2)$. The PyMC3 Python package [96] was used for ADVI and details on how it is used are described in [97]. Since the default stochastic gradient descent algorithm, Adagrad, showed relatively slow convergence, we used Adam [98] instead. We have also implemented random initialization with 100 initial points in the model training to get closer to the global solution of the variational inference problem.

4.2.3 Probability distributions of clustered occupant thermal preference profiles

Figure 4.3 shows the probability of an occupant belonging to each cluster before analyzing any data from the occupant, inferred by the revised generalized model. The uncertainty for the probabilities is visualized with box plots based on 1,000 samples from the variational distribution (approximate posterior distribution). Orange bars are the median value of the probabilities, and the upper and lower whiskers are the associated 95% credible intervals. This graph essentially shows the probability of each cluster being active. Since four clusters have meaningful probabilities, we concluded that the generalized model discovered four clusters (two with high probabilities and the other two with low probabilities) of people having similar thermal preference characteristics.

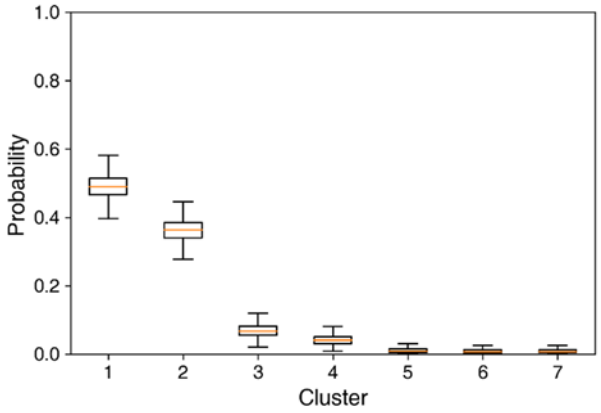

Figure 4.3. The probability of each cluster being active

The resulting predictive probability distributions (calculated with sub-models for the four clusters) of occupant thermal preferences (i.e., “want warmer”, “no change”, “want cooler”) are plotted on the left column of Figure 4.4. In order to visualize results in 2-D figures as a function of Ta, the other variables were set as follows: MRT = Ta, Spd = 0.05 m/s, RH = 50 %, Met = 1.2 met, and Clo = 0.6 clo. Solid lines represent the median values of the probabilities (i.e., median model), and shaded areas represent the associated 95% credible intervals (i.e., 2.5- and 97.5-

quantiles of the predictive probability). Note that the variational distribution we used ignores the correlation between model parameters and it can underestimate the model uncertainty.

The right column of Figure 4.4 shows the probability of each occupant belonging to each cluster. Each circle represents the probability for each occupant, and the color of each circle corresponds to the probability (i.e., dark red denotes high probability and dark blue means low probability). Most of the occupants belong to the first two clusters with high probabilities, thus the thermal preference of the majority of people can be explained with these two clusters, in accordance with Figure 4.3.

The differences in probability for "no change" preference (green curves) are clear between the four clusters. For the first and second cluster these preferences are maximized around 23 °C and 21 °C (when other factors are as mentioned above). Consequently, these two clusters describe occupants who prefer "relatively warmer" and "relatively cooler" conditions, respectively.

The third cluster represents occupants whose almost all of the responses were "prefer no change". In fact, there were 3 occupants whose data were all "no change" in our training data. Kim et al. [58] reported that they also observed such occupants in their study. Although the generalized model discovered this cluster from the data, it is arguable whether this cluster really represents a separate group of people in terms of thermal preference characteristics or not. The reasons are: (i) the number of data collected from each of such occupants is small; and (ii) most of them were not exposed to various thermal conditions. Indeed, the generalized model also shows this ambiguousness. The right figure shows that no occupants belong to this cluster with a probability close to 1. Therefore, the results imply that data collected from each of these occupants were not qualitatively and/or quantitatively adequate to classify these occupants into this cluster with high probability; their thermal preferences could be explained with other clusters.

The fourth cluster represents occupants preferring very warm conditions. Only a few (approx. 7 - 10) occupants are in this cluster with high probability, a relatively small number assuming that our training data are representative of the entire population. Thus, the uncertainty of the sub-model for this cluster is higher than the other sub-models. We expect that this high uncertainty decreases as we update the generalized model with new data.

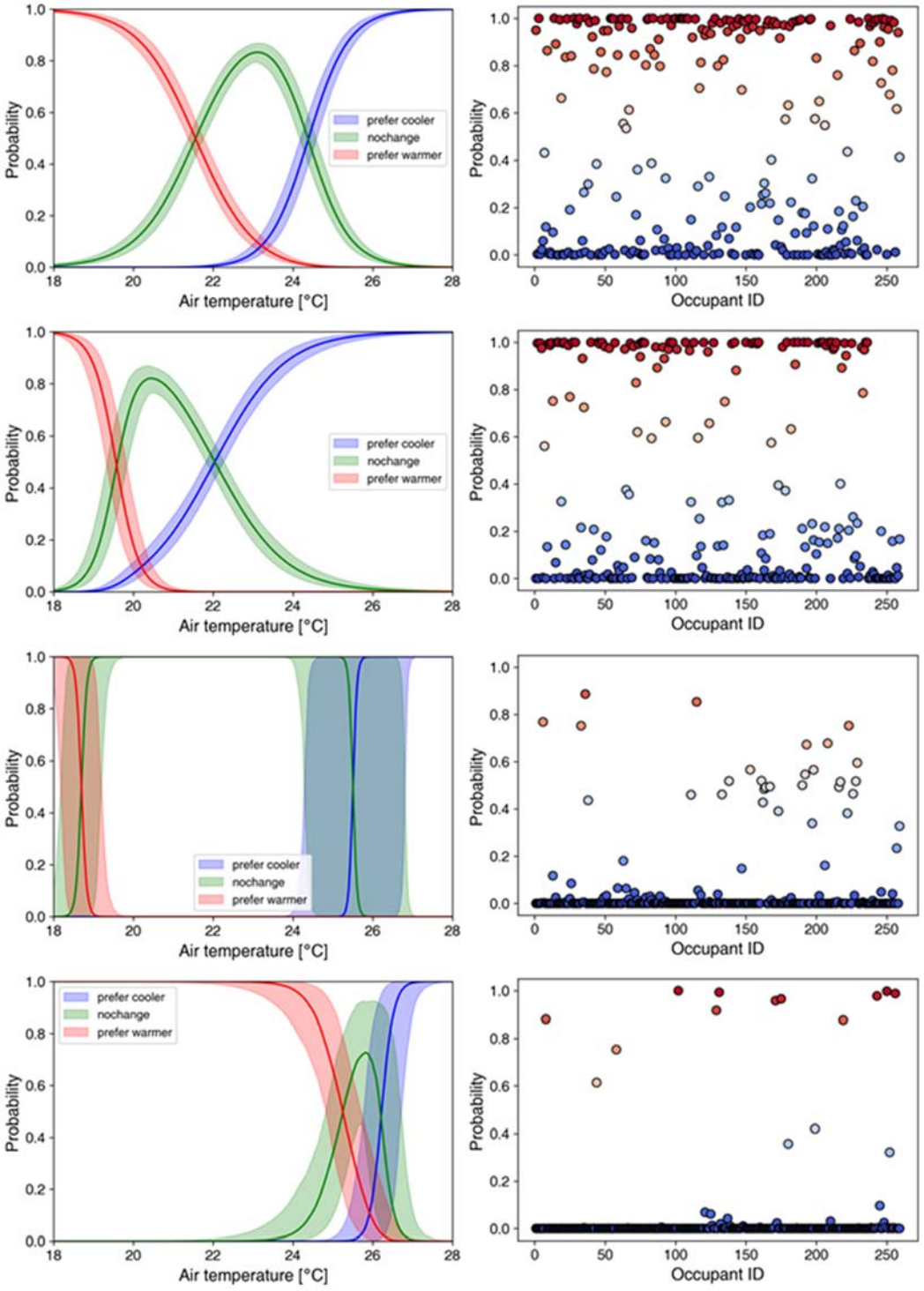

Figure 4.4. Predictive probability distributions calculated with sub-models for the four clusters (left column), and probability of each occupant belonging to each cluster (right column). The displayed probability distributions were calculated with the following settings: MRT = air temperature, air velocity = 0.05 m/s, relative humidity = 50 %, metabolic rate = 1.2 met, and clothing level = 0.6 clo.

4.3 Learning new occupants in the real world

4.3.1 Methodology for learning new occupants

If we could collect data for all the input variables (Ta, MRT, RH, Spd, Met and Clo) and output (thermal preference) from new individual occupants, we could learn their thermal preference profile without any additional treatment. Learning a new occupant would mean augmenting the generalized model by including data from the new occupant in the joint probability and inducing the updated posterior probability:

$$p\left(z_o, \boldsymbol{\theta} \middle| \mathbf{y}_o, \mathbf{X}_o, \mathbf{Data}_{org}\right) \propto p(\mathbf{y}_o|\mathbf{X}_o, z_o, \boldsymbol{\theta}) p(z_o|\boldsymbol{\theta}) p\left(\mathbf{Data}_{org} \middle| \boldsymbol{\theta}\right) p(\boldsymbol{\theta}) \tag{4-12}$$

where $\{\mathbf{y}_o, \mathbf{X}_o\}$ is the data from the new occupant, z_o is the thermal preference characteristic of the new occupant, and $\mathbf{Data}_{org}$ is the original training data (i.e., the subset of ASHRAE RP-884 DB). With this posterior probability, we can predict thermal preference of the new occupant (y_p) under certain conditions ($\mathbf{x}_p$) as:

$$p\left(y_p \middle| \mathbf{x}_p, \mathbf{y}_o, \mathbf{X}_o, \mathbf{Data}_{org}\right) = \int \sum_{z_o} p\left(y_p \middle| \mathbf{x}_p, \mathbf{y}_o, \mathbf{X}_o, \mathbf{Data}_{org}, z_o, \boldsymbol{\theta}\right) p\left(z_o, \boldsymbol{\theta} \middle| \mathbf{y}_o, \mathbf{X}_o, \mathbf{Data}_{org}\right) d\boldsymbol{\theta} \tag{4-13}$$

However, it is well-known that in real buildings, local air speed, metabolic rate, and clothing insulation level are very difficult to measure in practice. For Met and Clo, intrusive measurements and occupant monitoring are definitely required, and that is why these are usually estimated based on reference tables and guidelines [7]. So, one advantage of the generalized thermal preference model is that it can be used to learn new occupants in practice, by considering these three variables as hidden and assigning a probability distribution for them. Since the assigned probability distribution affects the inference of latent variables and predictions, it should be carefully chosen based on knowledge for the variables.

Figure 4.5 shows the joint probability of learning a new occupant (o). The simplest way to deal with the hidden variables ($Spd_{o,i}, Met_{o,i}, Clo_{o,i}$) is assigning a Dirac-$\delta$ function with a predefined fixed position for the PDF, which is equivalent to assuming constant values for these variables. However, this is an arbitrary guess and most importantly, these variables vary over time; therefore, other approaches are recommended as follows.

Metabolic rate probability distribution

The metabolic rate is a variable governed by body characteristics and activity pattern of each individual. We assume that these effects in an office space can be explained as a truncated Normal distribution:

$$p\left(Met_{o,i}\middle|\mu_{Met,o},\sigma^2_{Met,o}\right)=\text{Truncated Normal}\left(Met_{o,i}\middle|\mu_{Met,o},\sigma^2_{Met,o},a_{Met}\right) \quad (4\text{-}14)$$

where $\text{Truncated Normal}(\cdot\,|\mu,\sigma^2,a)$ is the probability density function (PDF) of a truncated normal distribution with parameters μ, σ, and a (mean and standard deviation of the original normal distribution, and lower bound of the distribution, respectively). We set $a_{Met}=0.7$. Since we do not have strong prior information about $\mu_{Met,o}$, we assign the respective probability distribution of Figure 4.2 to $\mu_{Met,o}$, which represents the population distribution for the metabolic rate:

$$p\left(\mu_{Met,o}\middle|\mu_{Met_p},\sigma^2_{Met_p},\omega_{Met_p}\right)=\text{Lognormal}\left(\mu_{Met,o}-\omega_{Met_p}\middle|\mu_{Met_p},\sigma^2_{Met_p}\right) \quad (4\text{-}15)$$

For $\sigma^2_{Met,o}$, since we believe that the metabolic rate of an individual would vary about ± 0.1 met in an office space, we assign the following probability: $p\left(\sigma^2_{Met,o}\middle|\lambda_{Met}\right)=\mathcal{E}\left(\sigma^2_{Met,o}\middle|\lambda_{Met}\right)$, where $\lambda_{Met}=400$.

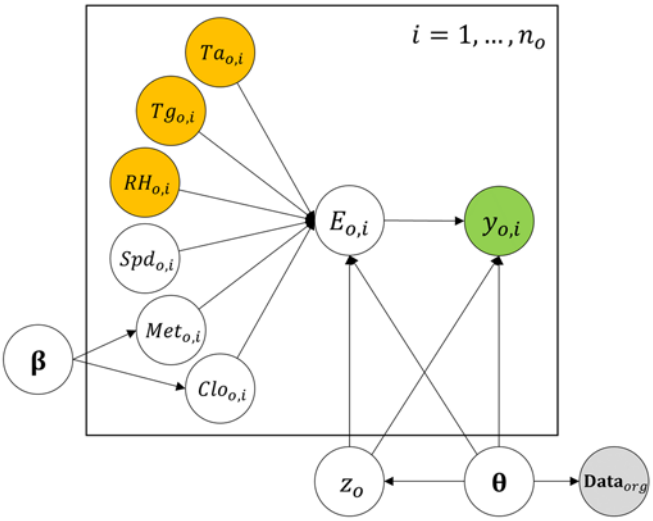

Figure 4.5. Graphical representation of the joint probability for the personalized thermal preference models.

Clothing level probability distribution

We make a similar assumption for the clothing insulation level:

$$p\left(Clo_{o,i}\middle|\mu_{Clo,o},\sigma^2_{Clo,o}\right)=\text{Truncated Normal}\left(Clo_{o,i}\middle|\mu_{Clo,o,i},\sigma^2_{Clo,o},a_{Clo}\right) \quad (4\text{-}16)$$

with $a_{Clo}=0$ and $p\left(\sigma^2_{Clo,o}\middle|\lambda_{Clo}\right)=\mathcal{E}\left(\sigma^2_{Clo,o}\middle|\lambda_{Clo}\right)$. Since we believe that the clothing level at a certain temperature could vary about ± 0.3 clo, we set $\lambda_{Clo}=20$. However, people might change their clothing to adapt to thermal conditions. To consider this adaptive behavior in the model, we can use a relationship between the clothing level and the air temperature. Here we use a linear relationship, expressed in the mean distribution value, $\mu_{Clo,o,i}$:

$$\mu_{Clo,o,i}=\left(-\beta_{1,o}\times\frac{T_{air_{o,i}}-22.5}{1.5}\right)\times 0.2+\beta_{2,o} \quad (4\text{-}17)$$

Other models can also be used, e.g., a logistic regression model between clothing and mean outdoor temperature [99]. In Eq. (4-17), the constants (22.5, 1.5, and 0.2) are introduced to just scale the variables. Since we know that $Tair_{o,i}$ and $Clo_{o,i}$ are negatively correlated, we assign the following prior to $\beta_{1,o}$: $p\left(\beta_{1,o}\middle|\lambda_{\beta_1}\right)=\mathcal{E}\left(\beta_{1,o}\middle|\lambda_{\beta_1}\right)$, and set $\lambda_{\beta_1}=1$. For $\beta_{2,o}$, we set the distribution of Figure 4.2 for clothing to the prior as:

$$p\left(\beta_{2,o}\middle|\mu_{Clo_p},\sigma^2_{Clo_p}\right)=\text{Lognormal}\left(\mu_{Clo,o}\middle|\mu_{Clo_p},\sigma^2_{Clo_p}\right) \quad (4\text{-}18)$$

Air speed probability distribution

Air velocity can vary significantly in office spaces. However, following thermal comfort and draft prevention recommendations [7], for low air speed ranges (<0.2m/s), the effect of change in air speed on heat transfer near human body is relatively small. So, the measured air speed probability distribution of Figure 4.2 is to $Spd_{o,i}$ as:

$$p\left(Spd_{o,i}\middle|\mu_{Spd_p},\sigma^2_{Spd_p}\right)=\text{Lognormal}\left(Spd_{o,i}\middle|\mu_{Spd_p},\sigma^2_{Spd_p}\right) \quad (4\text{-}19)$$

In cases where increased air speeds are used for cooling purposes, different probability distributions can be assigned, e.g.: $p\left(Spd_{o,i}\middle|S_{system}\right)$, where S_{system} denotes the operational status of the HVAC system.

The mean radiant temperature is estimated based on air temperature, globe temperature, and air speed with the following deterministic equation:

$$MRT_{o,i} = \left(Tglobe_{o,i}^4 + \frac{1.10 \times 10^8 Spd_{o,i}}{0.95 \times 0.15^{0.4}} \left(Tglobe_{o,i} - Tair_{o,i} \right) \right)^{0.25} \quad (4\text{-}20)$$

Once these probabilities are incorporated in the augmented model following Figure 4.1, we can learn and predict thermal preference of occupants without any data for Spd, Met, Clo and any occupant personal characteristics. Learning becomes inferring the joint posterior probability of the occupants' cluster value z_o, personal parameters $\boldsymbol{\beta}_o = \left(\mu_{Met,o}, \sigma_{Met,o}^2, \beta_{1,o}, \beta_{2,o}, \sigma_{Clo,o}^2 \right)$ for metabolic rate and clothing insulation level, and updated model parameters $\boldsymbol{\theta}$ as:

$$p\left(z_o, \boldsymbol{\beta}_o, \boldsymbol{\theta} | \mathbf{y}_o, \mathbf{X}'_o, \mathbf{Data}_{org} \right) \propto p(\mathbf{y}_o | \mathbf{X}'_o, z_o, \boldsymbol{\beta}_o, \boldsymbol{\theta}) p(z_o | \boldsymbol{\theta}) p(\boldsymbol{\beta}_o) p\left(\mathbf{Data}_{org} | \boldsymbol{\theta} \right) p(\boldsymbol{\theta}) \quad (4\text{-}21)$$

where $\mathbf{X}'_o = \left\{ \mathbf{x}'_{o,1}, \dots, \mathbf{x}'_{o,n_o} \right\}$ and $\mathbf{x}'_{o,i} = \left(Tair_{o,i}, Tglobe_{o,i}, RH_{o,i} \right)$. With this posterior probability, we can predict the thermal preference y_p of the new occupant under certain conditions $\mathbf{x}'_p$ as:

$$p\left(y_p | \mathbf{x}'_p, \mathbf{y}_o, \mathbf{X}'_o, \mathbf{Data}_{org} \right)$$
$$= \iint \sum_{z_o} p\left(y_p | \mathbf{x}'_p, \mathbf{y}_o, \mathbf{X}'_o, \mathbf{Data}_{org}, z_o, \boldsymbol{\beta}_o, \boldsymbol{\theta} \right) p\left(z_o, \boldsymbol{\beta}_o, \boldsymbol{\theta} | \mathbf{y}_o, \mathbf{X}'_o, \mathbf{Data}_{org} \right) d\boldsymbol{\beta}_o d\boldsymbol{\theta} \quad (4\text{-}22)$$

Even with using ADVI for Bayesian inference, updating the augmented model could be computationally heavy in real applications, since the inference problem includes the large dataset, $\mathbf{Data}_{org}$, and the large number of hidden variables for them. So instead of updating the whole augmented model, we construct a personalized model for a new occupant separately and feed the approximate posterior probability from the generalized model to the personalized model as a prior for the model parameters. In this way, computational time and memory consumption are significantly reduced.

4.3.2 Experimental data collection for model validation

To show the validity of our learning method, we designed and conducted an experimental study using three identical perimeter south-facing private offices (3.3m × 3.7m × 3.2m high) in October and November 2017. The offices (Figure 4.6) have one exterior curtain wall façade with 54% window-to-wall ratio, and a high-performance glazing unit with a selective low-emissivity coating (visible transmittance: 70%, solar transmittance: 33%). They are equipped with VAV systems, motorized shades and dimmable electric lights. A commercial BMS allows us to monitor, control and automate all building systems. In this study, we fixed the dimming level of the electric lights at 100 % and the shade position at 25 % to eliminate the potential impact of changing the

visual environment on the thermal preference of test-subjects. The study was approved by the Institutional Review Board (IRB Protocol #: 1503015873).

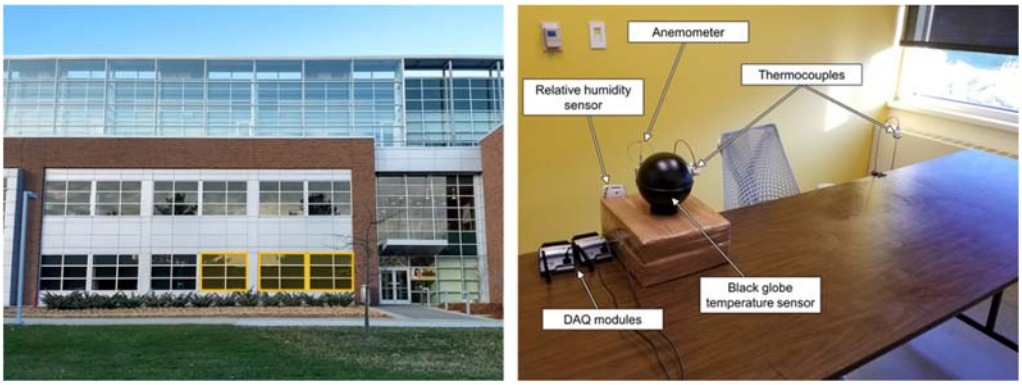

Figure 4.6. Exterior and interior view of the offices.

Nine test-subjects (20 - 40 years old), not familiar with this research, were recruited for the experiment. Three subjects participated in the experiment during each day (one in each office). They were asked to perform their usual workload (computer-related work, reading, writing, etc.) between 9:00 AM 4:00 PM. Each occupant participated for eight days and experienced all the temperature setpoint schedules listed in Table 4.2 (one for each day), while their thermal preference votes were collected. Very warm or cold conditions were not possible, however our goal was not to expose people to certain extreme conditions, but collect their preference under given conditions. All the subjects reported their thermal preference at 09:55 AM, 10:55 AM, 11:55 PM, 1:55 PM, 2:55 PM, and 3:55 PM each day. To ensure thermal adaptation with each condition, they were not allowed to leave the rooms for 30 minutes before each survey. They could leave the room shortly except this time and they had a 1-hour lunch break at 12:00 - 1:00 PM.

Table 4.2. Air temperature setpoint schedules (unit: °C)

Schedule #	9-10 AM	10-11 AM	11 AM-12 PM	1-2 PM	2-3 PM	3-4 PM
1	25	23.5	22	22	23.5	25
2	22	23.5	25	25	23.5	22
3	21	22	23	24	25	26
4	26	25	24	23	22	21
5	23	21.5	20	20	21.5	23
6	20	21.5	23	23	21.5	20
7	19	20	21	22	23	24
8	24	23	22	21	20	19

Air temperature, globe temperature and relative humidity were measured each minute. The air temperature was measured with two shielded T-type thermocouples on the left and right side

of the sitting location and the average value was used. The globe temperature and the relative humidity were measured with a black globe temperature sensor (μSMART TB1) and a relative humidity sensor (BA/H205-B4X-Z-CG-WMW) respectively using 5-minute average values. Local air speed and clothing were also recorded but were not used in this study according to our methodology. Figure 4.7 shows the distribution of collected data for air temperature, MRT, relative humidity and preference votes.

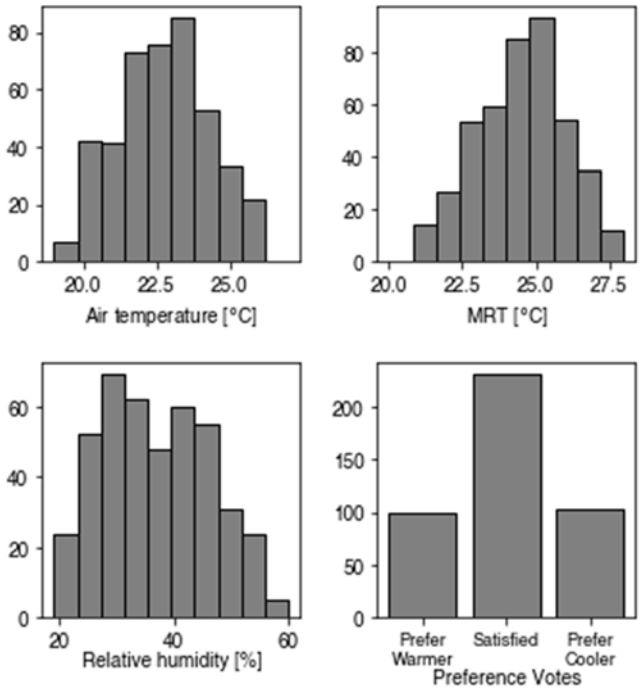

Figure 4.7. Distribution of data collected from the experiment

4.3.3 The inferred personalized profiles

Personalized models of the nine test-subjects were trained using the experimental data. We drew 1,000 samples from the approximate posterior for each test-subject and used them to illustrate results. Table 4.3 shows the induced cluster value and personal parameters of each test-subject, based on 48 data points (collected over the eight days of experiments for each subject). Subjects 2 and 9 were classified into the second cluster, and all the others were classified into the first cluster. The uncertainty for the cluster values was negligible. For the uncertainty of the personal parameters, 95% credible intervals along with median values were specified.

Table 4.3. Inferred cluster value (z_o) and personal parameters of the nine test-subjects

	Sub. 1	Sub. 2	Sub. 3	Sub. 4	Sub. 5	Sub. 6	Sub. 7	Sub. 8	Sub. 9
z_o	1	2	1	1	1	1	1	1	2
$\mu_{Met,o}$	1.12 (1.10, 1.14)	1.07 (1.06, 1.09)	1.10 (1.09, 1.12)	1.10 (1.08, 1.12)	1.01 (1.00, 1.03)	1.05 (1.04, 1.07)	1.14 (1.12, 1.15)	1.11 (1.09, 1.13)	1.07 (1.05, 1.08)
$\sigma^2_{Met,o}$	0.0049 (0.0032, 0.0069)	0.0025 (0.0016, 0.0035)	0.0037 (0.0025, 0.0055)	0.0040 (0.0026, 0.0057)	0.0033 (0.0022, 0.0047)	0.0028 (0.0019, 0.0041)	0.0038 (0.0026, 0.0056)	0.0042 (0.0029, 0.0063)	0.0026 (0.0017, 0.0038)
$\beta_{1,o}$	0.05 (0.01, 0.21)	0.04 (0.01, 0.16)	0.11 (0.04, 0.29)	0.29 (0.15, 0.58)	0.50 (0.37, 0.67)	0.21 (0.12, 0.40)	0.10 (0.04, 0.29)	0.66 (0.47, 0.92)	0.13 (0.06, 0.34)
$\beta_{2,o}$	0.58 (0.54, 0.62)	0.46 (0.44, 0.48)	0.73 (0.69, 0.76)	0.68 (0.63, 0.72)	0.55 (0.51, 0.58)	0.70 (0.67, 0.73)	0.70 (0.66, 0.74)	0.85 (0.80, 0.90)	0.68 (0.65, 0.71)
$\sigma^2_{Clo,o}$	0.0178 (0.0124, 0.0270)	0.0067 (0.0047, 0.0103)	0.0153 (0.0104, 0.0225)	0.0265 (0.0186, 0.0402)	0.0140 (0.0097, 0.0214)	0.0118 (0.0082, 0.0181)	0.0168 (0.0113, 0.0252)	0.0294 (0.0201, 0.0444)	0.0107 (0.0074, 0.0163)

Median (95% credible interval)

Figure 4.8 shows the inferred personalized profiles of the nine test-subjects corresponding to the personal parameters in Table 4.3. To plot the profiles with respect to air temperature, we set globe temperature = air temperature and relative humidity = 50 %. The personalized models show different profiles by having different sets of cluster values and personal parameters. In Figure 4.8, solid lines are the average values of the probabilities; darkly shaded areas represent the uncertainty caused by the uncertain parameters; and lightly shaded areas represent the uncertainty caused by the uncertain input variables (i.e., metabolic rate, clothing insulation level, and air speed). Therefore, the size of credible intervals in Table 4.3 correspond to the darkly shaded areas, and values of $\sigma^2_{Met,o}$ and $\sigma^2_{Clo,o}$ are related to the lightly shaded areas.

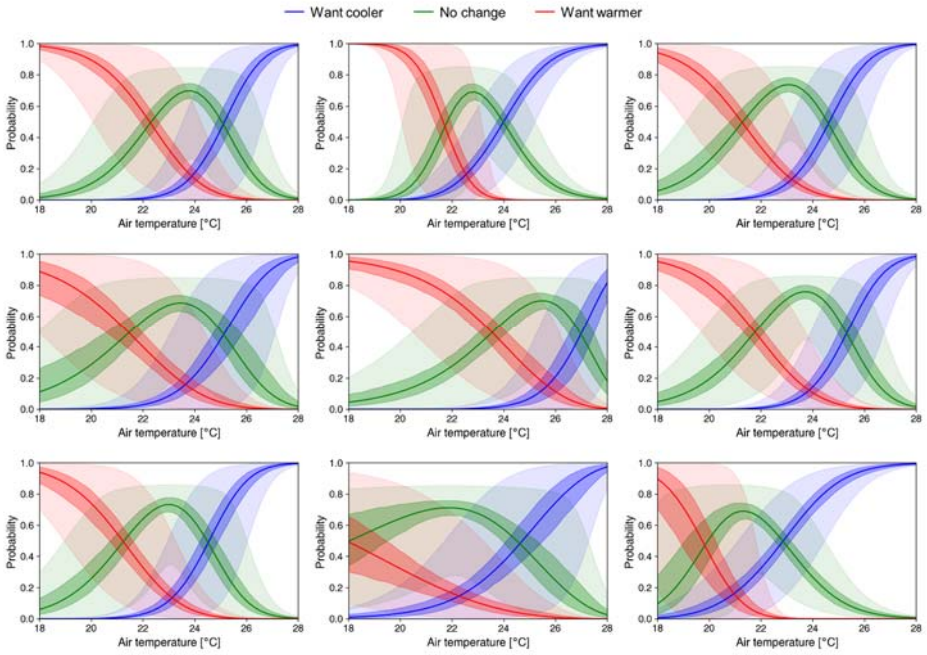

Figure 4.8. Personalized thermal preference profiles of the nine test-subjects

To further elaborate on the results, Figure 4.9 shows the profiles of subject 3 based on 6, 12, 18, 24, 30, 36, 42 and 48 data points (i.e., data for 1 to 8 days). The corresponding induced cluster value and personal parameters are also shown in Figure 4.10. Using just the first 6 data points, the model classified the subject into the first cluster with a low uncertainty. However, the uncertainty for personal parameters was high (wider darkly shaded areas in Figure 4.9 and wider box plots in Figure 4.10). As more data are fed into the model, the uncertainty for personal parameters decreases. The estimated $\sigma^2_{Met,o}$ and $\sigma^2_{Clo,o}$ do not change significantly –but this uncertainty can only be reduced by accurately observing uncertain variables (e.g. clothing level).

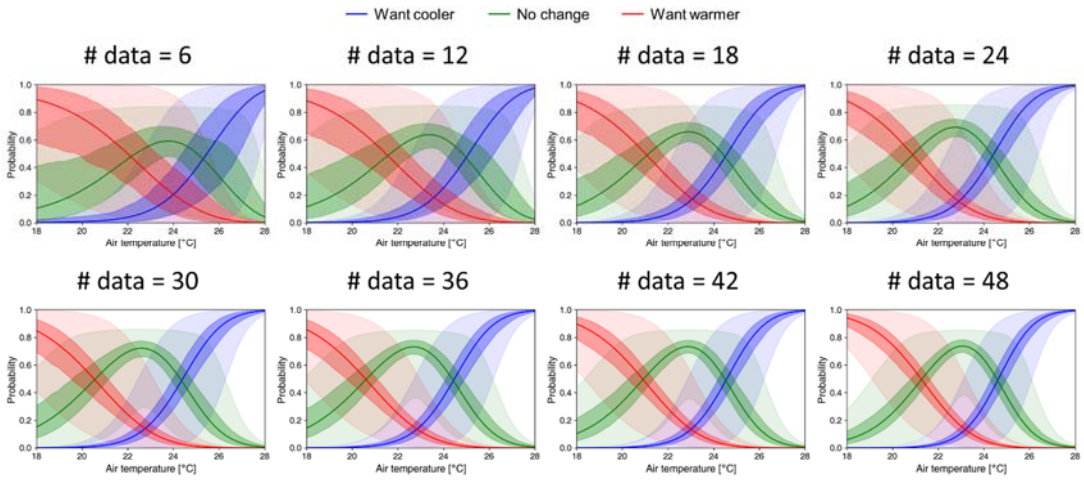

Figure 4.9. Thermal preference profile of subject 3 as a function of used data points (6-48).

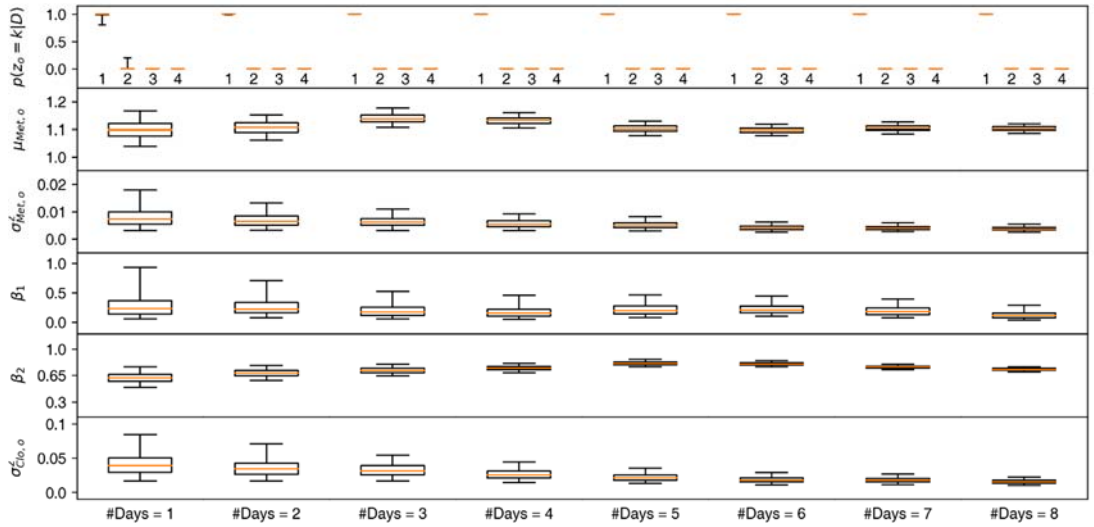

Figure 4.10. Induced cluster value and personal parameters of subject 3 as a function of used data points (6-48, or days 1-8).

4.3.4 Prediction performance of the personalized thermal preference models

The personalized profiles allow an understanding of thermal preferences of individuals with quantified uncertainty. To evaluate the prediction performance of the personalized models, a cross-validation was conducted. For each subject, we defined a set of data from each day (6 data points) as a unit dataset (i.e., 8 datasets total), and used one of these datasets for validation. To investigate the improvement of the prediction performance with respect to the training data size, personalized models were trained with 1~7 datasets; then, we computed a prediction performance metric over the validation set (not used to train the model). The number of possible combinations for setting training and validation sets are: $8 \times ({}_7\mathrm{C}_1 + {}_7\mathrm{C}_2 + {}_7\mathrm{C}_3 + {}_7\mathrm{C}_4 + {}_7\mathrm{C}_5 + {}_7\mathrm{C}_6 + {}_7\mathrm{C}_7) = 1016$, where ${}_n\mathrm{C}_r$ is the number of possible ways to choose r elements among n elements.

In this study, we use the area under the receiver operating characteristic curve (AUC) as the prediction performance metric. It represents the probability that a classifier will rank a randomly selected positive instance higher than a randomly selected negative one. Hence, AUC = 0.5 is equivalent to a random guesses and AUC = 1.0 indicates perfect predictions. Since AUC is a metric originally designed for binary classifiers, we compute the averaged AUC over the three classes using the micro-averaging scheme [100]. However, the absolute value of a metric may not always be sufficient, i.e., to conclude whether the value is high enough or not –comparison with competitive models (relative performance) provides additional useful information. Therefore, in this study, we compared 5 different methods to train the personalized models:

1. (Current method): Based on the generalized model assuming that the unmeasured metabolic rate, clothing level and air speed follow the distributions of Section 4.3.1.
2. Based on the generalized model assuming the following constant values for the unmeasured variables: metabolic rate = 1.1 met, clothing level = 0.5 clo, and air speed = 0.1 m/s.
3. Based on the generalized model assuming the following constant values for the unmeasured variables: metabolic rate = 1.1 met, clothing level = 1.0 clo, and air speed = 0.1 m/s.
4. Training a univariate multinomial logistic regression model which has the air temperature as the input variable from scratch with maximum likelihood estimation (MLE) method [100].

5. Training a multivariate multinomial logistic regression model having the three standard model input variables (Ta, Tg and RH) as inputs from scratch [100].

Figure 4.11 shows the learning curves (computed AUC with respect to the training data size) for each of the models. Comparing the current model with models 2 and 3 (constant unobserved variables), we can see that sometimes these simpler models might work reasonably well. Note that the generalized model retains some degree of freedom, allowing the personalized models to fit data (and also updating the model parameters to fit data). However, noticing the differences between models 2 and 3, we can tell that this might simply happen due to a random good guess for metabolic rate and clothing value (or air velocity). These differences are much larger for some of the occupants, indicating that selecting proper constant values for these variables is indeed a matter of luck, and therefore could result in wrong predictions. In addition, the generalized model should be continuously updated and revised as more data become available. Assuming incorrect constant values for these variables when updating the model will create further problems. So, the current model, which automates the learning process without assuming constant values for variable parameters, improves the reliability of the overall thermal preference learning process.

Comparing with model 4, one can note that the current method requires less data to converge (converges faster with training data size). With adequate training data (>30), the two models have similar overall prediction performance (although there are differences in the results for individual subjects). This is somewhat expected, since (i) Ta, MRT and RH during the experiments did not significantly vary independently from each other and (ii) in both of these models, no additional information was introduced for the other important variables (metabolic rate, clothing insulation level, and air velocity). This result supports that a pre-developed cluster model can be used to learn a new occupant even though we cannot measure some input variables of the cluster model for the occupant. Lastly, model 5 shows poor prediction performance; even 42 data points were not sufficient to train it. Training a model having such a high degree of freedom from scratch would not be practical to implement in real buildings.

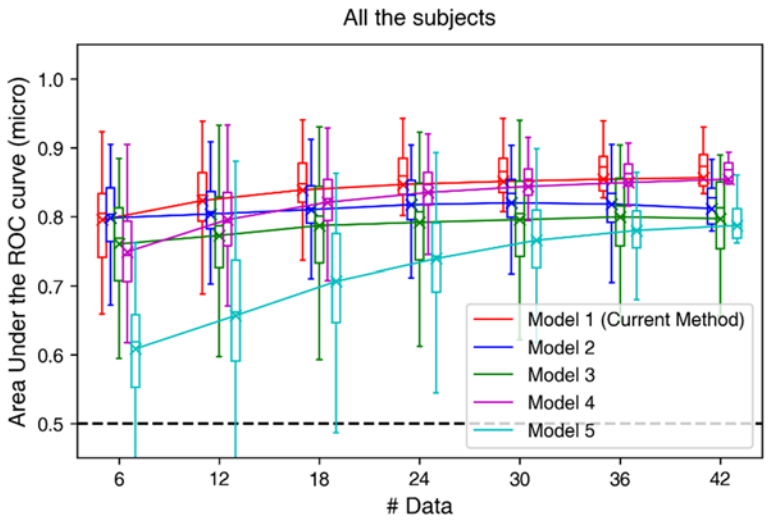

Figure 4.11. Comparison of learning curves for the different models.

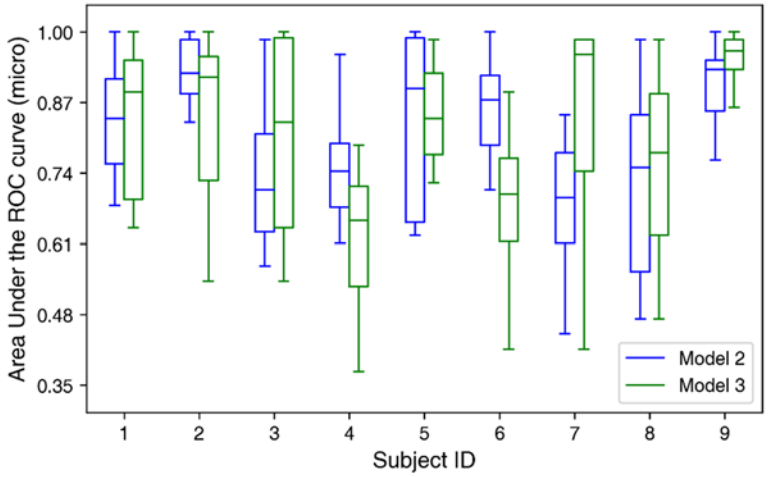

Figure 4.12. Comparison of AUC for Model 2 and 3 trained with 42 data points

4.3.5 Prediction performance with limited data

It is useful to understand the differences in prediction performance between the proposed model and model 4 when available data is limited. In such cases, the performance metrics value does not provide the required information. For that purpose, we take as an example the preference profile of Figure 4.9, which is now plotted using 6 data points from 4 different days in Figure 4.13, with the air temperature logistic regression model (model 4, top row) and with the current model (bottom row). Actual data points collected are shown with dots, while red, green and blue colors

represent “prefer warmer”, “no change”, and “prefer cooler”, respectively. Green dots are displayed on the top of each plot (and the rest on the bottom) to clearly identify this data.

The profiles of model 4 are totally different from each other if only 6 data points are used each time. In the first plot, only “no change” and “prefer cooler” votes were collected from that day. Therefore, the model trained with the data cannot predict that this occupant would prefer warmer conditions. In addition, the probability of “no change” increases as the air temperature decreases and is maximized at a very low temperature, which is unreasonable. The second plot shows the opposite result. In the third case, although there are votes of all the three classes, the model failed to create a reasonable profile because the number of votes is small and votes of “no change” and “prefer cooler” were collected from similar air temperatures. In the fourth case, since there were only “no change” votes, the model cannot be trained properly. Also note that these profiles are quite different from the profile developed with 48 data points in Figure 4.9.

These results show that the air temperature logistic regression MLE model cannot train reliable models with limited number of data, as the current model does. It is also evident that common performance metrics cannot always provide important information about the model accuracy, especially if limited data points are available.

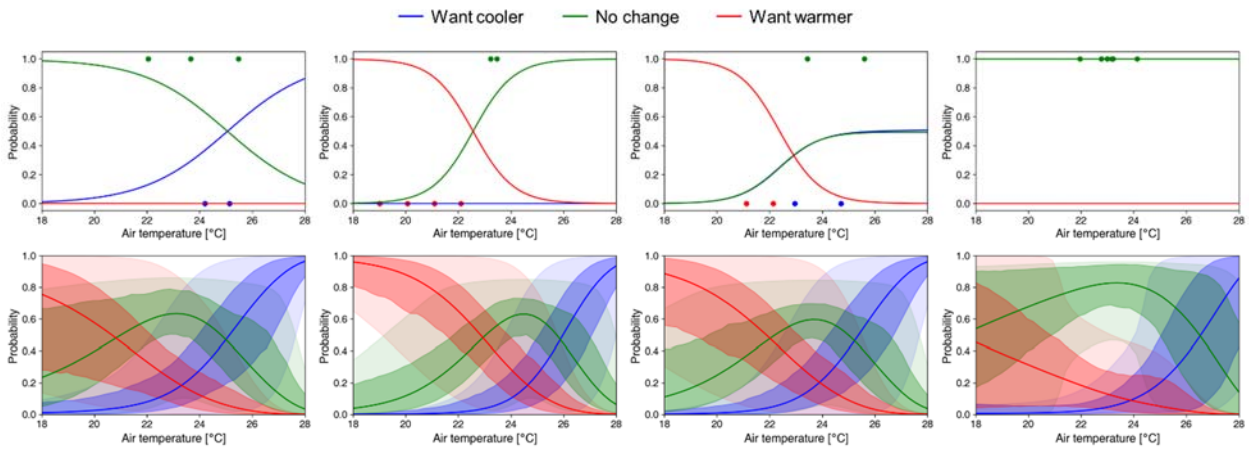

Figure 4.13. Personalized profiles developed based on model 4 (top row) and current model (bottom row) using four different sets of 6 data points.

A further analysis of the results using the current model is shown in Figure 4.14. The probability that the subject belongs to each cluster and the estimated personal parameters are displayed for the same four cases (four sets of 6 data points) discussed above. In the first three cases, the model classified the subject into the first cluster with high probability (however, the

profiles are not the same since the estimated personal parameters are different). For example, in the first case, the model did not classify the subject into the second cluster since the probability of a person voting "no change" when the air temperature is higher than 25 °C is very low. However, that probability is not zero since the metabolic rate and the clothing level might be very low at that moment. In the fourth case, only "no change" votes were collected in the day and the model uses a mixture of two sub-models to explain the subject.

Overall, the current model, described in Section 4.3.1, is able to estimate reasonable and reliable preference profiles and cluster values using limited data points. Comparing with the results of Figure 4.9 with 48 data points, there are significant similarities, thanks to information from the generalized model and our prior for the personal parameters: (i) the air temperature that maximizes the probability of "no change" is around 23-24 °C; and (ii) the probability of "prefer cooler" increases as air temperature increases and vice versa.

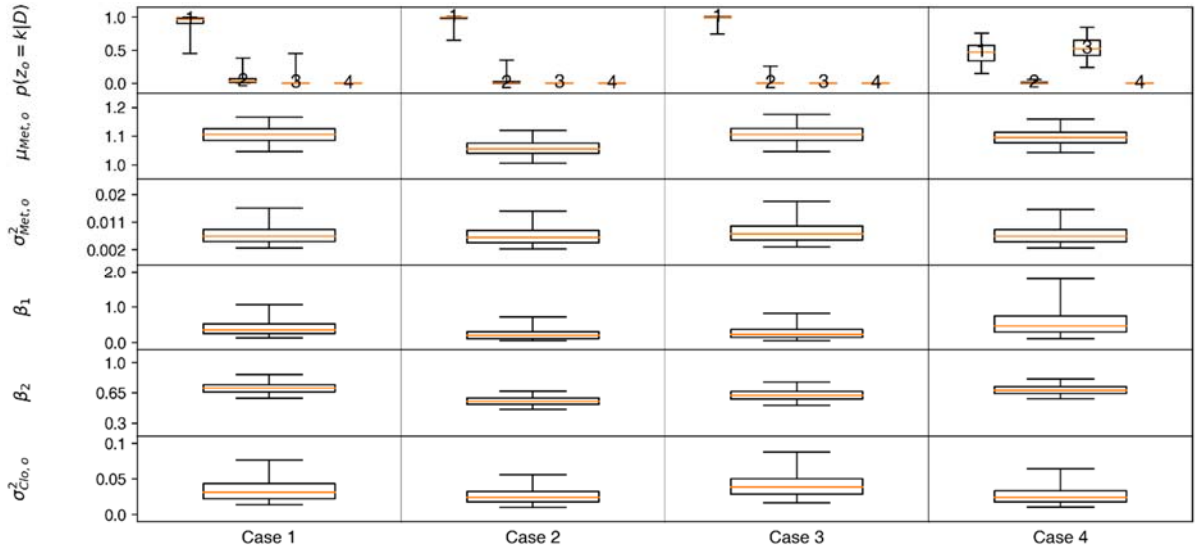

Figure 4.14. Induced cluster probability and personal parameters corresponding to profiles of the second row of Figure 4.13 (using four different sets of 6 data points).

4.4 Discussion

4.4.1 Importance of data efficiency and model complexity

Data-driven models, properly trained for each individual with adequate data, can predict occupant thermal preference, comfort, satisfaction or actions. However, collecting enough data can be a challenging task itself. Sanguinetti [61] reported that 77% of participants, who were asked

to use their participatory thermal sensing interface, submitted only 1-2 votes for six months; over the whole period, the mean number of votes per user was 2.23. This is an example of difficulties associated with collecting quantitatively enough data from each individual, and numbers will vary depending on conditions, interface type, etc. Data quality is also an important issue. Data-driven models require that data cover the entire space of interest (conditions). Models trained with data concentrated in specific areas of the space will probably lead to wrong predictions for other conditions. But if occupants are intentionally exposed to undesirable conditions to cover a larger space, we defeat the original purpose of preference learning: providing satisfactory conditions to each individual. The only exception is comparative preference learning [101], which is quite challenging for thermal preferences due to time required for thermal adaptation.

Therefore, the efficiency of a learning method in terms of required quantity and quality of data should be re-examined. One might argue that enough data can be collected over a long period of time. However, the final objective of learning is implementing the models into human preference-based control frameworks, and long learning periods are not practical for this purpose. In this regard, it is notable that the thermal preference learning method presented in this chapter, trained with limited but properly collected data, is more efficient than training a univariate multinomial logistic regression model, which is much simpler and theoretically requires less data.

Data efficiency is related with the model complexity, which is often explained with the number of free parameters (or the effective number of parameters) in the model. For a given training data set, a high-complexity model might over-fit the data and then it will not be able to predict future observations reliably (i.e., high variance). Conversely, to properly train a high-complexity model, a large dataset is needed (i.e., low data efficiency). This was the reason why the prediction performance of model 5 was lower than that of the others. One way to restrict model complexity is by reducing the number of parameters. However, an over-simplified model (e.g., using a linear model for a highly non-linear problem or using a univariate model for a multi-dimensional problem) may not be adequate to mimic the system (i.e., underfitting, high bias). Another way to control the model complexity is regularization, which means introducing additional information in the model to avoid overfitting.

In this regard, the Bayesian approach is powerful since we can introduce the additional information naturally by assigning informative priors. In our case, we encoded a lot of information over the whole learning process thanks to the benefit of Bayesian approach. More specifically, we

constructed the generalized model based on physical equations and introduced our prior knowledge of human thermal comfort and related variables in the model. In terms of learning new occupants, we use the generalized model as a prior for personalized models. In addition, we set informative priors to deal with unmeasured variables. These were ingredients that make our learning method efficient, although it is complex and considers multiple inputs, and it can be an example for future studies in this field.

4.4.2 Model updating for learning long-term variation effects

Previous studies [46,48,52] report that learning models should be continuously re-trained with updated datasets to capture long-term comfort/preference variation. Here, updating the training dataset means adding new data into it and removing old data from it. But is this always the best option?

If we could consider all the important variables in a model properly and measure or observe them, there would be no need to update the model. However, since that is not practically possible, we can simply ignore the unobserved variables (e.g., model 4) or assign a simple probability distribution for them (e.g., model 1). If these distributions do not change significantly, the predictions based on such methods would be satisfactory. Unfortunately, this is not the case. For example, suppose that a model was developed with the univariate multinomial logistic regression model (model 4) and trained with data collected during winter (i.e., "winter model"). In the summer, the occupant would change clothing and would prefer warmer conditions than those predicted by the "winter model". In this example, updating the model essentially means discarding the winter data and re-training the model with summer data (i.e., "summer model"), so removing and adding training data is meaningful.

However, this updating method has drawbacks: it requires collecting enough data with conditions causing dissatisfaction; plus, the model would need another updating after each "cycle" and so on. A promising alternative would be learning the variation of the distribution instead of discarding old data. If we know that this variation is highly correlated with a variable, e.g., correlation between clothing level and outdoor temperature, we can introduce that in the model as an input. Otherwise, we could set a hidden variable representing the state of the distribution in a model. Then, the model should be able infer the current state with limited data and make reliable predictions. Although learning the whole variation of distributions would take time, once it is done

properly, it does not need to be repeated. Finally, to avoid problems with high model complexity, it is possible to develop models with multilevel complexity, automatically unlocking the limited complexity of the current level as we gain more data.

4.4.3 An "ideal" model evaluation metric

As discussed in Section 4.3, evaluating models based on general performance metrics (e.g., AUC) is not always the best option. For the case of preference learning, there are two issues with using general metrics. First, it is highly probable that the test dataset distribution will be imbalanced (e.g., more than half of votes can be "no change"), which will negatively affect the reliability of the metric. Even in our experiment, which was designed to collect data under various conditions, data from some of the subjects were imbalanced. Second, costs for different misclassification cases are different (i.e., different costs to different cases in the confusion matrix), but general metrics do not consider the differences. For example, the cost for misclassifying an instance of "prefer warmer" as "prefer cooler" will be higher than the cost for misclassifying the same instance as "no change". In addition, different factors cause unequaled costs, e.g., occupant satisfaction cost and energy consumption cost and simply merging these costs into one measure is arguable.

A meaningful way to assess the prediction performance of a model is to quantify the anticipated benefit or cost of using the model within the context of the model application (i.e., the operating condition). This can be defined with a misclassification cost function and a class distribution Hern´andez-Orallo et. al. [102]. One way of estimating the cost is:

$$cost = \sum_{i=1}^{N} Q\left(y_i, y_{p,i}\right) \tag{4-23}$$

$$Q\left(y_i = k, y_{p,i}\right) = \frac{\pi_k}{N_k} \times C\left(y_i = k, y_{p,i}\right), \qquad k = 1,2,3 \tag{4-24}$$

where $y_{p,i}$ is the model prediction at instance i, $k = 1,2,3$ represents the classes (i.e., "prefer warmer", "no change", and "prefer cooler", respectively), π_k is a portion of each class in the operating condition, N is the number of test data, N_k is the number of test data for each class, and C is a misclassification cost function. The equation infers that model evaluation can be highly affected by the operating condition. To demonstrate how the anticipated cost can differ according to how we set the cost function, we use the following example. We compute the costs for two

personalized models of subject 2 from our dataset, developed based on methods 1 and 4 of Section 4.3.3 respectively, with three different cost matrixes. In this example, we define that the predicted class from a model at instance i is:

$$y_{p,i} = \underset{k}{\operatorname{argmax}}\, p\left(y_{p,i} = k | \mathbf{x}_{p,i}, \mathbf{Data}\right) \tag{4-25}$$

To simplify this example, we assume that the class distribution of the operating condition is equivalent to that of the test dataset. The cost at instance C can be determined based on the actual class y_i, the predicted class $y_{p,i}$, and a cost matrix. Figure 4.15 shows the three different cost matrixes we used for this example. Although we could not determine the exact cost (e.g., $ cost) for each case, if we determine the cost ratio between cases (i.e., relative importance), we can compute a normalized cost to compare models. In the first cost matrix, an equal cost (1) is assigned for misclassifying an instance of satisfied ("no change") to dissatisfied ("want warmer" or "want cooler") and vice versa. This implies that predicting one's satisfaction and dissatisfaction are equally important. A higher cost (4) is assigned for misclassifying an instance of "want warmer" or "want cooler" to each other considering the clear order between classes. In the second cost matrix, a cost of 1.9 is assigned for misclassifying a dissatisfied instance to satisfied, but a cost of 0.1 is used for the opposite case, i.e., correctly detecting dissatisfaction is much more important than detecting satisfaction. This approach can be used to design a controller that maximizes one's satisfaction (a satisfaction oriented cost matrix). The third cost matrix is the transpose of the second one (an energy-saving oriented cost matrix).

Equal

		Actual Class		
		Want warmer	No change	Want cooler
Predicted Class	Want warmer	0	1	4
	No change	1	0	1
	Want cooler	4	1	0

Satisfaction oriented

		Actual Class		
		Want warmer	No change	Want cooler
Predicted Class	Want warmer	0	0.1	4
	No change	1.9	0	1.9
	Want cooler	4	0.1	0

Energy-saving oriented

		Actual Class		
		Want warmer	No change	Want cooler
Predicted Class	Want warmer	0	1.9	4
	No change	0.1	0	0.1
	Want cooler	4	1.9	0

Figure 4.15. Three different cost matrixes.

Table 4.4. Computed cost with three different cost matrixes for personalized models of subject 2, developed based on models 1 and 4 as defined in Section 4.3.3.

Method	Cost		
	Equal	Satisfaction Oriented	Energy-saving Oriented
1	1.25 (0.66)	2.15 (1.47)	0.35 (0.59)
4	1.75 (1.20)	1.75 (1.51)	1.75 (1.18)

Table 4.4 shows the computed cost based on the three matrices. With the equal cost matrix, the anticipated cost of model 1 is lower than that of the model 4. The same result is obtained with the energy-oriented cost matrix, while model 4 is better when the satisfaction-oriented cost matrix is used. These results show that selecting the "best" model depends on the actual intend of application (operating condition), and that should be considered when the overall performance of models is evaluated.

If the operating condition is not known accurately, how can we select the "best" model? In such cases, we can calculate the expected cost over possible operating conditions $\boldsymbol{\psi}$ as: $\int cost(\boldsymbol{\psi})p(\boldsymbol{\psi})\,d\boldsymbol{\psi}$, where $p(\boldsymbol{\psi})$ is the probability distribution of the possible operating conditions Hern´andez-Orallo et. al. [102]. We can extend this concept to develop a new general metric, provided that we will define: (i) possible operating conditions and their distribution; and (ii) how to select the predicted class based on predictive probabilities (scores) from the model (Hern´andez-Orallo et. al. [102] used the term decision rule). We expect that a general metric will be developed based on future discussions and consensus about these issues so that researchers can evaluate and compare preference learning methods in a unified way.

4.5 Chapter conclusions

In this Chapter, a method for learning personalized comfort models in real buildings was introduced, where clothing level, metabolic rate and air speed cannot be measured.

The generalized model was revised considering two important issues: (1) inaccurately measured or estimated values for some variables in the training data (i.e., subset of ASHRAE RP-884 database used to train the model); (2) limited variation of thermal conditions in the training data. The revised model discovered 4 clusters of thermal preferences in the subset of ASHRAE RP-884 database. To develop personalized models without measured air speed, clothing level, and metabolic rate, hidden variables were introduced in the model structure.

A field study was conducted in private offices to validate the method and demonstrate a (human and physical) data collection process to properly train personalized preference models in the real world. The proposed method showed better prediction performance compared to previous methods (e.g., training a simple univariate multinomial logistic regression model, or using constant values for unobserved variables). In addition, our method provides better results when limited data are available, which is important for real world applications. Our Bayesian approach is powerful since we can introduce additional information by assigning informative priors –we can encode a lot of information over the whole learning process. This makes our learning method efficient, although it is complex and considers multiple inputs. It is notable that the thermal preference learning method presented in this paper, trained with limited but properly collected data, is more efficient than training a univariate multinomial logistic regression model, which is much simpler.

5. IMPLEMENTATION OF A SELF-TUNED HVAC CONTROLLER TO SATISFY OCCUPANT THERMAL PREFERENCES AND OPTIMIZE ENERGY USE

5.1 Overview

In this chapter, the objective is to develop a novel self-tuned HVAC controller that provides customized thermal conditions to satisfy occupant preferences while minimizing energy consumption, and to demonstrate its implementation in a real occupied open-plan office space (Section 5.2.1). In the self-tuned controller, the evolution of personalized thermal preference models (online-learning) (Section 5.2.2) and the delivery of thermal conditions with model predictive control (MPC-based HVAC operation) (Section 5.2.3) form a closed-loop. For the online-learning, we use a Bayesian clustering and online classification algorithm that has been extensively validated in our previous research by considering thermal comfort delivery conditions that are representative of typical office buildings [103,104]. To integrate these two parts into the self-tuned control loop, we propose a new algorithm that always provides a set of lower and upper operative temperature bounds for spaces (of both single and multiple occupancy) without tweaking the output of personalized comfort models nor solving computationally burdening multi-objective optimization (Section 5.2.4). We recruited nine occupants and implemented the self-tuned controller for 19 weekdays (Section 5.2.5). We present results with the self-tuned controller and evaluate the dissatisfaction level and energy consumption during the implementation period by comparing those with a baseline controller (Section 5.3). In addition to the experimental evaluation, we conduct a simulation study to demonstrate that users (e.g., occupants or building managers) can easily adjust the balance between the level of occupant satisfaction and energy consumption by changing a single parameter in the controller. In this way, decisions resulting in energy waste or dissatisfaction can be avoided and the energy is deployed where it is actually needed (Section 5.4).

5.2 Methodology

In this section, we present the development and implementation of a self-tuned controller in an actual open-plan office space conditioned with a radiant floor cooling system to evaluate its

performance in terms of occupant satisfaction and energy efficiency. The operation of the proposed self-tuned HVAC controller includes four processes (Figure 5.1) with two key modules that form a closed-loop: (i) collecting occupant feedback on the thermal conditions, (ii) developing/updating personalized thermal preference models based on daily feedback (learning module), (iii) updating the control bounds for the next day, and (iv) controlling the HVAC system with MPC given the updated operative temperature control bounds (MPC module). In the following sub-sections, we present the experimental details and the four processes of the controller operation.

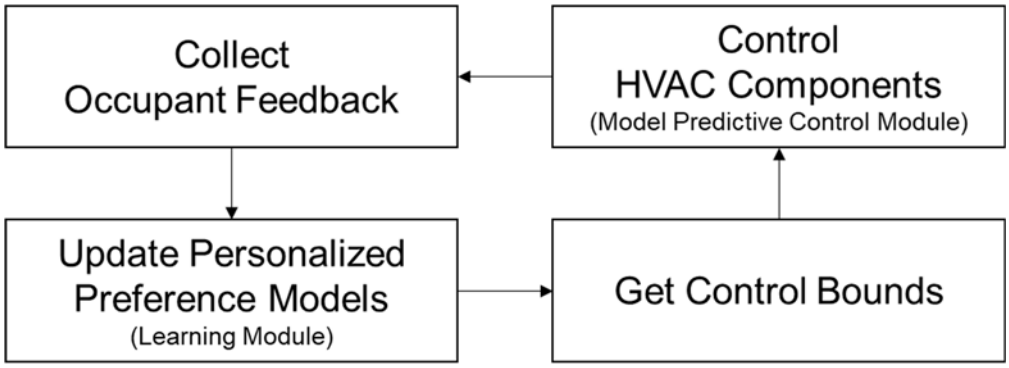

Figure 5.1. Sequence of processes in the self-tuned HVAC controller.

5.2.1 Office environment and sensor network

An open-plan office space (9.9 m by 10.5 m) was used as test-bed for this study. The building has a Building Management System (BMS) with Niagara/AX software framework and JACE controllers for the HVAC operation and data acquisition system. The space has a hydronic radiant floor system (Figure 5.2) and three wall diffusers for ventilation that are served from an Air Handling Unit (AHU). The radiant floor is separated into eight independently controlled loops so that localized thermal control can be provided to each sub-zone. RTD sensors (Digi-Key, 10K ohm, 1%) and thermocouples (Omega, T-type, ± 0.5°C) were installed in eight sections (0.6 m from the floor and on floor) to measure the air and slab surface temperatures (Figure 5.3, left). Ultrasonic flow meters (TUF-2000M, ± 1%) and thermocouples (Omega, T-type, ± 0.5°C) were attached and inserted at each pipe loop to monitor the cooling rate for each section (Figure 5.3, right). The incident solar radiation on windows was measured with a pyranometer (LI-COR 200-SL, resolution of 0.1 W/m2 and accuracy of 3%). A wireless data acquisition system (National Instruments) was deployed for the data collection.

Figure 5.2. Open-plan office space with radiant floor system and local control capabilities.

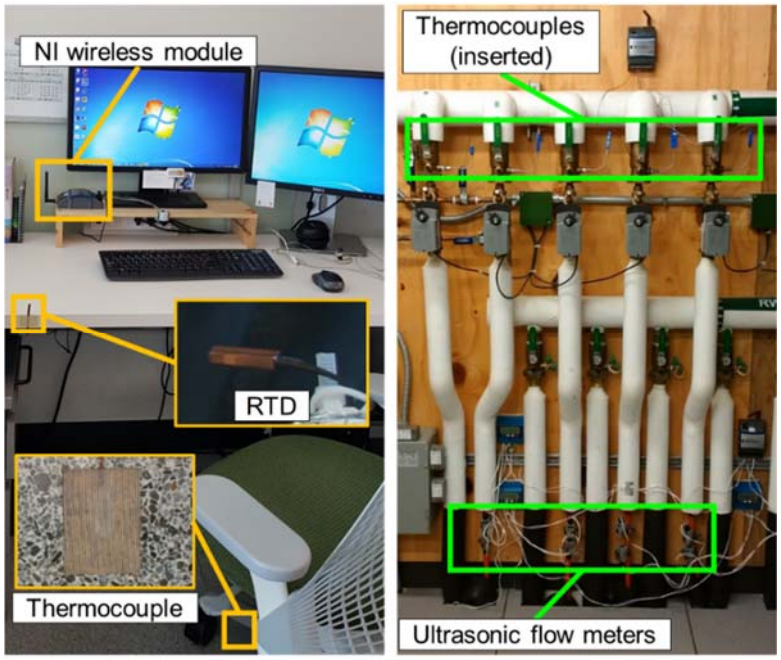

Figure 5.3. Local sensor network (left); pipe loops of the radiant floor system with temperature sensors and flow meters installed (right).

5.2.2 Learning module: personalized thermal preference modeling

The learning module, which learns thermal preferences of individual occupants by developing personalized preference models with their feedback, is the first key component of the self-tuned controller. To learn individuals efficiently, we use a Bayesian clustering and online

classification algorithm that combines two sub-problems: (i) discovery of thermal preference clusters using an existing dataset; (ii) online classification of new occupants', i.e., inferring their thermal preference cluster. The latter can be accomplished with much fewer observations than the development of different individual occupant models from scratch [104].

In this approach, first, we develop a generalized thermal preference model which classifies occupants into different clusters based on their thermal preference responses under different conditions, i.e., group of people having similar thermal preference characteristics. This generalized model includes sub-models, which explain the thermal preferences of people in each cluster. We constructed the model with the equations in Fanger's PMV model [1] and five additional parameters, and developed a probabilistic thermal preference model that is based on six well-known factors (air temperature, mean radiant temperature, air speed, humidity, clothing insulation level, and metabolic rate) and can be trained with limited data. The model was trained with a subset of ASHRAE RP-884 database [5] collected from air-conditioned office buildings in North America. Figure 5.4 shows the four sub-models in our generalized model [103]. Each of the plots is the predictive probability distribution of occupant thermal preference (i.e., "want warmer," "no change," "want cooler"). Solid lines represent the median values of the probabilities (i.e., median models), and shaded areas represent the associated 95% credible intervals (i.e., 2.5- and 97.5-quantiles of the predictive probability).

Second, we infer personalized models for new occupants using a mixture of sub-models in the generalized model based on their feedback. However, measuring air speed, clothing level and metabolic rate is difficult in real buildings. Hence, we introduced hidden personal parameters with informative priors to handle the uncertainty related to the unmeasured variables [103]. More specifically, we made the following assumptions: (i) the metabolic rate follows a truncated Gaussian distribution of which the mean and variance are hidden (ii) there is a linear relationship between air temperature and clothing level reflecting occupants' behavioral adaptation, and (iii) distribution of air speed follows the distribution in the subset of ASHRAE RP-884 database. We evaluated the performance of the proposed method with data collected from nine subjects (different from the occupants in this study) in a dedicated experiment. The proposed method showed better prediction performance compared to training a logistic regression model from scratch especially when the training data size is small, i.e., it is more efficient [103].

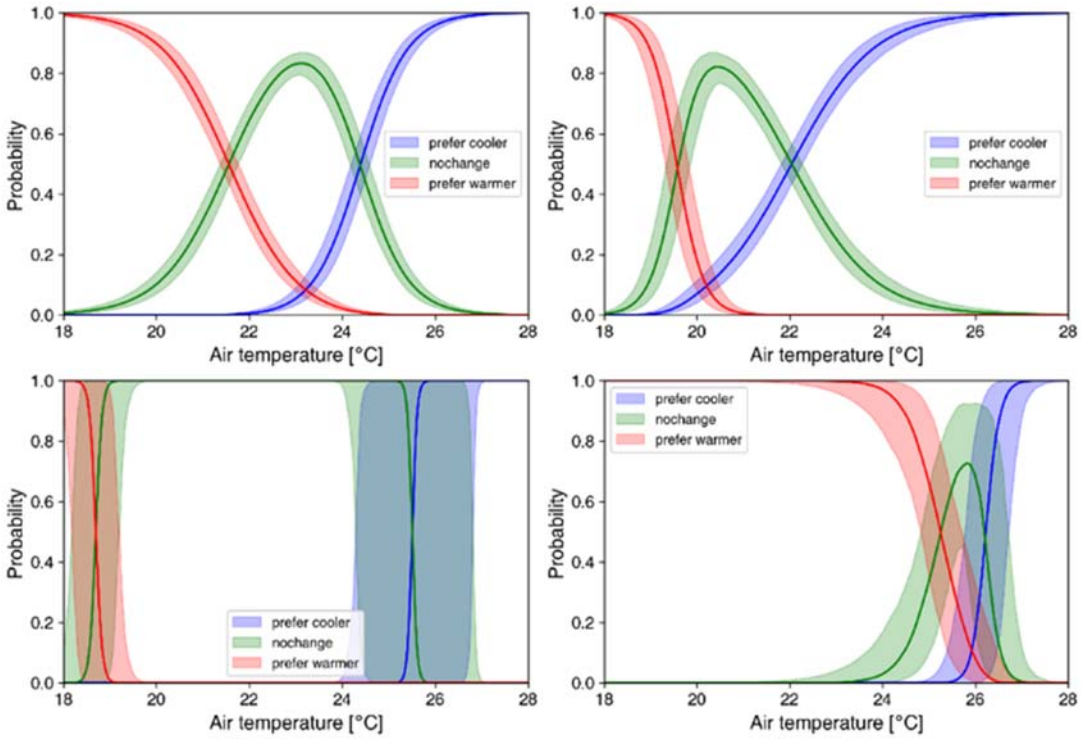

Figure 5.4. Predictive probability distributions calculated with sub-models for the four clusters. The displayed probability distributions were calculated with the following settings: MRT=air temperature, air speed=0.05 m/s, relative humidity=50 %, metabolic rate=1.2 met, and clothing level=0.6 clo.

Figure 5.5 shows the joint probability of learning a new occupant, o. Colored and white nodes in the figure correspond to observed and latent variables, respectively. y is the occupant thermal preference (i.e., "want warmer," "no change," and "want cooler"), E is the overall thermal stress level, and z is the thermal preference characteristic of the new occupant. T_{air}, MRT, RH, Spd, Met, and Clo represent air temperature, mean radiant temperature, air speed, humidity, clothing insulation level, and metabolic rate, respectively. $\boldsymbol{\theta}$ collects all the model parameters. E is predicted by the equations in PMV model with the five additional parameters, and y is predicted by a linear discriminant analysis (LDA) formulation. The index i labels each observation from the occupant. The variable **Data** is the training data used to develop the generalized model (i.e., the subset of ASHRAE RP-884 DB). In this study, we assume ${T_{\text{air}}}_o^{(i)} = \text{MRT}_o^{(i)} = {T_{\text{op}}}_o^{(i)}$ where T_{op} is the estimated operative temperature with measured air and floor surface temperatures. Since we do not measure Spd, Met, and Clo in the field experiment, we assign the probability distributions mentioned above with personal parameters $\boldsymbol{\beta}_o$. The posterior probability is all the parameters is:

$$p(z_o, \boldsymbol{\beta}_o, \boldsymbol{\theta} | \mathbf{y}_o, \mathbf{X}_o, \mathbf{Data}) \propto p(\mathbf{y}_o | \mathbf{X}_o, z_o, \boldsymbol{\beta}_o, \boldsymbol{\theta}) p(z_o | \boldsymbol{\theta}) p(\boldsymbol{\beta}_o) p(\mathbf{Data} | \boldsymbol{\theta}) p(\boldsymbol{\theta}) \quad (5\text{-}1)$$

where $\mathbf{y}_o = \left(y_o^{(1)}, \ldots, y_o^{(N)}\right)$, $\mathbf{X}_o = \left\{\mathbf{x}_o^{(1)}, \ldots, \mathbf{x}_o^{(N)}\right\}$, $\mathbf{x} = \left(T_{\mathrm{op}}, \mathrm{RH}\right)$, and $p(\mathbf{Data}|\boldsymbol{\theta})$ is the data likelihood we defined to develop the generalized model. We can predict the thermal preference of the new occupant $\left(y_p\right)$ under certain conditions $\left(\mathbf{x}_p\right)$ by employing the sum rule of probability theory:

$$p\left(y_p | \mathbf{x}_p, \mathbf{y}_o, \mathbf{X}_o, \mathbf{Data}\right) = \iint \sum_{z_o} p\left(y_p | \mathbf{x}_p, \mathbf{y}_o, \mathbf{X}_o, \mathbf{Data}, z_o, \boldsymbol{\beta}_o, \boldsymbol{\theta}\right) p(z_o, \boldsymbol{\beta}_o, \boldsymbol{\theta} | \mathbf{y}_o, \mathbf{X}_o, \mathbf{Data}) \, d\boldsymbol{\beta}_o d\boldsymbol{\theta} \quad (5\text{-}2)$$

The details of Eq. (5-1) and (5-2) are presented in our previous papers regarding the learning module [103,104].

We update the personalized thermal preference profiles every day after 6 p.m. with sensor data for indoor environment variables, and occupant feedback expressed through their preference votes, such as “want warmer,” “want cooler,” “no change.”

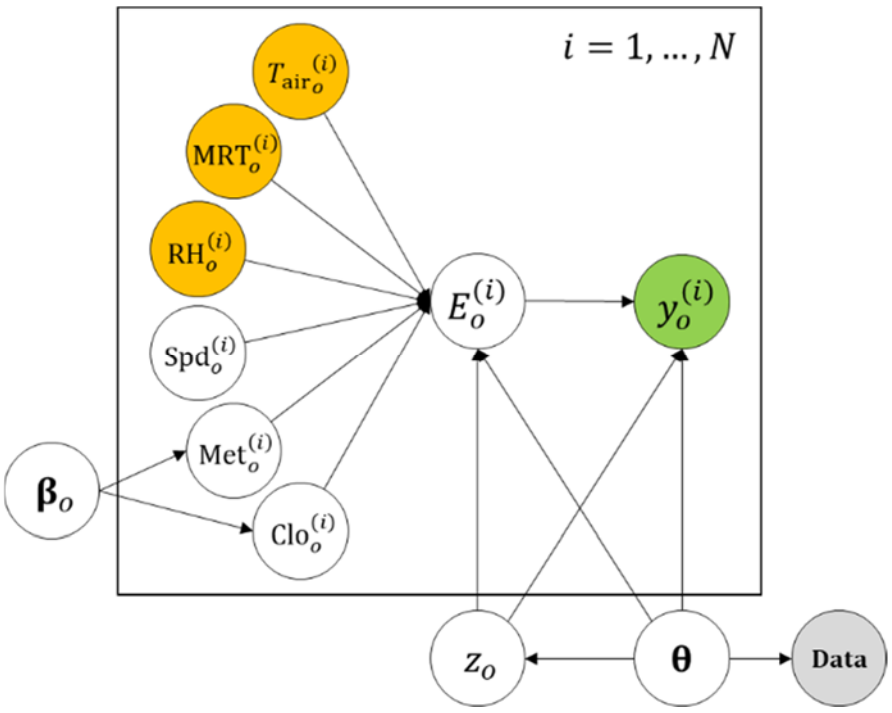

Figure 5.5. Graphical representation of the joint probability for the personalized thermal preference models.

5.2.3 Model predictive control module

In this section, we present the model predictive control module used in the self-tuned HVAC controller. First, we discuss the HVAC system, the control-oriented building model, and the optimization formulation. Subsequently, we explain the data communication and implementation settings.

Building model

A data-driven grey-box building model is constructed based on the state-space formulation as:

$$x[n+1] = A_d x[n] + B_{d,w} w[n] + B_{d,u} u[n] \tag{5-3}$$

Once this state-space formulation is stacked in time series, the control input ($\mathbf{u}$) and temperature trajectories ($\mathbf{X}$) are in an explicit linear relation as:

$$\underbrace{\begin{bmatrix} x[1] \\ x[2] \\ \vdots \\ x[n] \end{bmatrix}}_{\mathbf{X}} = \underbrace{\begin{bmatrix} A_d \\ {A_d}^2 \\ \vdots \\ {A_d}^n \end{bmatrix}}_{\Omega_x} \underbrace{x[0]}_{\mathbf{X_0}} + \underbrace{\begin{bmatrix} B_{d,w} & 0 & \cdots & 0 \\ A_d B_{d,w} & B_{d,w} & \cdots & 0 \\ \vdots & \vdots & \ddots & \vdots \\ {A_d}^{n-1} B_{d,w} & {A_d}^{n-2} B_{d,w} & \cdots & B_{d,w} \end{bmatrix}}_{\Omega_w} \underbrace{\begin{bmatrix} w[0] \\ w[1] \\ \vdots \\ w[n-1] \end{bmatrix}}_{\mathbf{w}} + \underbrace{\begin{bmatrix} B_{d,u} & 0 & \cdots & 0 \\ A_d B_{d,u} & B_{d,u} & \cdots & 0 \\ \vdots & \vdots & \ddots & \vdots \\ {A_d}^{n-1} B_{d,u} & {A_d}^{n-2} B_{d,u} & \cdots & B_{d,u} \end{bmatrix}}_{\Omega_u} \underbrace{\begin{bmatrix} u[0] \\ u[1] \\ \vdots \\ u[n-1] \end{bmatrix}}_{\mathbf{u}} \tag{5-4}$$

which is suitable for implementation in the optimization algorithm. The state and input matrix (A_d and B_d) consist of estimate parameters including the thermal capacity and resistance, as well as the coefficient multiplied to the heat flux input for the transmitted solar radiation and internal heat gain. The model includes five states: T_{cav} and T_{air} represent the cavity and air temperature, T_{sur}, T_{so}, and T_{si} represent the temperature of the slab surface, slab core where the pipe is located, and slab sink including the insulation layer, respectively. The cooling rates from the AHU (Q_{AHU}) and radiant floor system (Q_{rad}), are controlled inputs to T_{air} and T_{so} respectively. The exogenous disturbances from the internal heat gains (equipment, lighting, and people), Q_{int}, are multiplied with coefficients β_{air} and β_{sur} and are inputs to T_{air} and T_{sur}. The incident solar radiation measured on the exterior of the south façade (Q_{sol}) multiplied with coefficients α_{cav}, α_{air}, α_{sur}, is used as an input to T_{cav}, T_{air}, and T_{sur}.

The parameter estimation was carried out with a distributed system identification approach [105]. In this method, the zone is disassembled into sub-systems. To ensure sufficient excitation, cooling was provided to alternate floor sections for about six to twelve hours and the minimum

surface temperature for the floor was 18~19 °C. The sub-system models were initially estimated in parallel, reducing the scale of the estimation problem, and then integrated using the dual decomposition method [105]. The structure of the integrated model consists of 33 capacitances and 64 resistances (33C64R) with one boundary temperature which is the outdoor air temperature. Figure 5.6 shows only a portion of the model by excluding the repeated structure for simplicity. We used data collected for 17 days to estimate (with data of 5 days) and validate (with the rest of the data) the building model. The Root Mean Square Error (RMSE) during the estimation period for the air and slab surface temperature in each section ranges from 0.43 to 0.58 °C, and from 0.45 to 0.68 °C, respectively. This accuracy is considered to be reasonably good considering the complexity of the model. The details of the building model are presented in [105].

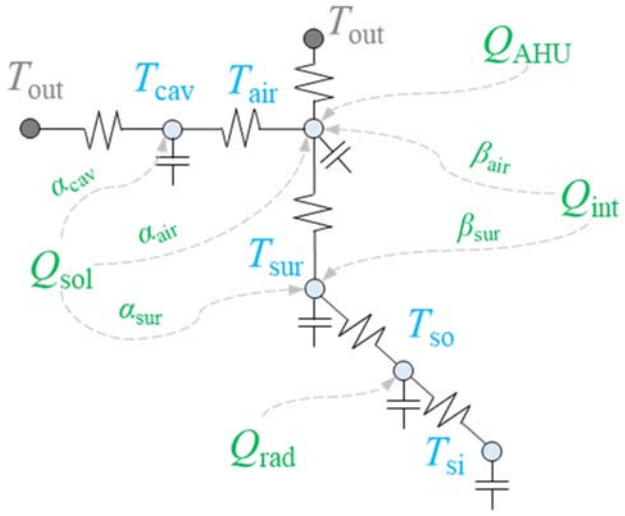

Figure 5.6. Grey-box model structure.

HVAC system and objective function

The cooling source in the actual test-bed is provided from the campus plant. However, because this type of configuration is not usual for typical office buildings, we assume that the chilled water is supplied by an air-cooled chiller to further generalize results. For this study, an air-cooled chiller model (Trane CGAM20) from EnergyPlus engineering reference is used. Its nominal capacity ($Q_{\mathrm{ref,Cap}}$) is 68.9 kW and it is scaled down to 8 %. The coefficient of performance ($C_{\mathrm{ref,COP}}$) is 2.67.

The objective function is the electricity consumption of the chiller, f_{chiller}, as:

$$\min f_{\text{chiller}}(\mathbf{u}) \tag{5-5}$$

subject to

$$\begin{bmatrix} \mathbf{C_T} \cdot \mathbf{\Omega_u} \cdot \mathbf{f_{cap}} \\ \vdots \end{bmatrix} \mathbf{u} \leq \begin{bmatrix} \mathbf{T_{bound}} - \mathbf{C_T} \cdot \left(\mathbf{\Omega_T} \cdot \mathbf{T_0} + \mathbf{\Omega_w} \cdot \mathbf{w} \right) \\ \vdots \end{bmatrix} \tag{5-6}$$

where

$$\begin{cases} f_{\text{chiller}} = f_{\text{Cap}} \cdot f_{\text{COP}} \cdot f_{\text{PLR}} \\ f_{\text{Cap}} = Q_{\text{ref,Cap}} \cdot \text{Curve}_{\text{biquad}}\left(T_{\text{leaving}}, T_{\text{outdoor}}\right) \\ f_{\text{COP}} = \dfrac{1}{C_{\text{ref,COP}}} \cdot \text{Curve}_{\text{biquad}}\left(T_{\text{leaving}}, T_{\text{outdoor}}\right) \\ f_{\text{PLR}} = \text{Curve}_{\text{quad}}\left(\dfrac{Q_{\text{load}}}{f_{\text{Cap}}}\right) = \text{Curve}_{\text{quad}}\left(\text{PLR}\right) \end{cases} \tag{5-7}$$

f_{Cap}, f_{COP}, and f_{PLR} represent the capacity, coefficient of performance (COP), and part load ratio (PLR), respectively. The fan and pump electricity use is neglected. The decision variable $\mathbf{u}$ is the Part Load Ratio (PLR) of the chiller. The dimension of the controlled input vector is 48 for a 24hr prediction horizon with 30 min time-step. The capacity and COP curves are biquadratic and require two control inputs. The leaving water temperature (T_{leaving}) is fixed at 13 °C which yields a quadratic polynomial with the outdoor air temperature known based on weather forecast. The resulting optimization problem has a convex form with linear inequality constraints. The first constraint represents the temperature bounds of the conditioned zone; $\mathbf{T}_{\text{bound}}$ is the upper or lower temperature bounds, and $\mathbf{C_T}$ is the matrix multiplied to all states to extract the target temperature states. For $\mathbf{T}_{\text{bound}}$, we apply eight sets of upper and lower bounds computed with personalized preference models to occupied hours (8 a.m. – 6 p.m.) and use 27 °C and 15 °C respectively to non-occupied hours. Additional bounds are used for certain states of the system, for example, the slab temperatures in the radiant system. The last constraint is set for the capacity of the HVAC source. $\mathbf{\Omega}$ represents the predefined matrices as shown in Eq. (5-4). This constraint quadratic programming is solved with quadprog in MATLAB environment. If the solver cannot find the optimal solution with $\mathbf{T}_{\text{bound}}$, we decrease the highest lower bound (among eight lower bounds for the eight sections) or increase the lowest upper bound (among eight upper bounds) for occupied hours by 0.5 °C, alternately, until it finds the solution.

Data communication

A schematic for the MPC implementation is shown in Figure 5.7. MPC calculations are performed in a server computer with MATLAB that has access to weather forecast data for 24 hours prediction. The optimal cooling rates are calculated and sent to Niagara server through Modbus communication. Then the valves in the radiant floor system are activated to satisfy the signal in each loop for a given time-step, 30 min. After each time-step, using sensor data for the zone and slab temperatures, the control and exogenous input are sent to the server computer, for the state estimation by the Kalman filter.

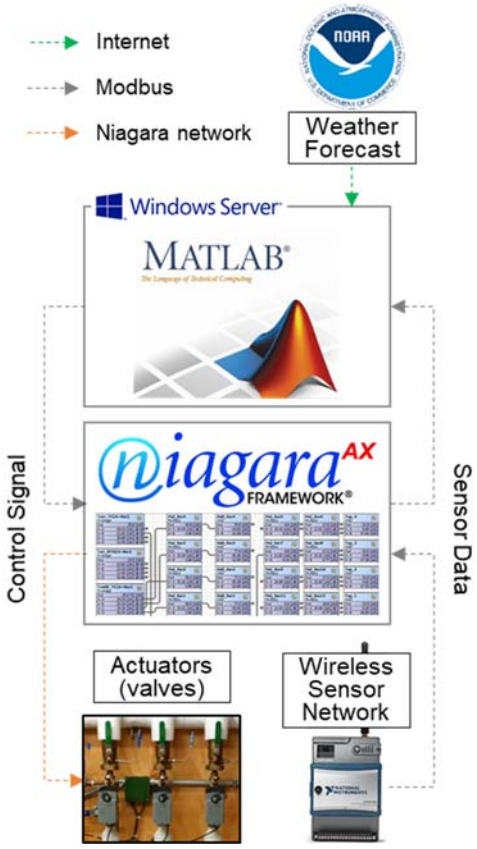

Figure 5.7. Data communication for MPC.

Implementation settings

In this section, we present information on disturbances and constraints used for the MPC implementation. For the disturbance prediction, the occupant and equipment heat gains are set to 65 and 50 W based on ASHRAE Standard 55 [7] and history data from the test-bed. The occupancy schedule is from 8 a.m. to 6 p.m. The air system provides ventilation by regulating the supply air

temperature to the average value of the lower and upper operative temperature bounds. The relative humidity of the zone is set to 55 % via the cooling coil control in AHU to eliminate the potential risk for condensation on the floor due to the low surface temperature. This requires additional conditioning, which is not considered in the MPC algorithm.

The operative temperature is a convex combination of the air and Mean Radiant Temperature (MRT). In this study, it is calculated using the measured air and slab surface temperatures as the air flow rate is less than 0.2 m/s [7]. A dedicated experiment was carried out to determine the weighting coefficients of the air and slab surface temperature which were found to be 0.77 and 0.23 [106].

The limit of the maximum difference between the air and slab surface temperature is set to be 7 °C [107,108], and the low-bound of the slab surface temperature is set to be 15 °C [109] to eliminate potential thermal discomfort of the occupants. The maximum available cooling capacity was set to be 5 kW based on maximum water flow rate of 12 gallon per minute and 15 °C minimum slab surface temperature.

5.2.4 Integrating preference learning and MPC: Operative temperature control bounds

To bridge the learning and MPC modules, we need to determine a set of lower and upper operative temperature control bounds using the personalized thermal preference models. The best set of lower and upper control bounds ($T_{\text{lb}}^*, T_{\text{ub}}^*$) minimizes the operational cost during the control period. Here, the cost includes both energy consumption and occupant satisfaction. Since we do not know the actual operational cost before applying the control bounds, we choose a set of control bounds ($T_{\text{lb}}, T_{\text{ub}}$) minimizing the expected cost as:

$$(T_{\text{lb}}^*, T_{\text{ub}}^*) = \underset{T_{\text{lb}}, T_{\text{ub}}}{\operatorname{argmin}} \mathbb{E}[f(T_{\text{lb}}, T_{\text{ub}})] \tag{5-8}$$

where $f(T_{\text{lb}}, T_{\text{ub}})$ is the cost with a set of control bounds T_{lb} and T_{ub}. We simplify this function by (i) defining the meaning of choosing a set of control bounds, and (ii) introducing a cost matrix C (Figure 5.8) to make the optimization feasible. Choosing a set of control bounds represents our expectation, $\hat{y}$, that the target occupant(s) would be satisfied within the bounds as:

$$\hat{y}(T_{\text{op}}, T_{\text{lb}}, T_{\text{ub}}) = \begin{cases} 1, & T_{\text{ub}} \leq T_{\text{op}} \\ 2, & T_{\text{lb}} < T_{\text{op}} < T_{\text{ub}} \\ 3, & T_{\text{op}} \leq T_{lb} \end{cases} \tag{5-9}$$

where $\hat{y} = 1, 2, 3$ represent “want cooler,” “no change,” and “want warmer,” respectively.

The cost matrix C defines costs for different misclassification cases. For example, if a person wants cooler conditions (y= 1), and the controller expects the person would want no change ($\hat{y} = 2$), then the misclassification cost for the instance is a (element $C_{1,2}$). We assign a higher cost (4) for misclassifying an instance of "want warmer" or "want cooler" to each other considering the clear order between classes.

		Predicted Class		
		Want cooler	No change	Want warmer
Actual Class	Want cooler	0	a	4
	No change	$2-a$	0	$2-a$
	Want warmer	4	a	0

Figure 5.8. Cost matrix for the calculation of operative temperature control bounds.

Eq.(5-7) can then be simplified to:

$$(T_{\text{lb}}^{*}, T_{\text{ub}}^{*}) = \underset{T_{\text{lb}}, T_{\text{ub}}}{\operatorname{argmin}} \int \sum_{y=1}^{3} C_{y,\hat{y}(T_{\text{op}}, T_{\text{lb}}, T_{\text{ub}})} p\left(y \middle| T_{\text{op}}, \text{RH}, \mathbf{y}_o, \mathbf{X}_o, \mathbf{Data}\right) p\left(T_{\text{op}}\right) dT_{\text{op}} \tag{5-10}$$

where $p\left(y \middle| T_{\text{op}}, \text{RH}, \mathbf{y}_o, \mathbf{X}_o, \mathbf{Data}\right)$ is the predictive distribution (Eq. (5-2)) of the target occupant personalized model, given T_{op} and RH, and $p\left(T_{\text{op}}\right)$ is the probability distribution of operative temperature. Here, we assume: (i) a uniform distribution for $p\left(T_{\text{op}}\right)$ for T_{op} between 15 – 29 ℃, and (ii) RH is 55 % (the relative humidity setpoint of AHU). This approach always gives the optimal control bounds regardless of the personalized model's shape.

In Figure 5.8, the parameter a controls the balance between the importance level of occupant satisfaction vs. energy consumption, i.e., the personalized comfort-energy tradeoff. Here, a should be greater than 0 and less than 2 to make the cost of misclassification always positive. If we use higher a, i.e., higher cost for misclassifying a dissatisfied instance as satisfied, but lower cost for the opposite case, it means that correctly detecting dissatisfaction is more important than detecting satisfaction. This will provide conservative control in terms of occupant satisfaction. Conversely, lower a will result in higher energy savings. Figure 5.9 shows how a modulates the control bounds

with a personalized model: lower/higher a results in wider/narrower control range, respectively. In our experimental implementation, we set $a = 1$.

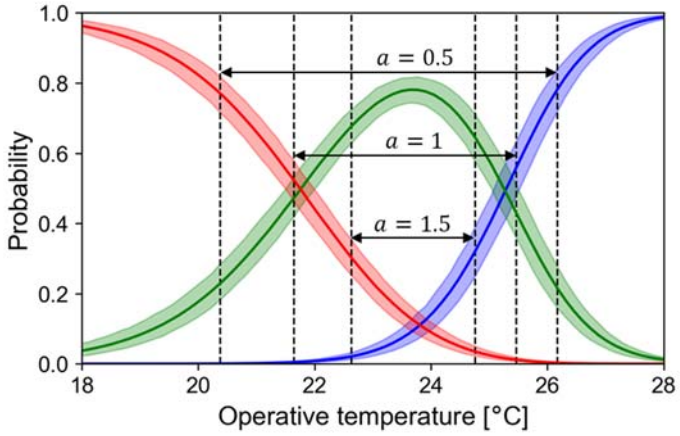

Figure 5.9. Three different control bounds with different a's.

We can easily extend this approach to calculate the optimal control bounds for a space shared by multiple occupants but conditioned by one radiant floor loop as:

$$(T_{\text{lb}}^*, T_{\text{ub}}^*) = \underset{T_{\text{lb}}, T_{\text{ub}}}{\operatorname{argmin}} \int \sum_{o=1}^{O} \sum_{y=1}^{3} C_{y,\hat{y}(T_{\text{op}}, T_{\text{lb}}, T_{\text{ub}})} p\left(y \middle| T_{\text{op}}, \text{RH}, \mathbf{y}_o, \mathbf{X}_o, \mathbf{Data}\right) p\left(T_{\text{op}}\right) dT_{\text{op}} \qquad (5\text{-}11)$$

where o means each occupant in the space.

5.2.5 Experimental implementation of self-tuned controller

We implemented a "baseline" and the self-tuned controller in the open plan office during August-October 2018. Here, the "baseline" controller is the MPC module with a set of default control bounds, i.e., no self-tuning with the learning module. We calculated the default control bounds, (21.1 °C and 25.5 °C), based on the generalized preference model with Eq. (5-9) and it was applied to all the eight sections. Note that the default control bounds were not set ad hoc, but they were the best option available before observing any data from the occupants, i.e., best option based on our prior knowledge.

Nine occupants, 22-33 years old, not familiar with this research, were recruited for the study. The feedback collection took place during weekdays between 9:00 a.m. and 6:00 p.m. Based on their meeting and work schedule, the occupants could enter and leave the office without restriction and performed their usual workload (computer-related work, reading, writing, etc.). Each occupant

participated in the experiment for a minimum of 16 days to a maximum of 25 days depending on his/her availability. The study was approved by the Institutional Review Board (IRB Protocol #: 1503015873).

The occupants reported their thermal preference every hour they were present in the office with the following survey question provided via a webpage: “How satisfied are you with current thermal conditions?” They could select one of the three answers: “I prefer warmer” / “I prefer cooler” / “I am satisfied with current conditions.” To ensure thermal adaptation, the occupants were asked to take the first survey one hour after their first (and intermediate) arrivals in the office. The desk location of each participant is shown in Figure 5.10, where the subject number and corresponding radiant floor loop section are marked. The subject numbers were used to record and track the individual thermal preference. The local air and floor surface temperature near the occupants were measured as described in Section 5.2.1.

For the first five days in August, the baseline controller was used. After this period, we implemented the self-tuned controller for 19 weekdays. Personalized preference models of the occupants were updated based on their daily feedback. Subsequently, the local control bounds in each thermal zone were updated with personalized preference models of occupants in that zone. Finally, we applied the baseline controller again for three days, for further data collection and validation checks.

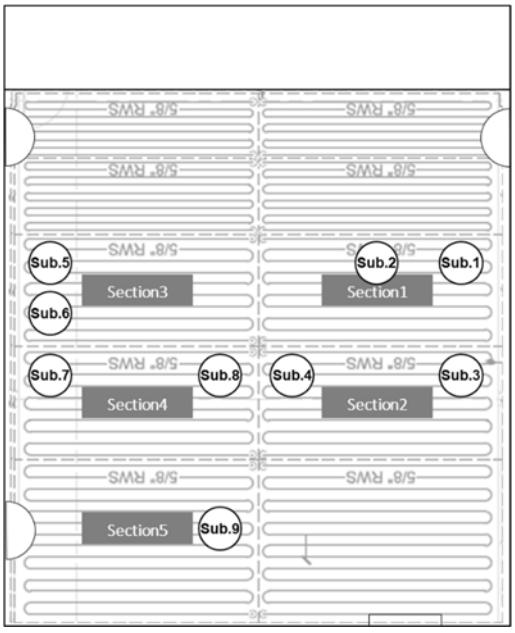

Figure 5.10. Space floor plan with occupant location and radiant floor control section.

5.3 Experimental results

Figure 5.11 shows the evolution of the upper and lower control bounds of operative temperature over the period with the self-tuned control, for each radiant floor section. Day 0 means the last day of the first baseline period. Subject 9 was not in the office for the first four days. The control bounds evolve fast during the first three days and converge after 7 to 13 days. The converged control ranges of sections 1, 2, and 5 are significantly lower than the default range, while that of section 3 is only wider for the low temperature side. The control range of section 4 is similar to the default.

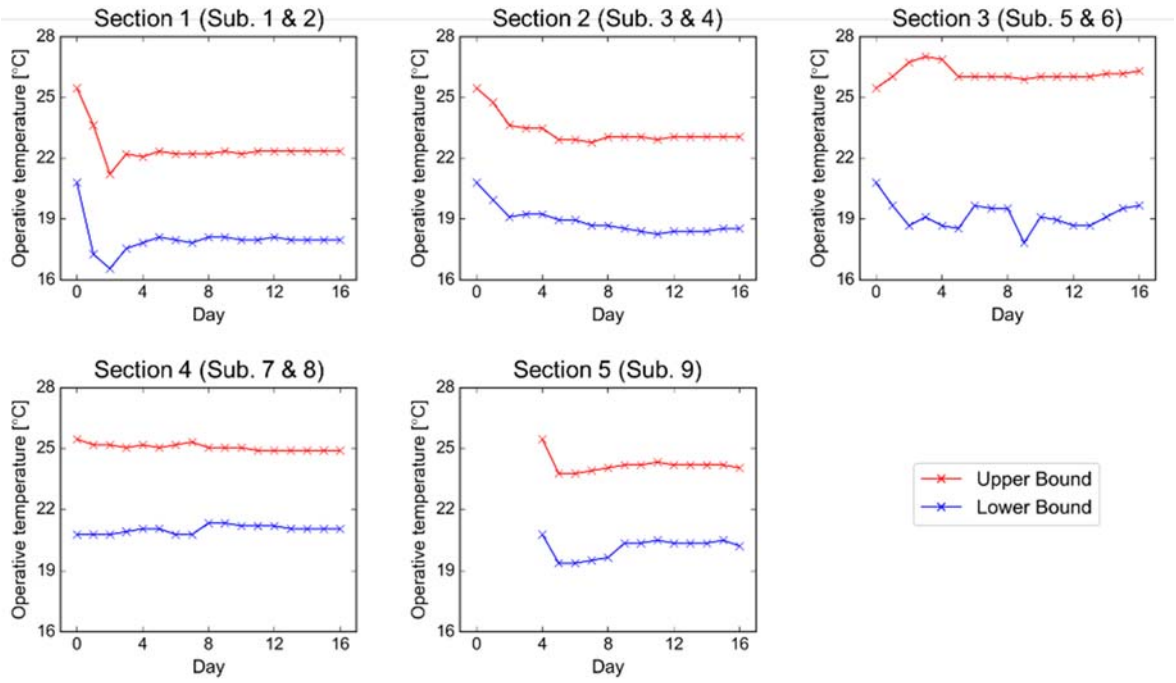

Figure 5.11. Evolution of the control bounds during the period with the self-tuned controller.

Figure 5.12 shows the personalized preference profiles of the nine subjects at the last day of the control implementation. The profiles developed with feedback from subjects 1, 2, 3, and 4 indicate that they preferred cooler conditions, i.e., green curves peak at lower temperatures compared to other subjects (and lower control range in sections 1 and 2 of Figure 5.11, corresponding to these subjects). Note that we computed the control bounds for shared spaces using Eq. (5-10). An interesting case, indicating the effect of individual preferences, is presented for subjects 7 and 9. Figure 5.12 shows very similar preference profiles for these two subjects,

however Figure 5.11 shows that the control range for subject 7 (seated in section 4) is higher than that of subject 9 (seated in section 5). The reason is that subject 7 shared section 4 with subject 8 who preferred relatively warmer conditions, as seen from Figure 5.12.

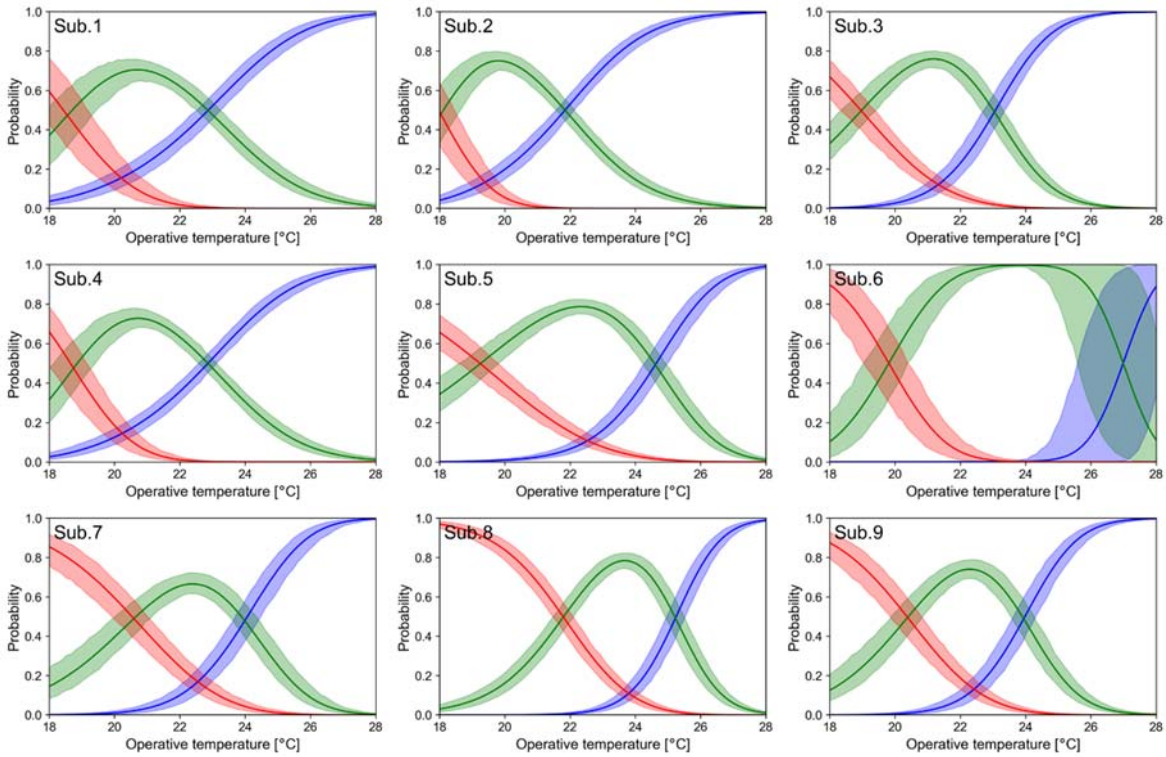

Figure 5.12. Personalized thermal preference profiles of the nine subjects.

The upper and lower control bounds and operative temperature of the five sections during a day after the bounds converged are presented in Figure 5.13. We can observe that the operative temperatures were low in the morning and gradually increased over time. This is because, the MPC controller pre-cooled the space in the morning when outdoor temperature is low, and the COP of the chiller is high to minimize cooling energy consumption. Theoretically, if cooling is required during the entire day, we expect that the temperature trajectory controlled by an optimal controller reaches the upper bound, if there are no other constraints. Nevertheless, in section 3, 4, and 5, the temperature did not reach the upper bounds. The reason was that the thermal dynamics of the five sections are interconnected (adjacent zones) and sections 1 and 2 had lower upper bounds.

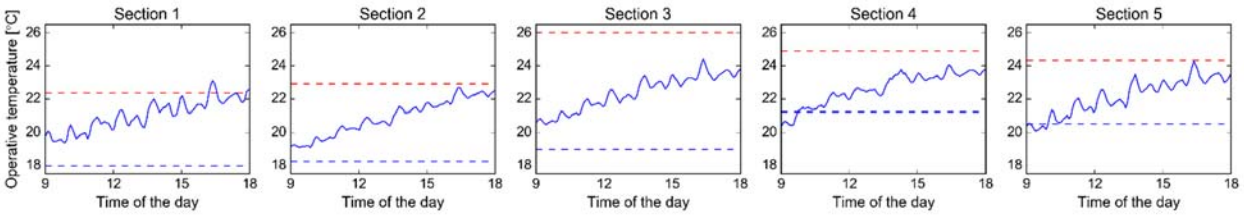

Figure 5.13. Operative temperature trajectory of the five sections in the office with the self-tuned controller. Red and Blue dashed lines represent operative temperature upper and lower bounds respectively.

Figure 5.14 shows the upper/lower control bounds and the operative temperature trajectory of section 1 in two different days with the default control bounds and self-tuned (converged) control bounds, respectively. Blue triangles and green circles represent "want cooler" and "no change" votes from subject 1, whose desk is in section 1. With the default control bounds, the subject mostly answered "want cooler," while the subject was satisfied with the converged control bounds and lowered operative temperature.

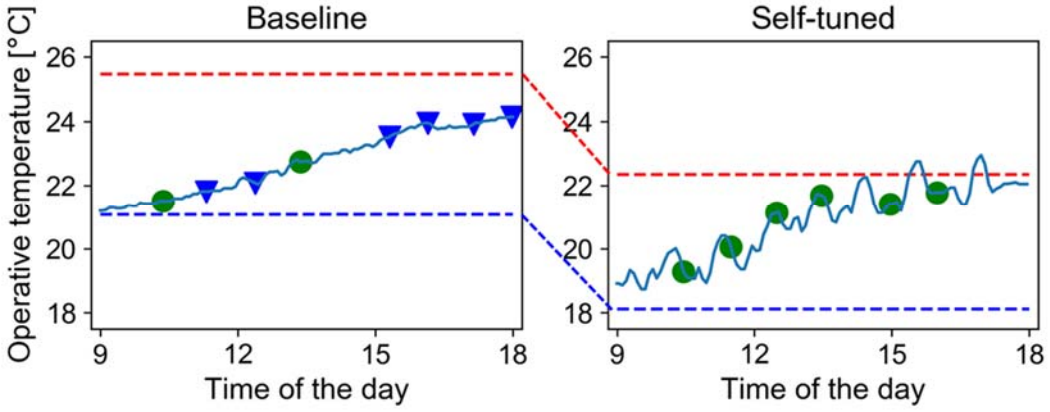

Figure 5.14. Thermal preference votes from subject 1 in two different days with the default control bounds and self-tuned control bounds. Blue triangles and green circles represent "want cooler" and "no change" votes, respectively. Dashed lines represent operative temperature upper and lower bounds.

To objectively evaluate the controller's performance in terms of occupant satisfaction, we compute a quantity which represents the level of dissatisfaction based on subjects' preference votes as:

$$\text{Dissatisfaction Level} = \frac{\text{number of dissatisfaction votes of all the subjects}}{\text{number of votes of all the subjects}} \tag{5-12}$$

where dissatisfaction votes include both "want warmer" and "want cooler."

Blue dots in Figure 5.15 indicate the daily dissatisfaction level over the entire period. Due to the high noise from the randomness in preference votes and the differences in the subjects' occupancy, the decreasing trend in dissatisfaction levels during the period with the self-tuned controller is not as visible. Therefore, a Bayesian Beta regression was conducted to investigate this further. The reason of using a Beta regression instead of a linear regression is that the dependent variable, dissatisfaction level, is within the unit interval. Details of the beta regression are presented in Appendix D. In Figure 5.15, the blue solid line and the orange shaded area respectively represent the median and 95% credible interval of mean of beta distributions (μ in Eq. (D-2)) over the self-tuned control period. The wider green shaded area represents the full uncertainty of the dissatisfaction level, and the blue dots indicate the dissatisfaction level calculated with the actual votes. This analysis helps to clearly realize the decreasing trend in dissatisfaction when the self-tuned controller is employed, compared to the baseline MPC control. Figure 5.16 shows the posterior distribution of the slope parameter of the Beta regression (β_1 in Eq. (D-2)). The posterior probability of the slope parameter being positive is nearly zero, which means that there is a high probability that there is a decreasing trend, i.e., the proposed controller improved the level of occupant satisfaction over time.

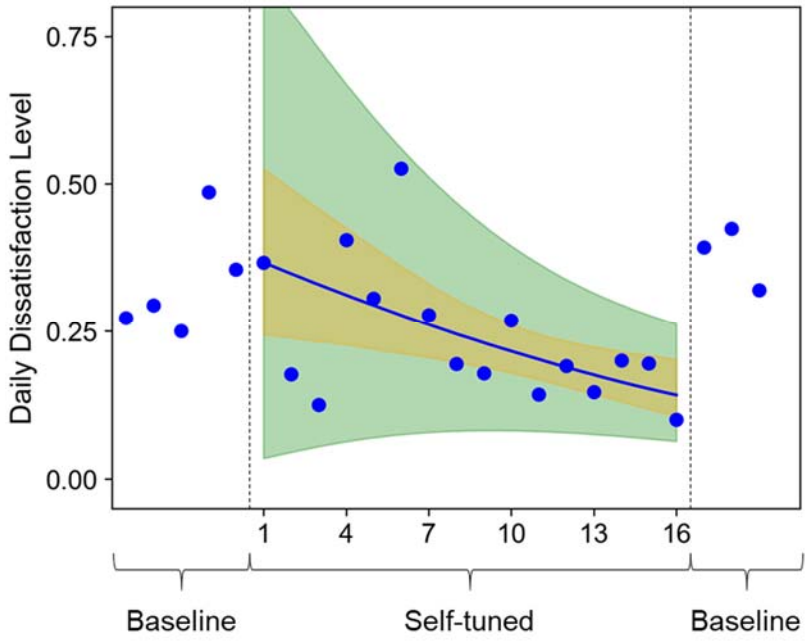

Figure 5.15. Daily dissatisfaction level during the entire period (blue dots) and a Beta regression model for the period with the self-tuned controller (blue line and shaded areas).

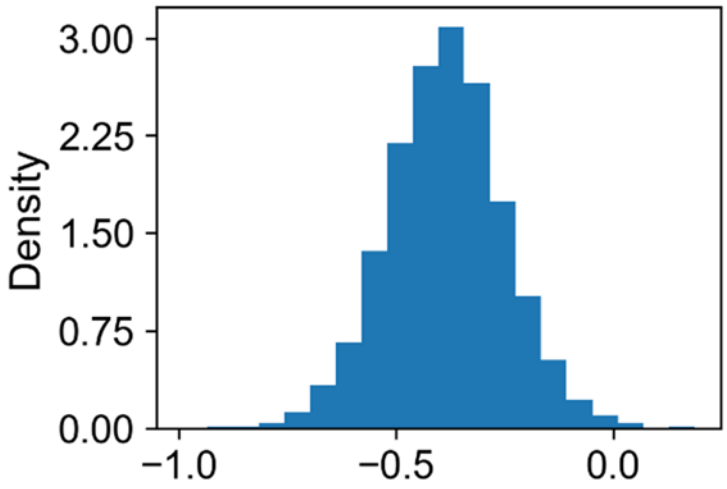

Figure 5.16. Posterior probability distribution of the slope parameter in the Beta regression model.

The distributions of the daily dissatisfaction level during the baseline MPC controller period and the proposed self-tuned controller period is shown in Figure 5.17. We used data from only the last eight days of the proposed controller implementation, to evaluate the dissatisfaction level with the converged control bounds. As shown in the figure, there is a notable difference in the dissatisfaction level between the two periods. This comparison also supports that the proposed controller improved the level of occupant satisfaction with the thermal environment.

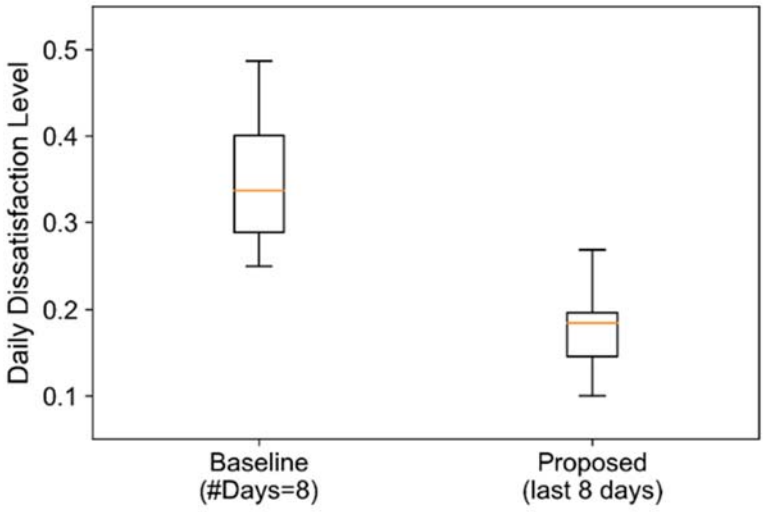

Figure 5.17. Distributions of the daily dissatisfaction level during two periods. Baseline refers the period with the baseline controller; Proposed refers to the last eight days of the period with the self-tuned controller.

In terms of cooling energy consumption, the results of Figure 5.11 indicate that the proposed controller would consume more cooling energy, since in general the self-tuned controls operative temperature bounds are lower than the default bounds. However, since cooling energy consumption is affected by outdoor temperature, a direct comparison between the two periods is not accurate –the impact of outdoor temperature should be considered. To overcome this problem, we quantified the effect of using one of the two controllers on energy consumption during the summer period by: (i) developing linear models for the relationship between the energy consumption and the mean outdoor temperature during the two control periods, and (ii) integrating out the mean outdoor temperature from the models. Details of this analysis are presented in Appendix E while Figure 5.18 shows the predictive probability distribution of the daily energy consumption with each controller induced by this analysis. We can observe that the proposed controller could increase the energy consumption by 23.13 % in mean and 30.47 % in median values. Note that the baseline controller in this study is the MPC module (described in Section 5.2.3) but not a traditional setpoint tracking controller with fixed setpoint schedule.

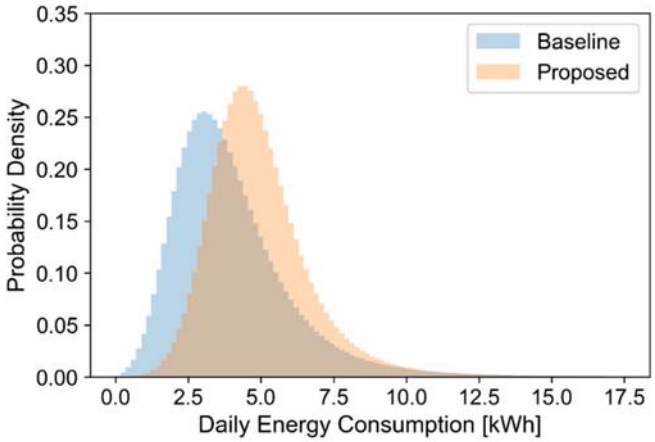

Figure 5.18. Predictive probability distributions of daily energy consumption with the baseline and self-tuned controllers.

From the experimental results, we conclude that the default control range, (21.1-25.5 ℃), was high for five out of nine subjects. Also, the proposed self-tuned controller adjusted the bounds based on subjects' preference votes, and reduced the level of occupant dissatisfaction while using more cooling energy as expected. The comparative satisfaction and energy results depends on how the default control bounds are set. For example, if the default bounds were low, e.g., (18-22 ℃), the energy consumption with the baseline case would increase, while the dissatisfaction level

would decrease. Finally, if we used a different α in the cost matrix of Figure 5.8, the results would differ. To further investigate this, a supplementary simulation study was conducted.

5.4 Simulation study

5.4.1 Simulation platform

A simulation framework consisting of multiple components was developed (Figure 5.19), which mimics the closed-loop processes of Figure 5.1. A building model, which is controlled by the MPC module (described in Section 5.2.3), returns the indoor operative temperature (T_{op}) with a timestep of 30 minutes. Here, we use the same RC model (Figure 5.6) and input data for both MPC and building simulation to eliminate other effects (e.g., accuracy of predictive model, error in disturbance forecast, etc.). We used nine synthetic occupants with the personalized preference models of Figure 5.12. They generate synthetic preference votes (y) every hour from 9:00 am to 5:00 pm (i.e., nine votes per person per day) using the resulting operative temperature at each time. The preference learning module trains/updates personalized preference models, while the control bounds ($T^*_{\mathrm{lb}}, T^*_{\mathrm{ub}}$) are updated at 6:00 pm every day. Here, the preference learning module does not have any information about synthetic occupants a priori. We run the simulation with measured weather data for the period of August 31st - September 20th, 2018. The simulation environment is developed in MATLAB and Python, including the MATLAB Engine API for Python.

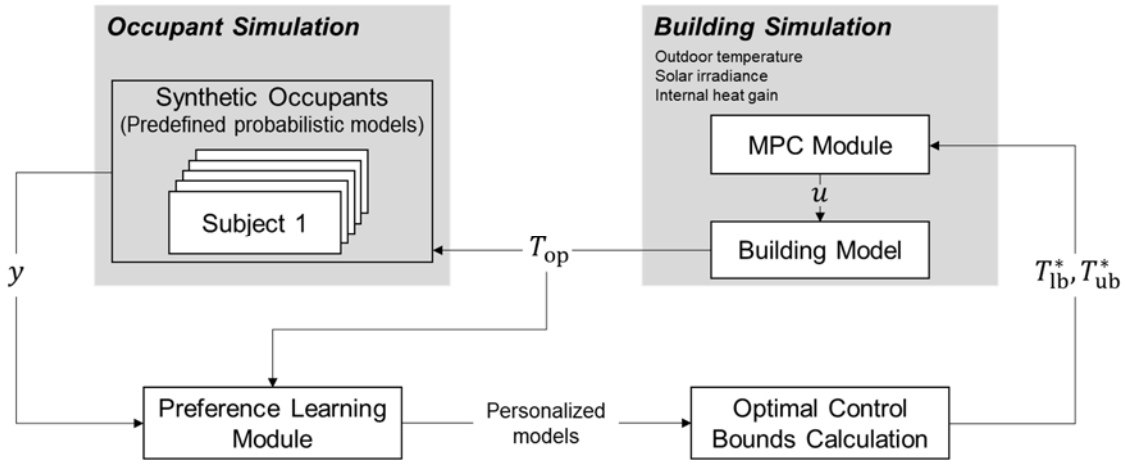

Figure 5.19. Simulation platform.

5.4.2 Simulation results

Figure 5.20 shows the evolution of control bounds with the self-tuned controller where $a = 1$. The results are in agreement with Figure 5.11 (evolution of control bounds in the experiment), indicating the individual differences between control sections.

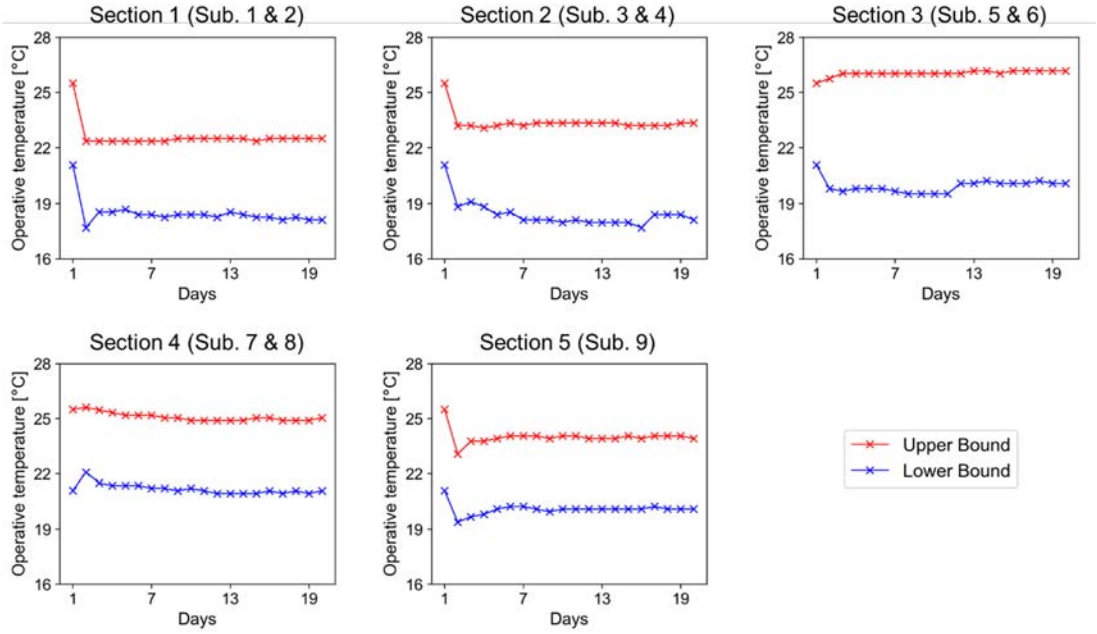

Figure 5.20. Evolution of the control bounds with the self-tuned controller in simulation.

The effect of two different sets of control bounds for the baseline controller (red box plots) and seven different a's for the proposed self-tuned controller (black box plots), on both dissatisfaction level and the mean daily energy consumption, are shown in Figure 5.21. We used results of days 5-20, i.e., after the control bounds converged with the self-tuned controller. Comparing the results with Figure 5.17 (baseline controller with control bounds of (21.1-25.5 ℃) and the proposed controller with $a = 1$), we can observe that: (i) dissatisfaction levels in both cases increased, and (ii) the difference between the two cases increased. The reason is that the synthetic occupants were assumed to be in the office from 9:00 am to 5:00 pm, while real occupancy was higher in the middle of the day.

Since the indoor temperature is low in the morning and gradually increases over time with the MPC, synthetic occupants experienced lower and higher temperatures more frequently compared to the real occupants. Note that a dissatisfaction level of 0.5 can be interpreted as occupants are being dissatisfied with the thermal conditions during the half of their workhours on

average. Therefore, the default control bounds (21.1-25.5 ℃) would not be suitable in real office buildings for people with similar thermal preference responses with the test-subjects of this study, even if they may result in energy savings, as shown in Figure 5.21. Comparing the baseline controller with control bounds of (18-22 ℃) and the proposed controller with $a = 1$, we can see that an ad hoc decision on control bounds can result in both higher dissatisfaction level and energy consumption.

To evaluate the effects of a on occupant satisfaction and energy consumption, we tested seven cases, $a = 0.25, 0.5, 0.75, 1, 1.25, 1.5, 1.75$. The results in Figure 5.21 show that a can effectively control the comfort-energy trade-off. For example, if there are complaints from occupants, the system will be able to self-tune and adjust automatically to satisfy more occupants, while consuming more energy. This process can be automated using the self-tuned controller developed in this study, instead of using uncertain decisions by building managers, resulting in energy waste or occupant dissatisfaction, can be minimized.

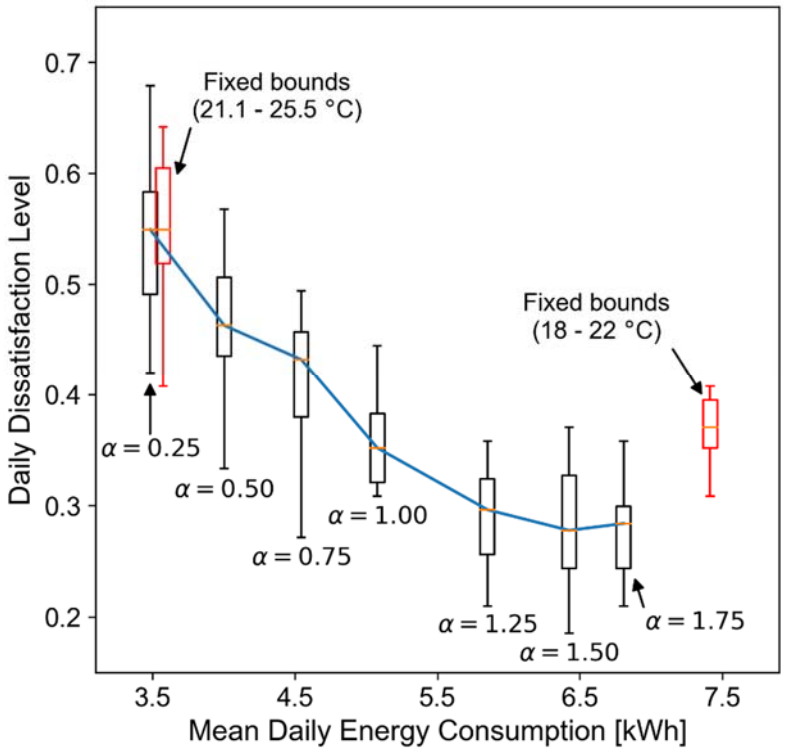

Figure 5.21. Daily dissatisfaction level (y-axis) and mean daily energy consumption (x-axis) of different baseline and self-tuned controllers.

5.5 Conclusions and Discussion

In this chapter, a novel self-tuned HVAC controller is presented, which improves occupant thermal satisfaction and energy efficiency. The controller learns the preferences of real occupants from their feedback, is automatically updated, and controls the system operation to optimize energy consumption. The evolution of personalized thermal preference models (online-learning) and the delivery of thermal conditions with model predictive control (MPC-based HVAC operation) form a closed-loop. To integrate these two parts into the loop, we propose a new method that always provides a set of lower and upper indoor temperature bounds for both private and shared spaces without tweaking the output of personalized comfort models nor solving computationally burdening multi-objective optimization. The control bounds are based on a decision-making algorithm which minimizes the expected cost, different from ad hoc rules proposed in previous research.

This study presents the first successful implementation of a controller that integrates model predictive control and personalized thermal preference models, in a real occupied office space. We implemented our self-tuned controller in an open-plan office space conditioned with a radiant floor cooling system, to facilitate local thermal environment control. Localized operative temperature bounds in each of the eight radiant floor loops are determined based on personalized thermal preference models, developed using a Bayesian clustering and online classification algorithm. The results showed that the self-tuned controller can decrease occupant thermal dissatisfaction votes compared to a baseline MPC controller. The relative comparison of satisfaction and energy results depends on how the default bounds are selected, as well as on the parameters used in the cost matrix for the proposed self-tuned controller.

To further evaluate the performance of the controller and generalize results, the self-tuned controller with local MPC and synthetic occupant preference profiles were incorporated into a building simulation platform. The learning module trains personalized preference models, while the control bounds are updated every day. The results show that an ad hoc decision on control bounds can result in both higher dissatisfaction level and energy consumption. In addition, the cost matrix tunable parameter can effectively control the comfort-energy trade-off; the system is able to adjust automatically to satisfy more occupants as required. In this way, uncertain decisions resulting in energy waste or occupant dissatisfaction can be minimized.

In long-term implementation scenarios, we think that personalized thermal preference models should be continuously or periodically updated to capture long-term comfort/preference variations due to the changes in clothing and activity pattern [103]. However, updating models requires feedback from occupants, and continuously asking their preference votes is not practical in the real world since it cannot avoid disturbing occupants. Hence, non-/less-intrusive ways of collecting/monitoring occupants' thermal preference would be required in the future.

6. BAYESIAN MODELING APPROACH FOR SMART AND LESS-INTRUSIVE USER-INTERFACE TOWARDS HUMAN-CENTERED HVAC OPERATION

6.1 Overview

In this chapter, we present a Bayesian modeling approach which allows incorporating voluntary feedback data (comfort-related responses), collected via participatory interfaces, along with requested feedback data, into the thermal preference learning framework. The incorporation is done by explicitly considering occupants' participation –a type of behavior –in the model. We evaluate the approach with two different datasets we collected from an experiment including two experimental setups with human test-subjects. Since the approach allows using both requested and participatory responses, we can (i) mainly rely on participatory responses and (ii) additionally request responses only when they are truly needed to learn one's thermal preference effectively and less-intrusively. To realize this, we propose a smart occupant feedback request algorithm, that determines whether to request feedback at each moment based on the quantified value of the request. To evaluate the algorithm, we conduct a simulation study with various scenarios.

6.2 Methodology

6.2.1 Experimental study

To collect data for the study, an experiment was conducted with five human test-subjects using three identical perimeter south-facing private offices (3.3m × 3.7m × 3.2m high) in West Lafayette, Indiana (Figure 6.1) in March and April 2019. The offices have one exterior curtain wall façade with 54% window-to-wall ratio, and a high-performance glazing unit with a selective low-emissivity coating (visible transmittance: 70%, solar transmittance: 33%). They are equipped with VAV systems, motorized shades, and dimmable electric lights. A commercial building management system (BMS) allows us to monitor, control and automate all building systems. In this study, we fixed the dimming level of the electric lights at 100 % and the shade position at 25 % to eliminate the potential impact of changing the visual environment on the thermal preference of test-subjects. The subjects performed their usual workload (computer-related work, reading, writing, etc.) during the experiment and wore similar clothes every time they participated. In each

room, one monitor was designated for a user-interface (Figure 6.2) that the subjects used to report their thermal preference by selecting one of the following three answers: “I prefer warmer” / “I prefer cooler” / “I am satisfied with current thermal conditions.” The study was approved by the Institutional Review Board (IRB Protocol #: 1503015873). The air temperature was measured each minute with two shielded T-type thermocouples on the left and right side of the sitting location, and the average value was used in this study. For the data acquisition, A wireless data acquisition system (National Instrument system consists of NIcRio-3024, NI9795, and WSN-3212) was deployed for the data collection. The globe temperature, relative humidity, and local air speed were also recorded but were not used in this study.

Figure 6.1. Exterior and interior view of the offices.

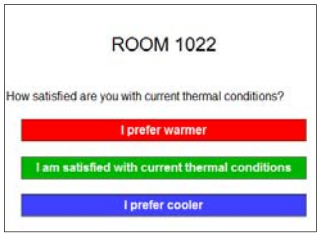

Figure 6.2. Interface.

In the experiment, two different experimental setups were used to collect two datasets from each person, which are “requested” and “participatory,” respectively. In the requested setup, the interface was activated if the subject stayed in the room for 30 minutes and the subjects were requested to report their thermal preference. Once they submitted a response, the 30-minute timer was reset, the interface became deactivated, and the room air temperature setpoint was changed to the next value in one of the pre-determined schedules listed in Table 6.1. If the subject left for a short break, the timer was reset when they came back, but the setpoint was maintained. The subjects were asked to report their thermal preference six times before and after lunch. Each subject participated in this setup for four days and experienced all the schedules. For each occupant, data collected in this setup is called a requested dataset.

Table 6.1. Setpoint schedules (°C) applied in the requested setup.

Sch.	1st	2nd	3rd	4th	5th	6th	Break	7th	8th	9th	10th	11th	12th
1	25	24.5	24	23.5	23	22.5	-	22	21.5	21	20.5	20	19.5
2	19.5	20	20.5	21	21.5	22	-	22.5	23	23.5	24	24.5	25
3	27	26.5	26	25.5	25	24.5	-	24	23.5	23	22.5	22	21.5
4	21.5	22	22.5	23	23.5	24	-	24.5	25	25.5	26	26.5	27

In the participatory setup, the interface was always activated (without any survey request), and the subjects could report their thermal preference, voluntarily, if and whenever they wanted. In this setup, the air temperature setpoint was changed based on the subject's thermal preference responses with the following rule (the subjects were informed that the room air temperature would be adjusted based on their responses without explaining the details):

- "prefer cooler" → decrease by 0.5 °C
- "satisfied" → no setpoint change
- "prefer warmer" → increase by 0.5 °C

To avoid frequent temperature changes, responses submitted within 20 minutes after entering the room or after the previous response were ignored. The subjects were asked to stay in the room for three hours before and after their lunch. Different initial temperature setpoints (i.e., 25, 22.5, 20 °C) were applied at the beginning of each session to avoid bias as much as possible. Each subject participated for three days (six sessions) in this setup and experienced each initial temperature setpoint twice. For each occupant, data collected in this setup is called a participatory dataset.

6.2.2 Personalized thermal preference models using requested and participatory data

Two different model structures are considered for developing personalized thermal preference models with the requested and participatory datasets (Figure 6.3). For the first one, we use the linear ordered probit model [110] considering the obvious order between the thermal preference responses (Model 1 in Figure 6.3). In other words, we assume that there is a latent quantity representing the thermal state of one's body and mind, l. If this quantity is below a certain threshold, τ_1, one will answer ″prefer warmer″; if it is above a certain threshold, τ_2, one will answer ″prefer cooler″; and in between, one will answer "satisfied." This quantity is affected by multiple factors, e.g., air temperature, mean radiant temperature, air speed, metabolic rate. In this study, a linear relationship between air temperature, t_a, and the latent quantity, l, is assumed, and the aggregated effect of all the unconsidered factors on the latent quantity, h_l, is assumed to follow the standard normal distribution, i.e., $p(l|t, \boldsymbol{\beta}) = \mathcal{N}(l|f(t), 1)$, where $t = (t_a - 23.25)/1.875$ is the scaled air temperature, $f(t) = \beta_0 + \beta_1 t$, $\mathcal{N}(\cdot\,|\mu, \sigma^2)$ is the PDF of a normal distribution with

mean μ and variance σ^2, and $\boldsymbol{\beta} = (\beta_0, \beta_1)$. We set $\tau_1 = -\tau_2$ to make the probability of the person being satisfied is maximized at $l = 0$, i.e., neutral state. Subsequently, the probability of y is modeled as

$$p(y = 1|t, \boldsymbol{\beta}, \tau) = p(l < -\tau|t, \boldsymbol{\beta}, \tau) = \Phi\big(-\tau - f(t)\big) \quad (6\text{-}1)$$

$$p(y = 0|t, \boldsymbol{\beta}, \tau) = p(-\tau < l < \tau|t, \boldsymbol{\beta}, \tau) = \Phi\big(\tau - f(t)\big) - \Phi\big(-\tau - f(t)\big) \quad (6\text{-}2)$$

$$p(y = -1|t, \boldsymbol{\beta}, \tau) = p(\tau < l|t, \boldsymbol{\beta}, \tau) = 1 - \Phi\big(\tau - f(t)\big) \quad (6\text{-}3)$$

where $\tau = \tau_2$, $\Phi(\cdot)$ is the CDF of the standard normal distribution and $y = -1,0,1$ represent "prefer cooler," "satisfied," and "prefer warmer," respectively (Figure 6.4). The key point in this model is that we consider the latent quantity, l, which is assumed to determine the occupant's response. This quantity plays a key role also in the second model structure.

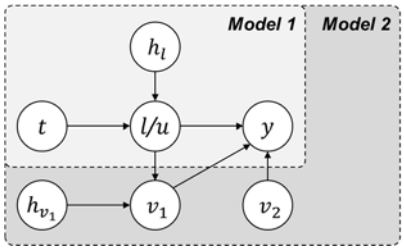

Figure 6.3. Model structures.

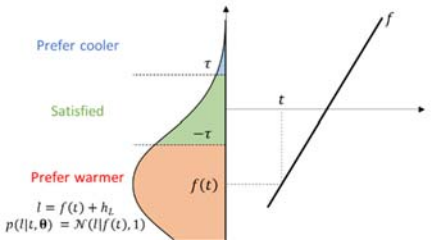

Figure 6.4. Application of the linear ordered probit model.

The second model structure in this study is designed to develop one's personalized preference model with participatory preference data (Model 2 in Figure 6.3). Relationships between t, l, and h_l are the same as described above. y has one more class, $y = 2$, representing an instance of no response in the participatory scenario. To model y, which is now one's participatory preference responses and instances of no response, we explicitly consider one's participations (i) triggered by one's thermal dissatisfaction/discomfort, v_1; (ii) due to other reasons, v_2. Regarding v_1, if the occupant is not satisfied with the current thermal condition, $|l| > \tau$, the chance of one's participation will increase as l goes far from zero. Here, even if we can observe the latent quantity l, we cannot perfectly predict v_1 since there are unconsidered factors, e.g., level of distraction/work load, affecting the process. h_{v_1} is the aggregated effect of such unconsidered factors, which we assume to follow a zero-mean normal distribution, $\mathcal{N}\big(h_{v_1}|0, \sigma_v^2\big)$. We assume that if u is smaller than $-\tau$ and $u + h_{v_1}$ is smaller than a threshold, δ, where $u = -|l|$, then the person will participate, $v_1 = 1$; otherwise, the person will not. i.e., the probability of v_1 is modeled as:

$$p(v_1 = 1|u, \delta, \sigma_v) = \begin{cases} 0, & u \geq -\tau \\ \Phi\left(\frac{\delta - u}{\sigma_v}\right), & u < -\tau \end{cases} \quad (6\text{-}4)$$

$$p(v_1 = 0|u, \delta, \sigma_v) = 1 - p(v_1 = 1|u, \delta, \sigma_v) \quad (6\text{-}5)$$

Regarding v_2, we model the probability of v_2 as a Bernoulli distribution:

$$p(v_2 = 0|q) = q \quad (6\text{-}6)$$

$$p(v_2 = 1|q) = 1 - q \quad (6\text{-}7)$$

where $0 < q < 1$. δ, σ_v, and q represent how active the person is in using the interface and how much aleatoric uncertain is in the prediction of the participation. Consequently, y is modeled as

$$p(y = 1|t, \boldsymbol{\theta}) = \big(1 - p(v_1 = 0|l < -\tau, \boldsymbol{\theta})p(v_2 = 0|\boldsymbol{\theta})\big)p(l < -\tau|t, \boldsymbol{\theta}) \quad (6\text{-}8)$$

$$p(y = 0|t, \boldsymbol{\theta}) = p(v_2 = 1|\boldsymbol{\theta})p(-\tau < l < \tau|t, \boldsymbol{\theta}) \quad (6\text{-}9)$$

$$p(y = -1|t, \boldsymbol{\theta}) = \big(1 - p(v_1 = 0|\tau < l, \boldsymbol{\theta})p(v_2 = 0|\boldsymbol{\theta})\big)p(\tau < l|t, \boldsymbol{\theta}) \quad (6\text{-}10)$$

$$p(y = 2|t, \boldsymbol{\theta}) = p(v_1 = 0|t, \boldsymbol{\theta})p(v_2 = 0|\boldsymbol{\theta}) \quad (6\text{-}11)$$

where $\boldsymbol{\theta} = (\beta_0, \beta_1, \tau, \delta, \sigma_v)$. In Appendix F, we describe how to compute $p(v_1 = 0|l < -\tau, \boldsymbol{\theta})$, $p(v_1 = 0|\tau < l, \boldsymbol{\theta})$, and $p(v_1 = 0|t, \boldsymbol{\theta})$.

The posterior parameter distribution of the two models can be written as

$$p(\boldsymbol{\theta}|\mathbf{y}, \mathbf{t}) \propto p(\mathbf{y}|\mathbf{t}, \boldsymbol{\theta})p(\boldsymbol{\theta}) \quad (6\text{-}12)$$

where $\mathbf{y} = \left(y^{(1)}, \dots, y^{(N)}\right)$, $\mathbf{t} = \left(t^{(1)}, \dots, t^{(N)}\right)$, i.e., training dataset of N observations. The likelihood can be decomposed as:

$$p(\mathbf{y}|\mathbf{t}, \boldsymbol{\theta}) = \prod_{i=1}^{N} p\left(y^{(i)}\middle|t^{(i)}, \boldsymbol{\theta}\right) \quad (6\text{-}13)$$

and we have discussed $p\left(y^{(i)}\middle|t^{(i)}, \boldsymbol{\theta}\right)$ in the two model structures above (Eq. (6-1)-(6-3), Eq. (6-8)-(6-11)). To estimate the posterior, we need to set the prior distribution, $p(\boldsymbol{\theta})$. For $p(\beta_0)$, $p(\beta_1)$, and $p(\tau)$, we first consider our prior knowledge: (i) β_0 would be around zero since the probability of satisfaction would be maximized between 20-26 °C; (ii) β_1 should be positive considering the obvious order between the thermal preferences. Then, to choose a specific distribution reflecting our prior knowledge, we test different distributions visually by plotting the predictive probability distributions with some samples from them (Figure 6.5). Finally, we set $p(\beta_0) = \mathcal{N}(\beta_0|0,2.5^2)$, $p(\beta_1) = \text{Gamma}(\beta_1|2,1.5)$, and $p(\tau) = \text{Gamma}(\tau|4,4)$, where $\text{Gamma}(\cdot\,|\alpha, \beta)$ represents the PDF of a gamma distribution with a shape α and a rate β parameters. For $p(q)$, we use $p(q) =$

$\mathcal{U}(\cdot\,|0,1)$, where $\mathcal{U}(\cdot\,|a,b)$ is the PDF of a continuous uniform distribution with upper and lower bounds, a, b, i.e., no informative prior knowledge. For $p(\delta)$, we expect that δ would be close to $-\tau$. However, since we do not have strong prior knowledge, we employ a hierarchical Bayesian approach and assign $p(\delta|\tau,\sigma_\delta) = \mathcal{N}\left(\delta\middle|-\tau,\sigma_\delta^2\right)$ and $p(\sigma_\delta) = \mathcal{E}(\sigma_\delta|10^{-1})$, where $\mathcal{E}(\cdot\,|\lambda)$ represents the PDF of an exponential distribution with a rate λ parameter, considering the scale of l. Similarly, for $p(\sigma_v)$, we assign $p(\sigma_v|\eta) = \mathcal{E}(\sigma_v|\eta^{-1})$ and $p(\eta) = \mathcal{E}(\eta|10^{-1})$.

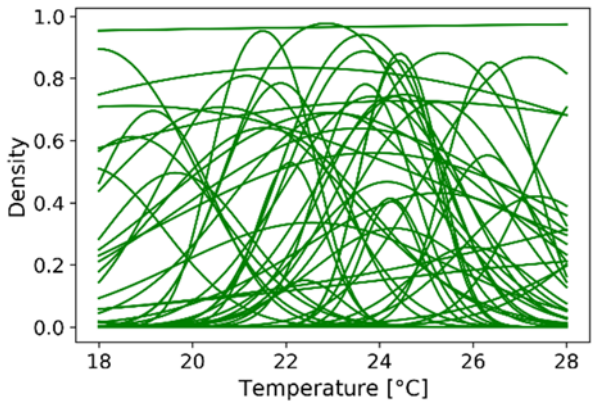

Figure 6.5. Predictive probability distributions with 50 prior samples.

To estimate the posterior distribution of the model parameters, which is intractable analytically, we use sequential Monte Carlo (SMC) [79], which is more efficient and effective than standard Markov chain Monte Carlo (MCMC). In Appendix G, we describe the algorithm. Table 6.2 shows SMC settings used in this study, which provided consistent results in multiple trainings with a reasonable computational cost.

Table 6.2. Settings for sequential Monte Carlo.

The number of particles	5000
The number of MCMC steps per SMC step	25
The threshold of the effective sample size	0.5
The reduction of the effective sample size per SMC step	0.95
MCMC step method	Metropolis-Hasting with a multivariate normal distribution as the proposal density (Scale of the proposal density were adjusted after each iteration to retain the acceptance rate between 0.2 and 0.5)

In real buildings, a target occupant's personalized model should be updated continuously as feedback responses are collected. In this regard, the standard way of updating is re-training the model with all the data we have repeatedly. However, even though SMC is efficient, the re-training computational cost will increase rapidly as the dataset size increases and might become intractable for local computers in real buildings. Hence, to resolve this problem, we develop a method for an efficient Bayesian model update.

Suppose that we already had samples approximating the posterior parameter distribution, $p(\boldsymbol{\theta}|\mathbf{y},\mathbf{t})$. We receive an additional data point, $(y_{\text{new}}, t_{\text{new}})$, and want to update the posterior with the data point, i.e., estimating $p(\boldsymbol{\theta}|\mathbf{y},\mathbf{t},y_{\text{new}},t_{\text{new}})$. If we write down the equation and rearrange it as:

$$p(\boldsymbol{\theta}|\mathbf{y},\mathbf{t},y_{\text{new}},t_{\text{new}}) \propto p(y_{\text{new}}|t_{\text{new}},\boldsymbol{\theta})p(\boldsymbol{\theta}|\mathbf{y},\mathbf{t}) \tag{6-14}$$

then we can estimate the posterior with the likelihood of the new datapoint using the previous posterior, $p(\boldsymbol{\theta}|\mathbf{y},\mathbf{t})$, as the prior. In other words, if we use the previous posterior directly in the estimation, we can update the model very efficiently. To this end, we use the samples approximating $p(\boldsymbol{\theta}|\mathbf{y},\mathbf{t})$ at the first SMC step and modify the likelihood part correspondingly. We describe the mathematical details in Appendix H. It is worth noting that this method can be used in other Bayesian model estimation problems where an efficient model update is needed.

6.2.3 Smart feedback request algorithm: quantifying the value of information gain

As shown in Figure 6.3, Model 1 is nested in Model 2, and they share three parameters: β_0, β_1, τ, which are used to predict the probability of one's preference. In other words, we can construct an augmented model structure to learn one's thermal preference with both requested and participatory preference responses. The likelihood of the augmented model is:

$$p(\mathbf{y}|\mathbf{t},\boldsymbol{\theta},\mathbf{r}) = \prod_{i=1}^{N} p\left(y^{(i)}\middle|t^{(i)},r^{(i)},\boldsymbol{\theta}\right) \tag{6-15}$$

where $\mathbf{r} = \left(r^{(1)},\dots,r^{(N)}\right)$, and $r^{(i)} = 0$ or 1 indicate whether $y^{(i)}$ is participatory or requested, respectively. Therefore, if $r^{(i)} = 0$, $p\left(y^{(i)}\middle|t^{(i)},r^{(i)},\boldsymbol{\theta}\right)$ is calculated with Eq. (6-8)-(6-11); if $r^{(i)} = 1$, $p\left(y^{(i)}\middle|t^{(i)},r^{(i)},\boldsymbol{\theta}\right)$ is calculated with Eq. (6-1)-(6-3).

Since frequent response requests are intrusive, requesting regularly or randomly is not efficient nor effective. The ideal way would be (i) mainly relying on participatory responses and

(ii) additionally requesting responses only when they are truly needed. Here, the question is how to quantify the value (importance) of requesting a response at a given moment (under specific conditions). The value of information gain at any given condition also varies with our current state of knowledge regarding the person's thermal preference. For example, if the current temperature is 30 °C, and if we are already quite certain that the person will prefer a cooler temperature, an additional requested response at that moment will not improve our state of knowledge –therefore, the value of a request would be low, and we do not need to disturb the person.

The theory of Bayesian experimental design provides a general probability-theoretical framework for such a problem [111], which is based on the theory for decision-making under uncertainty. The objective of Bayesian experimental design is to maximize the expected utility/value when designing the experiment. In our case, we want to decide whether to request or not, i.e., designing an experiment, to maximize the information gain, i.e., utility. The utility can involve the cost of performing the experiment. More specifically, assume that we have a personalized model trained with a dataset, $\mathbf{D} = \{\mathbf{y}, \mathbf{t}, \mathbf{r}\}$, collected from a person, i.e., the posterior parameter distribution, $p(\boldsymbol{\theta}|\mathbf{D})$. In the next instance, we want to quantify the expected information gain with/without a feedback request. We use the Kullback–Leibler divergence (D_{KL}) between $p(\boldsymbol{\theta}|\mathbf{D})$ and $p(\boldsymbol{\theta}|\mathbf{D}, y_{\text{new}}, t_{\text{new}}, r_{\text{new}})$ as the measure for the information gain:

$$D_{KL}\big(p(\boldsymbol{\theta}|\mathbf{D}, \mathbf{d}_{\text{new}}) \parallel p(\boldsymbol{\theta}|\mathbf{D})\big) = \int p(\boldsymbol{\theta}|\mathbf{D}, \mathbf{d}_{\text{new}}) \log \frac{p(\boldsymbol{\theta}|\mathbf{D}, \mathbf{d}_{\text{new}})}{p(\boldsymbol{\theta}|\mathbf{D})} d\boldsymbol{\theta} \tag{6-16}$$

where $\mathbf{d}_{\text{new}} = (y_{\text{new}}, t_{\text{new}}, r_{\text{new}})$ are the datapoint of the next instance. In statistics, the Kullback–Leibler divergence (also called relative entropy) shows how one distribution is different from another [112]. In other words, the quantity shows how different the updated and the original posterior distributions are. Since we cannot know y_{new} before we observe it, we use the expected D_{KL},

$$\begin{aligned} U(t_{\text{new}}, r_{\text{new}}) &= \mathbb{E}_y\big[D_{KL}\big(p(\boldsymbol{\theta}|\mathbf{D}, \mathbf{d}_{\text{new}}) \parallel p(\boldsymbol{\theta}|\mathbf{D})\big)\big] \\ &= \int \sum_{y_{\text{new}}} p(\boldsymbol{\theta}|\mathbf{D}, \mathbf{d}_{\text{new}}) p(y_{\text{new}}|\mathbf{D}, t_{\text{new}}, r_{\text{new}}) \log \frac{p(\boldsymbol{\theta}|\mathbf{D}, \mathbf{d}_{\text{new}})}{p(\boldsymbol{\theta}|\mathbf{D})} d\boldsymbol{\theta} \end{aligned} \tag{6-17}$$

The computation of this quantity is described in Appendix I.

Based on $U(t_{\text{new}}, r_{\text{new}} = 0)$ and $U(t_{\text{new}}, r_{\text{new}} = 1)$, we can decide whether to request a response or not, i.e., a smart request algorithm. In this study, we make decisions by simply comparing the magnitude of the two quantities: if $U(t_{\text{new}}, r_{\text{new}} = 1) > U(t_{\text{new}}, r_{\text{new}} = 0)$,

request a response, otherwise, do not request. Note that other quantities, e.g., D_{KL} between the updated and original predictive probability distributions, could also be used to quantify the value of a data point. In addition, the cost of requesting a response, e.g., how intrusive/disturbing it is, can be considered to make decisions.

To evaluate the effectiveness of the smart request algorithm, we conducted a simulation study with a synthetic occupant which provides thermal preference responses. The synthetic occupant is the augmented model (Eq. (6-15)) with parameters, $\boldsymbol{\theta}_{\text{true}}$, pre-determined by us. In the simulation, the parameters are assumed to be unknown. Figure 6.6 shows the flowchart of the simulation study. For the second process, i.e., computing the temperature control range with a personalized preference model, we use the method proposed in Chapter 5. With a control range, there are multiple different ways to actually operate an HVAC system. In the third process, to make the simulation results more conservative, instead of assuming a specific control scheme, we randomly draw a temperature sample from the control range. Here, we test two different probability distributions. Distribution 1 is $p\left(t_{a,\text{new}}\middle|t_{\text{lb}},t_{\text{ub}}\right)=\mathcal{U}\left(t_{a,\text{new}}\middle|t_{\text{lb}},t_{\text{ub}}\right)$. Distribution 2 is $p(\xi|\alpha,\beta)=\mathcal{B}(\xi|5,1)$, where $t_{a,\text{new}}=\xi\times(t_{\text{ub}}-t_{\text{lb}})+t_{\text{lb}}$, $\mathcal{B}(\cdot\,|\alpha,\beta)$ is the PDF of a Beta distribution with two positive shape parameters, α,β. Figure 6.7 shows the PDF of the two distributions where $t_{\text{lb}}=22.5$ and $t_{\text{ub}}=25.0$ as an example. The uniform distribution would represent a case where indoor temperature varies frequently within the control range; the beta distribution would represent a case where indoor temperature is maintained near the upper bound to save energy. For the fourth process, we test four different scenarios: (i) Request Only, i.e., requesting occupant's feedback at every instance; (ii) Participatory Only, i.e., relying only on participatory responses (no request); (iii) Random request, i.e., requesting randomly with the probability of 0.5; (iv) Proposed, i.e., request occupant's feedback based on the proposed algorithm. Considering the two distributions and four scenarios, we tested eight cases, with 200 simulations for each case.

In each simulation, as the loop in Figure 6.6 is iterated, the personalized preference model becomes similar to the augmented model of the synthetic occupant, i.e., the true model. The difference between the two models can be used to quantify the learning progress. As a measure for the difference, we use the following quantity:

$$\iint D_{KL}\left(p\left(y_p\middle|x_p,\boldsymbol{\theta}\right)\parallel p\left(y_p\middle|x_p,\boldsymbol{\theta}_{\text{true}}\right)\right)p\left(x_p\right)p(\boldsymbol{\theta}|\mathbf{D})\,dx_p d\boldsymbol{\theta} \tag{6-18}$$

where $p(y_p|x_p, \boldsymbol{\theta})$ is the predictive probability of y_p given x_p and $\boldsymbol{\theta}$, i.e., how different the predictive probability of the personalized model and that of the true model is. We set $p(x_p) = \mathcal{U}(x_p|15{,}30)$. By comparing the quantity of the eight cases, we evaluate the effectiveness of the smart request algorithm.

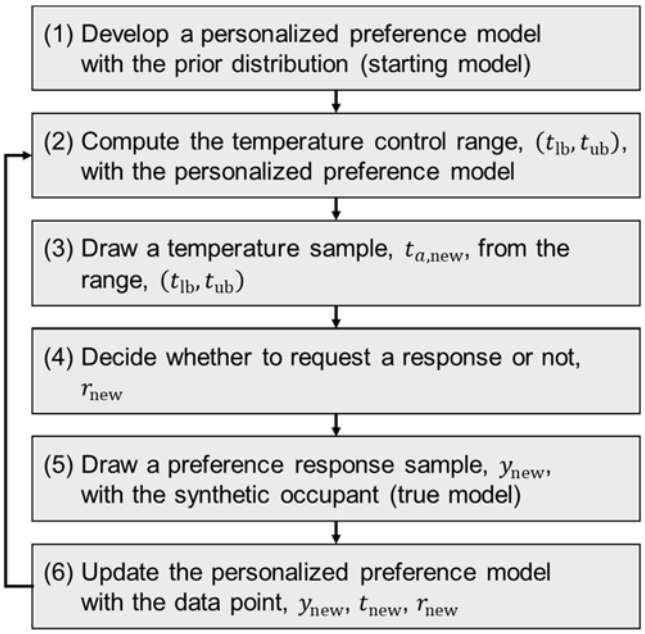

Figure 6.6. Flow chart of a simulation study.

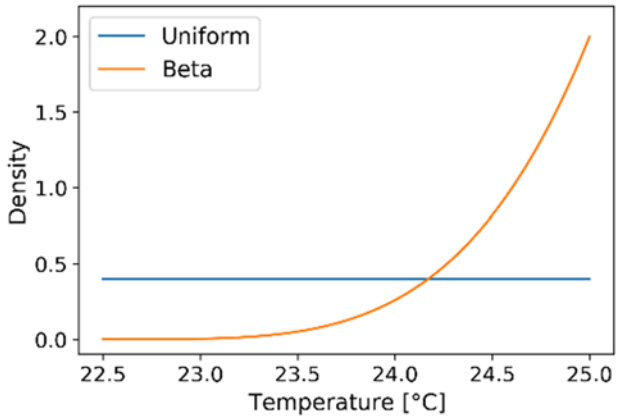

Figure 6.7. Probability distributions used to draw a temperature sample with the control range of $(22.5{,}25)$.

6.3 Results

6.3.1 Personalized Thermal Preference Models

Figure 6.8 shows data collected from the five test-subjects in the "requested" and "participatory" setups. The portion of "satisfied" responses is significantly lower in the participatory preference data. This observation corresponds to one of our hypotheses: "occupants would rarely report their thermal preference using a participatory interface under comfortable conditions." The data also show the differences in thermal preferences between individuals for both setups.

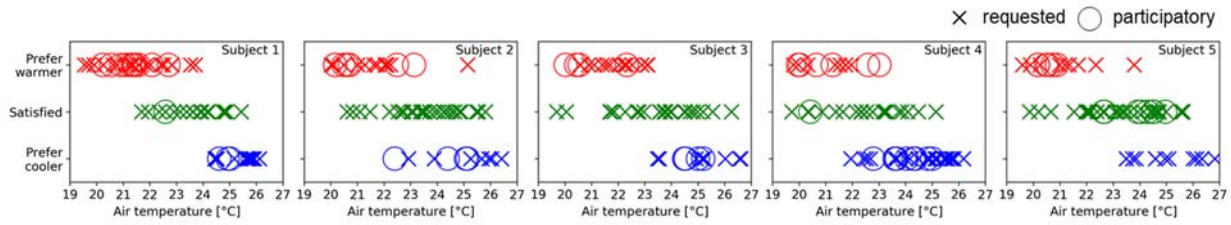

Figure 6.8. Thermal preference responses from five subjects (request and participatory setups).

To realize the difference between the requested and participatory datasets and their impact on personalized preference models, three personalized models were developed and compared for each subject: (i) Model 1 trained with the requested dataset; (ii) Model 1 trained with the participatory dataset; (iii) Model 2 trained with the participatory dataset. Each graph in Figure 6.9 shows the predictive probability distribution with respect to air temperature computed from the personalized preference models. Solid lines represent the median values of the probabilities, and shaded areas represent the associated 95% credible intervals (i.e., 2.5- and 97.5-quantiles of the predictive probability).

Comparing graphs in the first and second rows (Model 1 trained with one's requested and participatory datasets, respectively), we can see that the predictive probability of models developed with Model 1 and participatory data, can be highly distorted. More specifically, the probability of the person being satisfied decreases significantly due to the lack of "satisfied" responses, i.e., the green curves are shrunk for Subjects 1-4. Even in the case of Subject 5, who submitted quite a few "satisfied" responses, we can see that the temperature range in which red and green areas cross moved to the right. Although we may be able to infer the temperature that each occupant most

likely prefers with such models, we cannot compute the satisfaction probability; therefore determining the proper range of controlled thermal conditions becomes difficult.

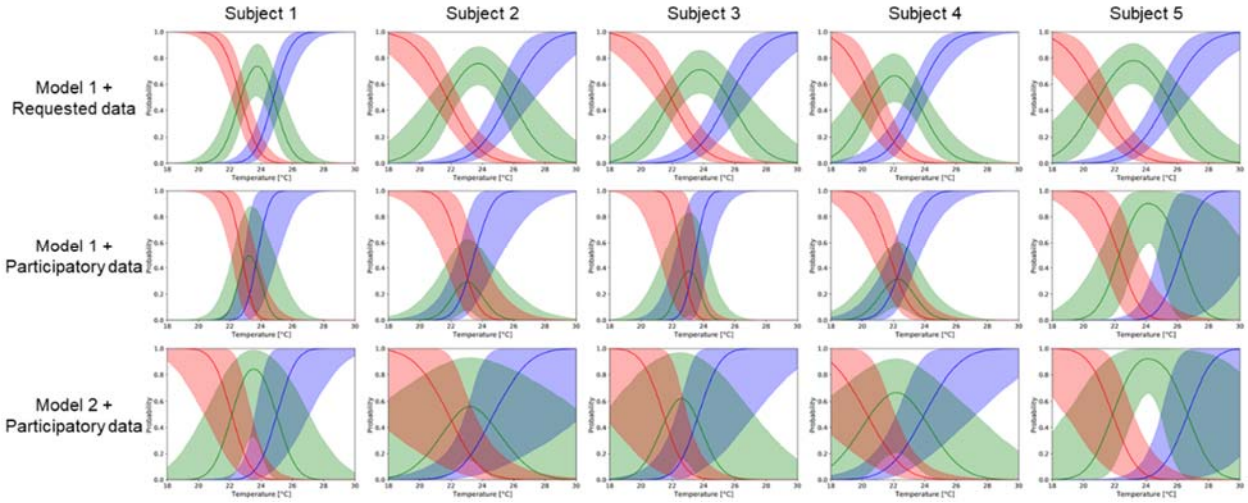

Figure 6.9. Predictive probabilities from different personalized preference models trained with requested and participatory data (5 subjects).

The graphs in the third rows of Figure 6.9 show the predictive probability of models trained with Model 2 and the participatory datasets. The uncertainty areas cover the graphs of the first row. In other words, Model 2 properly keeps the uncertainty due to the unobserved thermal preferences with the participatory interface as is, instead of returning distorted predictive probabilities. This is important not only for avoiding wrong predictions but also for estimating the value (importance) of information gain (a new data point) with and without a response request at a moment.

To evaluate the models more quantitatively, we compute the expected squared error with the models over the requested datasets as

$$\sum_{i=1}^{N}\sum_{y=-1}^{1}\left(y_{\text{obs}}^{(i)}-y\right)^2 p\left(y\middle|t_{\text{obs}}^{(i)},\boldsymbol{\theta}_j\right) \tag{6-19}$$

where $\boldsymbol{\theta}_j$ is a sample from the posterior distribution, $p(\boldsymbol{\theta}|\mathbf{y},\mathbf{t})$, of a model, $p\left(y\middle|t,\boldsymbol{\theta}_j\right)$ is the predictive probability with the parameter values in $\boldsymbol{\theta}_j$, $\left(y_{\text{obs}}^{(i)},\ldots,y_{\text{obs}}^{(N)}\right)$ and $\left(t_{\text{obs}}^{(i)},\ldots,t_{\text{obs}}^{(N)}\right)$ are data in one's requested dataset. We choose this quantity as the metric for the comparison due to the obvious order between classes. Note that each $\boldsymbol{\theta}_j$ is a plausible set of model parameter values from the Bayesian model estimation.

Figure 6.10 shows the expected squared error of the three cases (three rows of Figure 6.9). Each boxplot shows the distribution of the quantity with 5,000 sets of model parameters values, $\boldsymbol{\theta}_{1:5000}$. In this evaluation, the expected squared error values of models developed with Model 1 and the requested datasets (the first row of Figure 6.9) provide ideas regarding the maximum prediction performance of the linear ordered probit model for the datasets. The error values of models developed with Model 2 and participatory datasets are always lower than those of models developed with Model 1 and participatory datasets. This result also supports that Model 2 is more preferable to learn one's thermal preference from participatory feedback data.

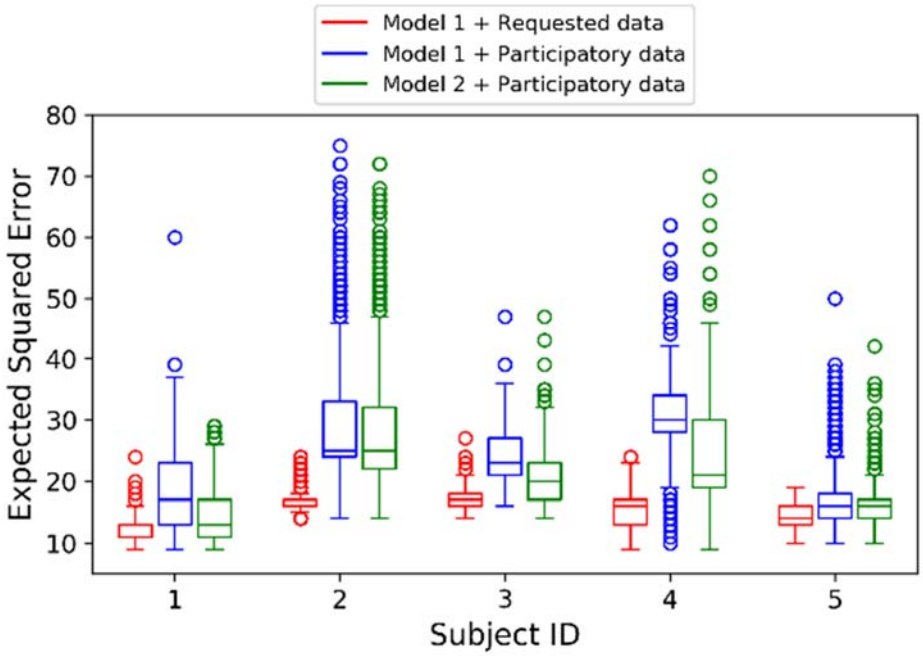

Figure 6.10. Prediction performance of different personalized thermal preference models.

6.3.2 Value of Information Gain With/Without a Request

With the augmented model structure (Eq. (6-15)), we can quantify the value of a feedback request at an instance. The upper left plot in Fig 6.11 shows the predictive probability distribution of Subject 1's personalized model trained with the participatory dataset. Assuming that the model is our current state of knowledge, the lower left plot shows the corresponding expected Kullback–Leibler divergence (Eq. (6-16)) with and without a request under different temperature conditions for the next instance. Bigger difference, $U(t_{\text{new}}, r_{\text{new}} = 1) - U(t_{\text{new}}, r_{\text{new}} = 0)$, represents higher value of the request (e.g., for 22 °C or 25 °C). We observe that $U(t_{\text{new}}, r_{\text{new}} = 0)$ is similar

or higher than $U(t_{\text{new}}, r_{\text{new}} = 1)$ if the temperature is lower than 19 °C or higher than 28 °C. This is because the model is already certain of the occupant's preferences with "extreme" temperature conditions. Under such conditions, not requesting is better to estimate δ, σ_v, and q, i.e., learning how active the person is in using the interface. To present how the quantity changes as the model is updated, we update the model with seven preference data points collected between 21.5-22.5 °C in the request setup. The upper right plot of Figure 6.11 is the predictive probability distribution of the updated model, and the lower right plot shows the corresponding expected Kullback–Leibler divergence. Like the model uncertainty in the predictive probability, the expected Kullback–Leibler divergence for 22 °C decreased significantly, i.e., the value of a request under 22 °C was reduced as data points were added. The expected Kullback–Leibler divergence for higher temperatures also decreased to some extent. This is because we use a model structure of low flexibility, and consequently, the update in the posterior parameter distribution with the data points also decreases the uncertainty in high-temperature ranges. Model structures of higher flexibility would result in higher differences.

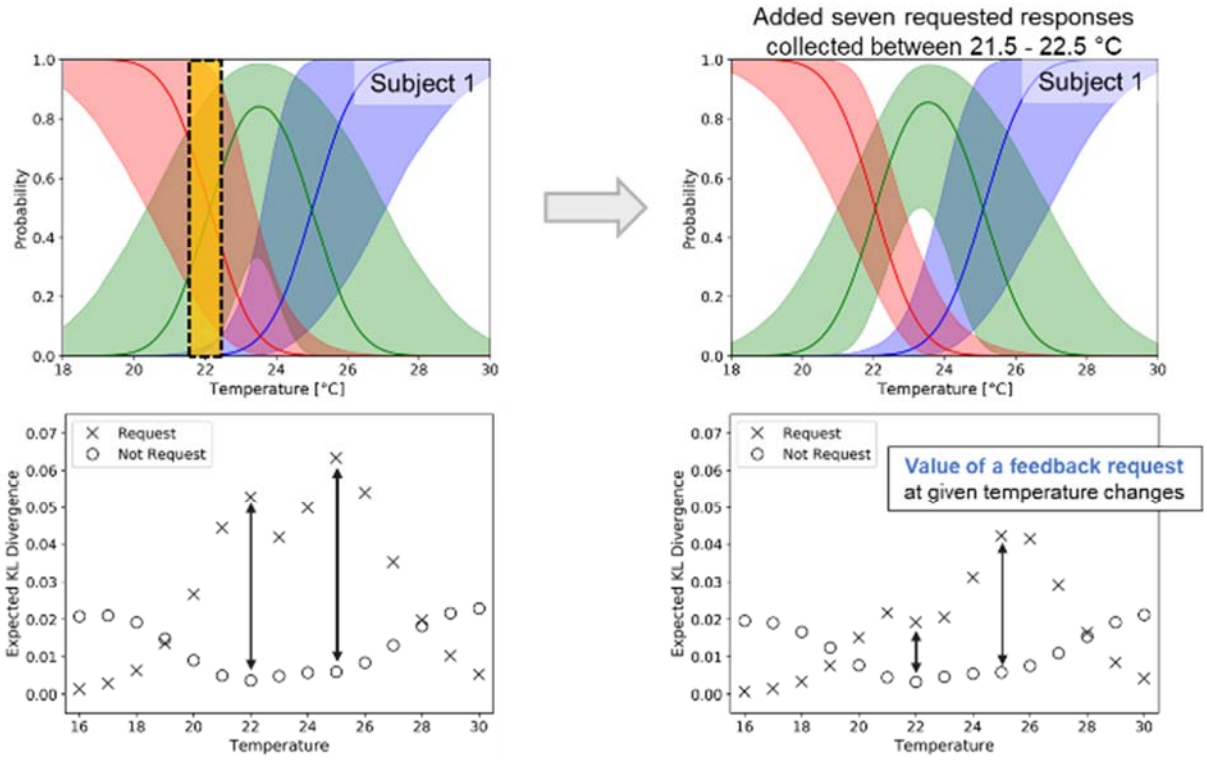

Figure 6.11. Expected entropy difference of the updated model with/without response request.

6.3.3 Simulation Results

Figure 6.12 shows the progress of learning in the different cases described in Section 6.2.3. For the synthetic occupant in the simulation, we use the following values for the model parameters, $\boldsymbol{\theta}_{\text{true}}$: $\beta_0 = -0.496$, $\beta_1 = 3.104$, $\tau = 1.477$, $q = 0.018$, $\sigma_\delta = 2.920$, $\delta = -4.911$, which is a sampled set of parameter values from the posterior parameter distribution of Subject 1's personalized preference model, trained with both requested and participatory datasets. In Figure 6.12, the x-axis is the number of iterations, i.e., the number of data points used to train the personalized model. The y-axis is the model divergence computed with Eq. (6-18). The left plot shows the results with Distribution 1, and the right plot shows those with Distribution 2. Each boxplot shows the distribution of the model divergence over 200 simulations. Table 6.3 shows the mean, median, and standard deviation of the number of requests in the simulations. Requesting the occupant's feedback at every instance, i.e., the Request Only scenario, is the fastest way to learn the occupant's thermal preference while it is most disturbing, i.e., highest number of requests. On the other hand, relying only on the occupant's participatory feedback, i.e., Participatory Only scenario, is the slowest but least disturbing way.

From Figure 6.12, we can see that the learning progress in the Proposed scenario, i.e., deciding whether to request or not with the proposed algorithm, is competitive with that in the Request Only scenario with both distributions. A notable point is that these results were achieved with 33.33 and 37.50 % less (in median) numbers of requests, i.e., less-intrusive but still effective. Another observation is that, with Distribution 2, the difference in the learning progress between Proposed, Random, and Participatory Only scenarios is bigger. The reason is that a model requires responses under low-temperature conditions to learn the occupant's preference properly, while most of sampled temperatures are near the upper bound with Distribution 2. In Proposed scenario, the proposed algorithm actively requests responses when the sampled temperatures are low, which are rare but important moments. We can also see that the number of requests in Proposed scenario with Distribution 2 is lower than that with Distribution 1. The reason is that the algorithm reduced the frequency since responses under high-temperature conditions are sufficient due to the biased sampled temperatures.

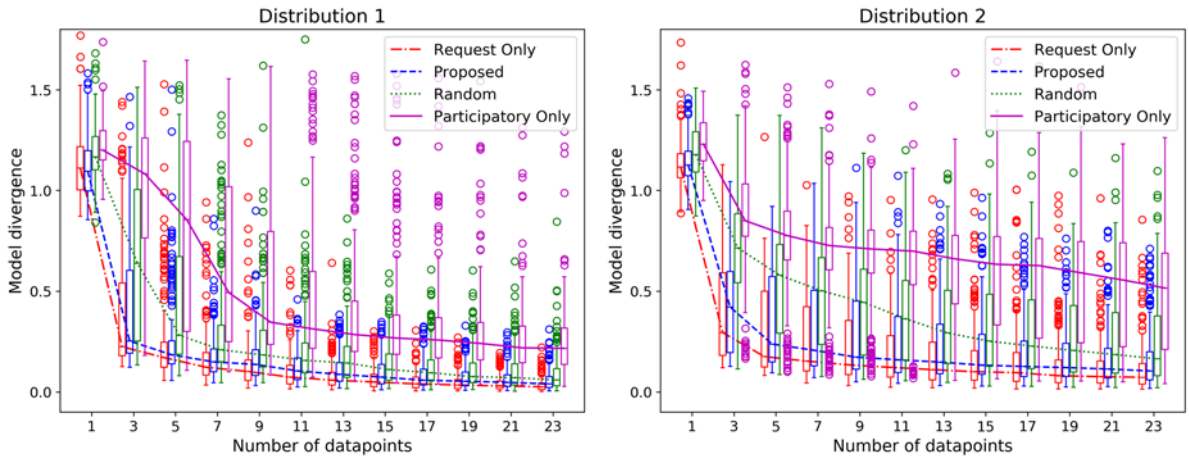

Figure 6.12. Progress of learning in the different simulation scenarios.

Table 6.3. The number of feedback requests in different scenarios.

	Distribution 1	Distribution 2
Request Only	24 / 24 / 0	24 / 24 / 0
Participatory Only	0 / 0 / 0	0 / 0 / 0
Random	12.29 / 12 / 2.55	11.87 / 12 / 2.46
Proposed	16.27 / 16 / 1.36	14.69 / 15 / 1.55

Mean / Median / Standard deviation

6.4 Conclusion and Discussion

In this chapter, a Bayesian modeling approach was presented, which allows using both participatory preference data (collected via participatory interfaces) and requested preference data for learning individual occupants' thermal preference. This is achieved by explicitly considering occupant participation, a type of behavior, in the model structure. An experiment was conducted with two different setups to collect occupants' thermal preference responses (with both ways), which were used to develop personalized thermal preference models. The modeling results showed that the proposed modeling approach allows maintaining the uncertainty in a model, which corresponds to the lack of satisfaction responses with a participatory interface, i.e., sampling bias, instead of returning distorted predictive probabilities.

In addition, we proposed a smart occupant feedback request algorithm to determine whether to request feedback at each moment based on the quantified value, i.e., information gain, of the request. The value was computed using the expected Kullback-Leibler divergence between the

current and updated posterior parameter distributions. A simulation study was conducted to evaluate the performance of the algorithm. The simulation results showed that the algorithm allows us to collect sufficient data to learn one's thermal preference with reduced number of feedback requests, i.e., effective but less-intrusive.

This is an initial study regarding feedback collection from occupants, and there is room for improvement. The assumptions we set in the model structures can be released. Model 1, which predicts one's thermal preference response, could have other input variables explicitly instead of including them in h_l; the relationship between the inputs and the latent quantity does not need to be linear; moreover, it does not need to be based on the probit structure as many studies mentioned in Section 2.2 showed.

Model 2, which predicts one's participation, can be also improved and expanded. Occupants' participation behavior could be affected by other factors, such as elapsed time from the previous response, time of the day, and level of work load or distraction. Such factors, which were not explicitly considered in this study, could be used as separate input variables for v_2 and v_2. However, if one agrees that a portion of occupants' participations are triggered by their dissatisfaction, having a latent quantity that affects both preference response and participation in a model will be beneficial with any improvement. We believe that this treatment, i.e., having the latent quantity, would allow us to learn an occupant's thermal preference with his/her thermal comfort-related behaviors, e.g., thermostat adjustment, use of local fan/heater, etc., alongside with requested/participatory responses.

Regarding the request algorithm, one may design a smarter algorithm by simply considering the cost of feedback request, e.g., comparing $U(t_{\text{new}}, r_{\text{new}} = 0)$ with $U(t_{\text{new}}, r_{\text{new}} = 1) + \alpha$ or $\alpha U(t_{\text{new}}, r_{\text{new}} = 1)$ to control the number of requests with the algorithm, i.e., number of requests decreases as bigger α is used. However, even smarter algorithms could be developed. The proposed algorithm makes a decision which simply maximizes the expected information gain at each moment, i.e., greedy algorithm. Although a greedy algorithm is simple and intuitive, it does not guarantee the optimality of its solution for the entire problem. In other words, there are cases where such a greedy algorithm underperforms. For example, if we want to request a response once per day, the proposed algorithm cannot answer when would be the best time to request during the day even if we know how the HVAC system would be operated. If the HVAC system adjusts its operation in real time based on occupants' responses at the current moment and this adjustment

influences the temperature in the subsequent moments significantly, the solution from the greedy algorithm would be far from the optimal. A Bayesian sequential experimental design approach can be applied to solve this decision-making problem [113], which will allow to make a decision that maximizes the expected information gain over a period of time via approximate dynamic programming.

7. FUTURE WORK

Future work for subtopics in this Thesis has been discussed in chapter discussion sections extensively and deeply. Hence, this chapter includes more general ideas for future work towards human-in-the-loop, human-centered, smart and user-interactive HVAC systems.

7.1 Holistic Human-Building Interaction Research Framework

Compared to the level of our knowledge regarding physical systems, e.g., heat/mass transfer and thermodynamics in buildings, we have limited knowledge on human needs and behaviors in buildings. Hence, towards smart and user-interactive HVAC systems, we need to increase the depth and breadth of this knowledge. Various and changing human needs are what the buildings need to recognize and satisfy; human behaviors are closely related to these needs. In previous research, each of the needs or behaviors has been studied "separately" focusing merely on its "prediction" based on the correlation with related variables. The outcomes, i.e., predictive models, have provided bases for fundamental design/operational guidelines or have been used to mimic occupants in simulation studies. However, the studies are quite limited in helping to satisfy human needs effectively and efficiently by controlling, adjusting, or intervening upon their causal factors, since they do not examine/explain causal relationships between variables explicitly. In fact, investigating the causal relationships around human needs and behaviors in buildings is quite challenging because of two significant hurdles.

First, the processes of human perception and consequent effects are interrelated and involve/share multiple variables. Thus, holistic investigations on the causality between the human factors are required; necessarily, an enormous amount of data is needed. Second, even if we have enough data, it is tricky to untangle the causal from the merely correlative with traditional statistical or machine learning techniques unless the data comes from a controlled experiment. In reality, conducting a controlled experiment which covers all of our interests for the holistic investigations is impossible; hence, we cannot but conduct smaller but more specific experimental studies sequentially, and at the same time, rely heavily on observational data which are collected from the real world.

To overcome this limitation in the future, I plan to develop a research framework for understanding human-building interactions with two emerging statistical methodologies: Bayesian data analysis and statistical causal inference. Bayesian approaches will allow (i) encoding prior knowledge from previous studies in formal probabilistic ways; (ii) combining available data from different sources with hidden variables for the heterogeneity. Variables that are important but not investigated yet at the current stage will be modeled as epistemic uncertainty to evaluate the necessity and direction of the subsequent investigations. Statistical causal inference methods will be used to test hypotheses in the Bayesian models so that it can be used to explain the causalities, and eventually, help us satisfy human needs, i.e., optimal building design and operation.

7.2 Incorporation of Advanced Sensing Technologies in Human-Building Interaction Research

Previous human-building interaction research relies only on data of representative environmental conditions (e.g., air temperature, illuminance), monitored behaviors, and subjective responses from surveys, i.e., limited information. The uncertainty in our understanding of human-building interactions has been regarded as randomness (aleatoric uncertainty), even though a considerable portion of the uncertainty comes from the missing information (epistemic uncertainty).

Following the development of smart devices, IoT, and computing technologies, collecting and processing physiological data (e.g., blood volume pulse, skin temperature, electrodermal activity, body movement) and high-dimensional data (e.g., electroencephalography, digital images, videos) becomes possible. The biggest challenge is improving our knowledge by mapping the data and human factors. To this end, I plan to adopt Bayesian nonparametric methods (e.g., Gaussian process regression) due to their flexibility regarding both fitting data and encoding prior knowledge. However, they may not be sufficient to deal with high-dimensional data such as electroencephalography and digital images. Hence, I will also consider using Bayesian convolutional neural networks (Bayesian deep learning).

7.3 Interactive Interfaces and Information Design

User interfaces in buildings enable human-building interaction, i.e., occupants can control the systems and request their needs; and the systems can provide information to the occupants to

assist in their decision-making. Hence, the interfaces and information should be carefully designed to promote efficient and human-centered building operation. Within this context, I plan to investigate two important concepts: i) instructive feedback; ii) trust in human-building interactions, which have not been studied systematically. Instructive feedback from building systems can inform occupants of beneficial behaviors; and contribute to energy-savings and higher levels of occupant satisfaction for given contextual factors (e.g., layout, system capacity). This will be an extension of the building's role from a responsive system to a cooperative system. Occupants' trust in building systems prevents them from making unnecessary overrides which degrade the optimality in operation. Future research will include a set of experiments with human subjects, interfaces with different level and types of information and advanced sensing technologies.

7.4 Optimal Operation of Buildings Considering Human-Building Interactions

Optimal operation of buildings is not trivial because of the uncertainty occupant preferences and behaviors. As a result, traditional control techniques (i.e., heuristic rule-based and deterministic optimal controls) cannot maximize the energy efficiency of the systems. Moreover, in scenarios where the demand response and resilience of integrated energy systems are important, control can easily fail because of the uncertainty.

To resolve this issue, I plan to apply stochastic optimal control techniques with outcomes of topics above. Both model-predictive control (MPC, receding horizon control) and approximate dynamic programming (ADP, reinforcement learning) will be evaluated in terms of the computational cost and capability of dealing with the uncertain variables. The models or agents will be fine-tuned as the controller explores various mechanisms in its target building. This exploration process will be constrained with the domain knowledge encoded in the models, i.e., fast and efficient, but less-intrusive learning.

APPENDIX A. RE-LABELING SMC SAMPLES

Figure A-1 shows the SMC samples for the parameters before re-labeled which is equivalent to Figure 3.7. As shown in the figure, although the estimation process found 2 distinctive sets of parameters, however, some samples have opposite labels (i.e., label-switching), and consequently, blue and green dots are mixed in the figure. Although predictions made by a model are independent from the label-switching problem, since a sub-model for each cluster cannot be identified with the mixed labels, the samples should be re-labeled.

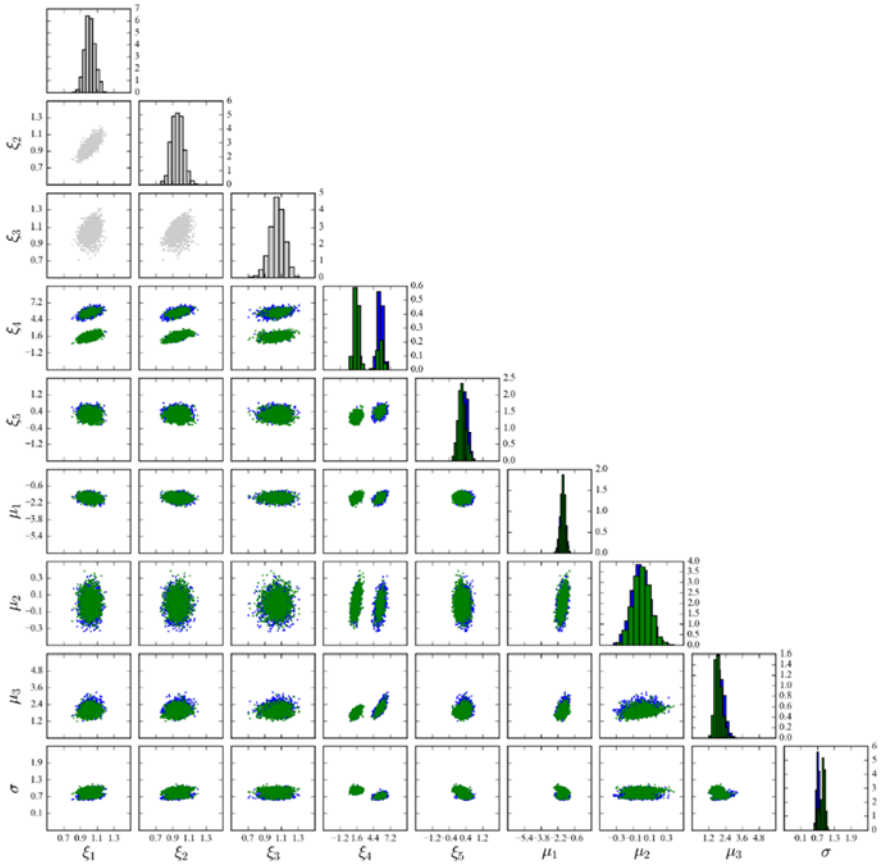

Figure A-1. SMC samples for parameters in case of the model having two clusters before re-labeled

In this study, SMC samples were re-labeled by following procedures.

- Find a sample which has the highest posterior among the samples, and set its $z_{1:D}$ as a reference, $z_{1:D,\mathrm{ref}}$.
- Define a permutation ψ of the labels $1, \ldots, K$, where $\psi \in \Psi_K$, the set of all the permutations of the labels.

- For each sample, find ψ_{relabel} which maximizes the following:

$$\psi_{\text{relabel}} = \arg\max_{\psi \in \Psi_K} \prod_{d=1}^{D} P\left(\mathbf{y}_d \middle| \mathbf{X}_d, z_{d,\text{ref}}, \boldsymbol{\mu}_{\psi_{z_{d,\text{ref}}}}, \sigma_{\psi_{z_{d,\text{ref}}}}, \boldsymbol{\xi}_{\psi_{z_{d,\text{ref}}}}\right) \quad \text{(A-1)}$$

- Re-label the sample based on ψ_{relabel}.
- For example, if $K = 3, \psi_{\text{relabel}} = (2,1,3)$, then $\boldsymbol{\theta}_{\text{relabeled},1} = \boldsymbol{\theta}_2, \boldsymbol{\theta}_{\text{relabeled},2} = \boldsymbol{\theta}_1, \boldsymbol{\theta}_{\text{relabeled},3} = \boldsymbol{\theta}_3$, where $\boldsymbol{\theta}_k = (\boldsymbol{\mu}_k, \sigma_k, \boldsymbol{\xi}_k)$.

APPENDIX B. METHOD FOR DISCOVERING THE OPTIMAL NUMBER OF CLUSTERS

Bayesian model selection

In Bayesian model selection Bayes rule is applied to quantify the posterior probability of a model being right. Let $\mathcal{M} = \{M_1, \dots, M_R\}$ be the set of all models that we would like to compare, θ_i be the M_i model parameters with prior $P(\theta_i|M_i)$, $\mathcal{D}$ be the experimental data, $P(\mathcal{D}|\theta_i, M_i)$ the likelihood of model M_i, and $P(M_i)$ the prior probability we assign to M_i being the right model, e.g., $P(M_i) = \frac{1}{R}$ if we are indifferent. Each model is trained using Bayes inference to compute the posterior of the parameters:

$$P(\theta_i|\mathcal{D}, M_i) = \frac{P(\mathcal{D}|\theta_i, M_i)P(\theta_i|M_i)}{P(\mathcal{D}|M_i)} \tag{B-1}$$

where the normalization constant,

$$P(\mathcal{D}|M_i) = \int P(\mathcal{D}|\theta_i, M_i)P(\theta_i|M_i)d\theta_i \tag{B-2}$$

is known as the model evidence. The model evidence is notoriously difficult to evaluate using MCMC [94]. However, the SMC sampling approach we adopted in Section 3.2.3 provides a robust estimator [95]. The evidence $P(\mathcal{D}|M_i)$ gives the probability that the dataset is observed conditioned on model M_i being the best one. Using Bayes rule, the probability that model M_i is the best conditioned on the observed data $\mathcal{D}$ is:

$$P(M_i|\mathcal{D}) \propto P(\mathcal{D}|M_i)P(M_i) \tag{B-3}$$

This distribution over models quantifies our state of knowledge about which model is best after we have seen the data. If we had to select one of them, we would pick the maximum a posteriori estimate (MAE):

$$i^* = \arg\max_{i=1,\dots,R} P(M_i|\mathcal{D}) \tag{B-4}$$

If we are a priori indifferent, this MAE is the model with the maximum evidence:

$$i^* = \arg\max_{i=1,\dots,R} P(\mathcal{D}|M_i) \tag{B-5}$$

This process automatically avoids overfitting by choosing the simplest model that adequately explains the data, see [74]. Note that the absolute value of the model evidence does not provide information about the validity of a model. The model evidence can only be used to compare the validity of two or more models. As shown above, it can be used to quantify the probability that

any given model in a set of candidate models is valid, albeit conditioned on the belief that at least one of them is valid. To compare two models to each other, we can use the ratio of the evidence which is known as the Bayes factor (BF). When we are a priori indifferent, the BF is nothing more than the ratio of the probabilities of each model being the right one.

$$BF_{1,0} \triangleq \frac{P(D|M_1)}{P(D|M_0)} \tag{B-6}$$

In practice, we use the Jeffrey's scale of evidence [96] to interpreting BF (Table B-1).

Table B-1. Jeffrey's scale of evidence for interpreting Bayes factors

Bayes factor $BF_{1,0}$	**Interpretation**
$BF_{1,0} < \frac{1}{100}$	Decisive evidence for M_0
$\frac{1}{100} < BF_{1,0} < \frac{1}{10}$	Strong evidence for M_0
$\frac{1}{10} < BF_{1,0} < \frac{1}{3}$	Moderate evidence for M_0
$\frac{1}{3} < BF_{1,0} < 1$	Weak evidence for M_0
$1 < BF_{1,0} < 3$	Weak evidence for M_1
$3 < BF_{1,0} < 10$	Moderate evidence for M_1
$10 < BF_{1,0} < 100$	Strong evidence for M_1
$100 < BF_{1,0}$	Decisive evidence for M_1

Dirichlet process prior

A DP defines a probability measure over a space of probability measures. To narrow down the discussion, let us consider the space of probability measures over the space of model parameters:

$$\mathcal{P} = \{G: \Theta \to \mathbf{R}_+ : \mathrm{G \text{ is a probability measure}}\} \tag{B-7}$$

This is the space where the prior probability distribution we assign to all model parameters, θ, lives. A DP assigns a probability measure on $\mathcal{P}$. Mathematically, a DP is characterized by a base probability measure $G_0 \in \mathcal{P}$ and a concentration parameter $\alpha_0 > 0$. We write $\mathrm{DP}(\mathrm{G}_0, \alpha_0)$ and we read "the DP with base measure G_0 and scale parameter α_0". For the formal definition see [97]. The DP has a special property that makes it extremely useful in clustering applications. Namely, it can be shown [98] that all sampled measures G from $\mathrm{DP}(\mathrm{G}_0, \alpha_0)$ are discrete distributions, i.e., they can be written as:

$$G(\theta) = \sum_{k=1}^{\infty} \pi_k \delta(\theta - \theta_k) \tag{B-8}$$

where δ is the Dirac δ-function, with point masses distributed according to the base measure, i.e., $\theta_i \sim G_0$, weights π_k decaying at a rate specified by α_0. So, the idea is that, if we assign this prior probability measure on the prior distribution of the model parameters, θ, then we automatically get a model with an arbitrarily large number of clusters. To be consistent with our existing model, the base measure must be the prior probability distribution we assigned to θ is Section 3.2.2, $G_0(\theta) \equiv P(\theta)$. The choice of α_0 controls how many clusters we believe there are a priori. At the extreme, a choice of $\alpha_0 = 0$ corresponds to the belief that there is a single cluster. Small α_0 corresponds to the a priori belief that the number of clusters is small, and large α_0 to the a priori belief that the number of clusters is large. Once this connection of the DP to the prior of the model of Section 3.2.2 has been established, we may proceed with Bayesian inference and let the data decide how many clusters are needed.

Bayesian inference in the DP-based model is not trivial. Fortunately, one may exploit the "stick-breaking" construction [99] of the DP to proceed. This "stick-breaking" construction is equivalent to assigning the following prior over the cluster value z [97],

$$P(z_{1:D}|\mathbf{v}) = \prod_{d=1}^{D} \pi_{z_d}(\mathbf{v}) \tag{B-9}$$

where

$$\pi_k(\mathbf{v}) = v_k \prod_{i=1}^{k-1} (1 - v_i) \tag{B-10}$$

and

$$P(\mathbf{v}|\alpha_0) = \prod_{k=1}^{\infty} \mathcal{B}\text{eta}(v_k|1, \alpha_0) \tag{B-11}$$

In other words, the π_k's can be interpreted as the probability of cluster k being active. To close the model, we need to pick a value for the concentration parameter α0. For lack of better alternatives, we employ a hierarchical Bayesian approach and assign an exponential distribution to it, i.e., $\mathrm{P}(\alpha_0) = \mathcal{E}(\alpha_0|1)$. In practice, the products of Eq. (B-11) are truncated at a large, but finite, $K_{\max}$. To be safe, this value must be picked to be much bigger than the maximum number of cluster we anticipate to find. In our work, we find that the choice $K_{\max} = 7$ is adequate. Once

these connections have been established, inference proceeds with SMC with just one additional parameter: the fractional "stick" $\boldsymbol{\nu}$. Although DP-based model is useful and gives additional information, $P(z_{1:D}|\boldsymbol{\nu})$, since it needs further investigation, it is exploited only for discovering the optimal number of clusters in this work.

APPENDIX C. MATHEMATICAL DETAILS FOR LEARNING THE PERSONAL PREFERENCE PROFILES

The following is the derivation of factorization in Eq. (3-32):

$$\int \sum_{z_{1:D}} P(z_{\text{new}}, z_{1:D}, \boldsymbol{\theta} | \mathbf{y}_{\text{new}}, \mathbf{X}_{\text{new}}, \mathbf{y}_{1:D}, \mathbf{X}_{1:D})\, d\boldsymbol{\theta}$$

$$= \int \sum_{z_{1:D}} P(z_{\text{new}} | \mathbf{y}_{\text{new}}, \mathbf{X}_{\text{new}}, \mathbf{y}_{1:D}, \mathbf{X}_{1:D}, z_{1:D}, \boldsymbol{\theta}) P(z_{1:D}, \boldsymbol{\theta} | \mathbf{y}_{\text{new}}, \mathbf{X}_{\text{new}}, \mathbf{y}_{1:D}, \mathbf{X}_{1:D})\, d\boldsymbol{\theta}$$

$$\approx \int \sum_{z_{1:D}} P(z_{\text{new}} | \mathbf{y}_{\text{new}}, \mathbf{X}_{\text{new}}, \mathbf{y}_{1:D}, \mathbf{X}_{1:D}, z_{1:D}, \boldsymbol{\theta}) P(z_{1:D}, \boldsymbol{\theta} | \mathbf{y}_{1:D}, \mathbf{X}_{1:D})\, d\boldsymbol{\theta} \quad \text{(by the assumption)}$$

$$= \int \sum_{z_{1:D}} \frac{P(\mathbf{y}_{\text{new}} | \mathbf{X}_{\text{new}}, \mathbf{y}_{1:D}, \mathbf{X}_{1:D}, z_{1:D}, \boldsymbol{\theta}, z_{\text{new}}) P(z_{new})}{P(\mathbf{y}_{\text{new}} | \mathbf{X}_{\text{new}}, \mathbf{y}_{1:D}, \mathbf{X}_{1:D}, z_{1:D}, \boldsymbol{\theta})} P(z_{1:D}, \boldsymbol{\theta} | \mathbf{y}_{1:D}, \mathbf{X}_{1:D})\, d\boldsymbol{\theta} \quad \text{(C-1)}$$

$$= \int \sum_{z_{1:D}} \frac{P(\mathbf{y}_{\text{new}} | \mathbf{X}_{\text{new}}, \boldsymbol{\theta}, z_{\text{new}}) P(z_{new})}{P(\mathbf{y}_{\text{new}} | \mathbf{X}_{\text{new}}, \boldsymbol{\theta})} P(z_{1:D}, \boldsymbol{\theta} | \mathbf{y}_{1:D}, \mathbf{X}_{1:D})\, d\boldsymbol{\theta}$$

$$= \int \sum_{z_{1:D}} P(z_{\text{new}} | \mathbf{y}_{\text{new}}, \mathbf{X}_{\text{new}}, \boldsymbol{\theta}) P(z_{1:D}, \boldsymbol{\theta} | \mathbf{y}_{1:D}, \mathbf{X}_{1:D})\, d\boldsymbol{\theta}$$

$$= \frac{1}{C_1} \int \sum_{z_{1:D}} P(\mathbf{y}_{\text{new}} | \mathbf{X}_{\text{new}}, \boldsymbol{\theta}, z_{\text{new}}) P(z_{\text{new}}) P(z_{1:D}, \boldsymbol{\theta} | \mathbf{y}_{1:D}, \mathbf{X}_{1:D})\, d\boldsymbol{\theta}$$

The following equation shows how the right-hand side of Eq. (3-32) can be computed efficiently with the SMC particles:

$$\int \sum_{z_{1:D}} P(\mathbf{y}_{\text{new}} | \mathbf{X}_{\text{new}}, \boldsymbol{\theta}, z_{\text{new}}) P(z_{\text{new}}) P(z_{1:D}, \boldsymbol{\theta} | \mathbf{y}_{1:D}, \mathbf{X}_{1:D})\, d\boldsymbol{\theta}$$

$$\approx \sum_{i=1}^{\#\, Particles} w^{(i)} P\left(\mathbf{y}_{\text{new}} \middle| \mathbf{X}_{\text{new}}, \boldsymbol{\theta}^{(i)}, z_{\text{new}}\right) P(z_{\text{new}}) \quad \text{(by the particle approximation)} \quad \text{(C-2)}$$

where w is the weight of each particle (in this study, every particle has the same weight since they were scaled, i.e., w = 1/3000). The following equation shows how Eq. (3-33) can be computed efficiently with the SMC particles:

$$\int \sum_{z_{\text{new}}} \sum_{z_{1:D}} P\left(y_{\text{p}} = j \middle| \mathbf{x}_{\text{p}}, z_{\text{new}}, \boldsymbol{\theta}\right) P(\mathbf{y}_{\text{new}} | \mathbf{X}_{\text{new}}, \boldsymbol{\theta}, z_{\text{new}}) P(z_{\text{new}}) P(z_{1:D}, \boldsymbol{\theta} | \mathbf{y}_{1:D}, \mathbf{X}_{1:D})\, d\boldsymbol{\theta}$$

$$\approx \sum_{k=1}^{K} \sum_{i=1}^{\#Particles} w^{(i)} P\left(y_{\text{p}} = j \middle| \mathbf{x}_{\text{p}}, z_{\text{new}} = k, \boldsymbol{\theta}^{(i)}\right) P\left(\mathbf{y}_{\text{new}} \middle| \mathbf{X}_{\text{new}}, \boldsymbol{\theta}^{(i)}, z_{\text{new}} = k\right) P(z_{\text{new}} = k) \quad \text{(C-3)}$$

APPENDIX D. BETA REGRESSION

We assume that the likelihood of observing the dissatisfaction level, y, in a day follows a Beta distribution. The probability density function of the beta distribution is parametrized as:

$$B(y|\mu,\phi) = \frac{\Gamma(\phi)}{\Gamma(\mu\phi)\Gamma\big((1-\mu)\phi\big)} y^{\mu\phi-1}(1-y)^{(1-\mu)\phi-1}, \qquad 0 < y < 1 \tag{D-1}$$

where $0 < \mu < 1$, $\phi > 0$, and $\Gamma(\cdot)$ is the gamma function [61]. Here, the mean and variance of y are μ and $\mu(1-\mu)/(1+\phi)$, respectively.

Subsequently, to link the number of elapsed days, x, and shape of Beta distributions over the period, we construct the following linear relationships:

$$g_1\big(\mu^{(i)}\big) = \beta_0 + \beta_1 x^{(i)} \tag{D-2}$$

$$g_2\big(\phi^{(i)}\big) = \beta_2 + \beta_3 x^{(i)} \tag{D-3}$$

Here, $g_1(\cdot)$ and $g_2(\cdot)$ are link functions which are used to transform values and ensure the constraints, $0 < \mu < 1$, $\phi > 0$. We use the logit function ($g_1(\mu) = \log(\mu/(1-\mu))$) and log function ($g_2(\phi) = \log(\phi)$) for $g_1(\cdot)$ and $g_2(\cdot)$, respectively [62].

The likelihood of the Beta regression is:

$$p(\mathbf{y}|\boldsymbol{\mu},\boldsymbol{\phi}) = \prod_{i=1}^{N} B\big(y^{(i)}\big|\mu^{(i)},\phi^{(i)}\big) \tag{D-4}$$

where $\mathbf{y} = \big(y^{(1)}, \dots y^{(N)}\big)$, $\boldsymbol{\mu} = (\mu^{(1)}, \dots, \mu^{(N)})$, $\boldsymbol{\phi} = (\phi^{(1)}, \dots, \phi^{(N)})$, $B(\cdot\,|\mu,\phi)$ is the probability density function of a Beta distribution in Eq. (D-1).

To carry out the regression in a fully Bayesian way, we assign priors to the coefficients $\boldsymbol{\beta} = (\beta_1, \beta_2, \beta_3, \beta_4)$. We assign a zero mean Gaussian prior as $p(\boldsymbol{\beta}|\alpha) = \mathcal{N}(\boldsymbol{\beta}|0, \lambda\mathbf{I})$, where $\mathcal{N}(\cdot\,|\boldsymbol{\mu},\boldsymbol{\Sigma})$ is the probability density function of a multivariate Gaussian distribution with mean $\boldsymbol{\mu}$ and covariance matrix $\boldsymbol{\Sigma}$, $\mathbf{I}$ is the 4-dimensional unit matrix. We set $\lambda = 10{,}000$ since we do not have specific prior knowledge.

We use Python PyMC3 [63] package to code the model as well as sample from the posterior of $\boldsymbol{\beta}$ using Markov chain Monte Carlo (MCMC). After analyzing the traces, we decide to burn the first 100,000 samples and gather 5,000 samples by keeping one MCMC sample out of every 100. Figure D-1 shows the posterior probability distribution of $\boldsymbol{\beta}$. The posterior probability of β_1 (the slope parameter) being positive is nearly zero, which means that there is a high probability of a

negative correlation existing between x and $g_1(\mu)$ in Eq. (D-2). From the posterior, we conclude that the proposed controller reduced the dissatisfaction level over time.

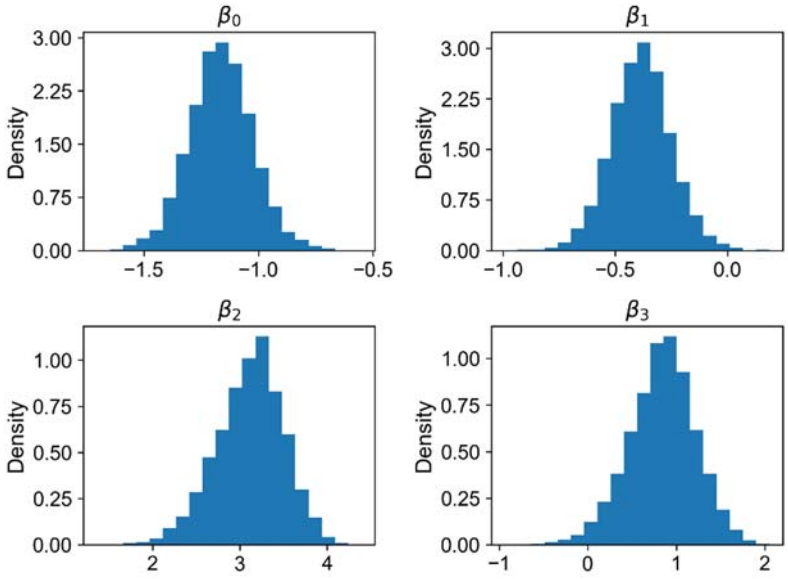

Figure D-1. Posterior distribution of the parameters.

APPENDIX E. ENERGY CONSUMPTION WITH DIFFERENT CONTROLLERS

We can quantify the effect of using different controllers on cooling energy consumption by coding causal relationships in a Bayesian model. In this study, we consider two input variables: (i) use of different controllers; (ii) mean outdoor air temperature, which directly affect the energy consumption, and train linear models. Before proceeding, we confirm our belief that there will be a positive correlation between the energy consumption and the mean outdoor temperature by plotting the two variables (Figure E-1). Then, we preprocess the data for the modeling: (i) we work with the logarithm of the energy consumption since it is a positive variable; (ii) we standardize the energy values by subtracting their mean and dividing by their standard deviation.

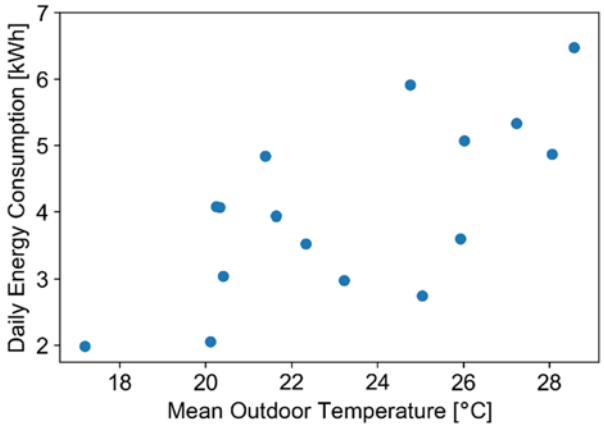

Figure E-1. Daily energy consumption and mean outdoor temperature during the entire period.

Instead of training two linear regression models for the baseline and proposed controllers separately, we train one model including both cases to encode the order between the two cases in the energy consumption.

The likelihood of the model is:

$$p\left(\mathbf{y}_j \middle| \boldsymbol{\mu}_j, \sigma_j^2\right) = \prod_{j=1}^{2} \prod_{i=1}^{N_j} \mathcal{N}\left(y_j^{(i)} \middle| \mu_j^{(i)}, \sigma_j^2\right) \tag{E-1}$$

$$\mu_j^{(i)} = \beta_{j,0} + \beta_{j,1} x_j^{(i)} \tag{E-2}$$

where $j = 1{,}2$ represents the baseline and proposed controller, respectively, $\mathbf{y}_j = \left(y_j^{(1)}, \dots, y_j^{(N_j)}\right)$, $\boldsymbol{\mu}_j = \left(\mu_j^{(1)}, \dots, \mu_j^{(N_j)}\right)$, y and x are the preprocessed energy consumption and mean outdoor temperature, respectively. Here, we strictly encode the order by forcing $\mu_1 \leq \mu_2$ whenever the mean outdoor temperature is higher than 18 °C, i.e., when a positive cooling load could exist. We set the following priors: $p(\beta_{j,0}|\lambda) = \mathcal{N}(\beta_{j,0}|0, \lambda)$, $p(\beta_{j,1}|\lambda) = \mathcal{E}(\beta_{j,1}|\lambda)$, and $p(\sigma|\lambda) = \mathcal{E}(\sigma|\lambda)$, which mean $\beta_{j,0}$ are real numbers while $\beta_{j,1}$and σ are positive real numbers. We set $\lambda = 10000$ since we do not have specific prior knowledge.

We sample from the posterior of the model parameters using Markov chain Monte Carlo (MCMC). We burn the first 100,000 samples and gather 2,000 samples by keeping one MCMC sample out of every 250.

Figure E-2 shows the two sub-models for the two cases, respectively. In each plot, blue dots are actual data points, blue line and shaded area with orange color respectively represent the median and 95% credible interval of mean of normal distributions (μ_j in Eq. (E-2)). Shaded area with green color represents the full uncertainty of the daily energy consumption.

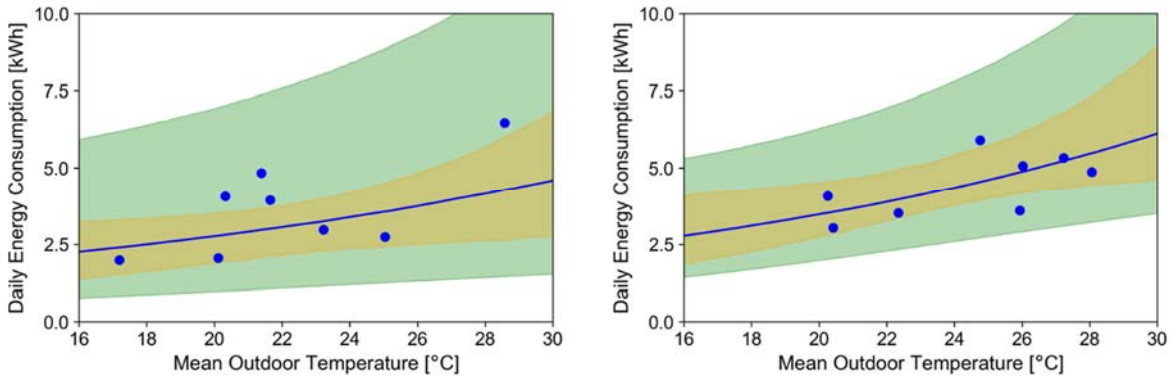

Figure E-2. Bayesian linear regression models for the relationship between daily energy consumption and mean outdoor temperature with the baseline (left) and the self-tuned controller (right)

Then, we can calculate the predictive probability distribution of the daily energy consumption during summer period by integrating the mean outdoor temperature out from the sub-models as:

$$p(y|j, \mathbf{Data}) = \iint p(y|j, x, \boldsymbol{\theta}) p(x) p(\boldsymbol{\theta}|\mathbf{Data})\, d\boldsymbol{\theta}\, dx \tag{E-3}$$

where $\boldsymbol{\theta} = (\beta_{0,0}, \beta_{0,1}, \beta_{1,0}, \beta_{1,1}, \sigma)$ are the model parameters, **Data** are the training data, $p(\boldsymbol{\theta}|\mathbf{Data})$ is the posterior probability distribution, and $p(x)$ is the probability distribution of the mean outdoor temperature. For the latter, we fit a skewed normal distribution [64] to the mean outdoor temperature measured between July 1st to September 30th, 2018 (Figure E-3) and use it for $p(x)$. For the fitting, we use stats function in Python SciPy [65] package. Figure 5.18 shows the predictive probability distribution of the daily energy consumption (Eq. (E-3)).

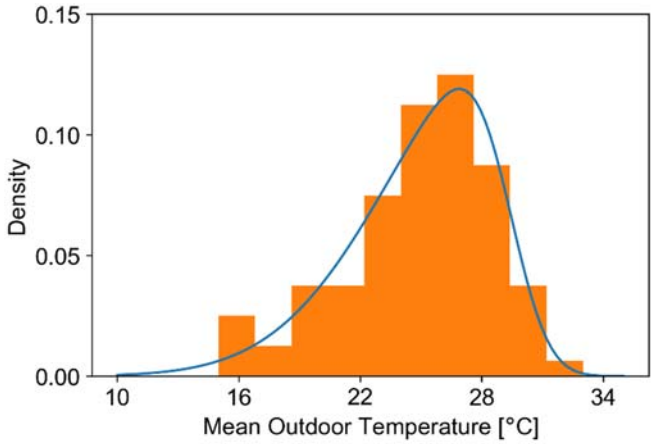

Figure E-3. Distribution of mean outdoor temperature measured between July 1st to September 30th, 2018 (normalized histogram) and probability density of a skewed normal distribution fitted with the measured data (blue line).

APPENDIX F. PROBABILITY CALCULATION

Let A and B represent $|l|$ and h_{v_1}, respectively. Since the PDF of the sum of two random variables equals the convolution of PDFs of the two variables, we can compute $p(v_1 = 0|t, \boldsymbol{\theta})$ as

$$\begin{aligned} &p(v_1 = 0|t, \boldsymbol{\theta}) \\ &= p(-A + B > \delta|t, \boldsymbol{\theta}) \\ &= 1 - p(-A + B < \delta|t, \boldsymbol{\theta}) \\ &= 1 - \int p(B < \delta + A|A, t, \boldsymbol{\theta}) p(A|t, \boldsymbol{\theta})\, dA \end{aligned} \tag{F-1}$$

where

$$p(A|t, \boldsymbol{\theta}) = \mathcal{FN}(A|f(t), 1) \tag{F-2}$$

$$p(B|\boldsymbol{\theta}) = \mathcal{N}(B|0, \sigma_v^2) \tag{F-3}$$

$\mathcal{FN}(\cdot\,|\mu, \sigma^2)$ is the PDF of a folded normal distribution with mean μ and variance σ^2.

Now, let A and B represent l and h_{v_1}, respectively. Then, we can compute $p(v_1 = 0|l < -\tau, \boldsymbol{\theta})$ as

$$\begin{aligned} &p(v_1 = 0|l < -\tau, \boldsymbol{\theta}) \\ &= p(A + B > \delta|t, \boldsymbol{\theta}) \\ &= 1 - \ p(A + B < \delta|t, \boldsymbol{\theta}) \\ &= 1 - \int p(A < \delta - B|B, t, \boldsymbol{\theta}) p(B|\boldsymbol{\theta})\, dB \end{aligned} \tag{F-4}$$

where

$$p(A|t, \boldsymbol{\theta}) = \mathcal{TN}(A|f(t), 1, -\infty, -\tau) \tag{F-5}$$

$$p(B|\boldsymbol{\theta}) = \mathcal{N}(B|0, \sigma_v^2) \tag{F-6}$$

$\mathcal{TN}(\cdot\,|\mu, \sigma^2, \text{lb}, \text{ub})$ is the PDF of a truncated normal distribution with mean μ, variance σ^2, lower bound lb, and upper bound ub.

Similarly, we can compute $p(v_1 = 0|l > \tau, \boldsymbol{\theta})$ as

$$\begin{aligned} &p(v_1 = 0|l > \tau, \boldsymbol{\theta}) \\ &= p(-A + B > \delta|t, \boldsymbol{\theta}) \\ &= 1 - \ p(-A + B < \delta|t, \boldsymbol{\theta}) \\ &= 1 - \int p(-A < \delta - B|B, t, \boldsymbol{\theta}) p(B|\boldsymbol{\theta})\, dB \end{aligned} \tag{F-7}$$

where

$$p(A|t,\boldsymbol{\theta}) = \mathcal{TN}(A|f(t),1,\tau,\infty) \tag{F-8}$$

$$p(B|\boldsymbol{\theta}) = \mathcal{N}(B|0,\sigma_v^2) \tag{F-9}$$

Since, Eq. (F-1), (F-4), (F-7) cannot be computed analytically, we use Gauss-Hermite quadrature [114] with 100 points to compute it numerically.

APPENDIX G. SEQUENTIAL MONTE CARLO

Let us suppose that our joint probability is:

$$p(\boldsymbol{\theta}|\mathbf{D}) = \frac{p(\mathbf{D}|\boldsymbol{\theta})p(\boldsymbol{\theta})}{p(\mathbf{D})} \tag{G-1}$$

where $\mathbf{D}$ is a dataset of N observations and $\boldsymbol{\theta}$ is model parameters. We define a family of distributions that will take us from the prior to the posterior with increasing complexity:

$$p(\boldsymbol{\theta}|\mathbf{D},\gamma) \propto \pi_\gamma(\boldsymbol{\theta}) \coloneqq p(\mathbf{D}|\boldsymbol{\theta})^\gamma p(\boldsymbol{\theta}) \tag{G-2}$$

subject to $0 \leq \gamma \leq 1$. Here, $\gamma = 0$ corresponds to the prior:

$$p(\boldsymbol{\theta}|\mathbf{D},\gamma = 0) \propto \pi_0(\boldsymbol{\theta}) = p(\boldsymbol{\theta}) \tag{G-3}$$

$\gamma = 1$ means the posterior:

$$p(\boldsymbol{\theta}|\mathbf{D},\gamma = 1) \propto \pi_1(\boldsymbol{\theta}) = p(\mathbf{D}|\boldsymbol{\theta})p(\boldsymbol{\theta}) \tag{G-4}$$

The particle approximation to the distribution is:

$$p(\boldsymbol{\theta}|\mathbf{D},\gamma) = \sum_{i=1}^{I} w_{r,i}\delta\left(\boldsymbol{\theta}_{\gamma,i} - \boldsymbol{\theta}\right) \tag{G-5}$$

where $\boldsymbol{\theta}_{\gamma,i}$ is a sample (particle) from $\pi_\gamma(\boldsymbol{\theta})$:

$$\boldsymbol{\theta}_{\gamma,i} \sim \pi_\gamma(\boldsymbol{\theta}) = p(\mathbf{D}|\boldsymbol{\theta})^\gamma p(\boldsymbol{\theta}) \tag{G-6}$$

$$\sum_{i=1}^{I} w_{r,i} = 1 \tag{G-7}$$

For two consecutive gammas, $0 \leq \gamma_t < \gamma_{t+1} \leq 1$, we update the weights as:

$$w_{\gamma_{t+1},i} = \frac{W_{\gamma_{t+1},i}}{\sum_{j=1}^{I} W_{\gamma_{t+1},j}} \tag{G-8}$$

where

$$W_{\gamma_{t+1},i} = w_{\gamma_t,i}\frac{\pi_{\gamma_{t+1}}\left(\boldsymbol{\theta}_{\gamma_t,i}\right)}{\pi_{\gamma_t}\left(\boldsymbol{\theta}_{\gamma_t,i}\right)} \tag{G-9}$$

and sample particles, $\boldsymbol{\theta}_{\gamma_{t+1},1:I}$, from

$$\boldsymbol{\theta}_{\gamma_{t+1},i} \sim \pi_{\gamma_{t+1}}(\boldsymbol{\theta}) = p(\mathbf{D}|\boldsymbol{\theta})^{\gamma_{t+1}} p(\boldsymbol{\theta}) \tag{G-10}$$

by doing a few steps of MCMC.

To select intermediate gammas, we introduce the Effective Sample Size (EES, [115]),

$$\mathrm{ESS}(\gamma) = \frac{1}{\sum_{i=1}^{I} w_{r,i}^2} \tag{G-11}$$

and define an acceptable reduction in the ESS between two consecutive gammas as

$$\mathrm{ESS}(\gamma_{t+1}) \geq 0.95\mathrm{ESS}(\gamma_t) \tag{G-12}$$

If $\mathrm{ESS}(\gamma_t) \leq 0.5I$, we resample particles.

A benefit of using SMC is that we can compute the normalization constant of the posterior, $p(\mathbf{D})$, a.k.a., model evidence, as

$$Z = \prod_{t}^{T} \sum_{i=1}^{I} W_{r_t,i} \tag{G-13}$$

which is normally used for Bayesian model selection. In this study, this quantity is used in Appendix H.

For further details regarding SMC, please refer to [79].

APPENDIX H. BAYESIAN MODEL UPDATE WITH SEQUENTIAL MONTE CARLO

Let us suppose that we already estimated the posterior parameter distribution given some data, $\mathbf{D}$. We get new data points $\mathbf{D}_{\text{new}}$, and we want to update the posterior with it. Then, our joint probability is:

$$p(\boldsymbol{\theta}|\mathbf{D},\mathbf{D}_{\text{new}}) = \frac{p(\mathbf{D},\mathbf{D}_{\text{new}}|\boldsymbol{\theta})p(\boldsymbol{\theta})}{p(\mathbf{D},\mathbf{D}_{\text{new}})} \tag{H-1}$$

If $\mathbf{D}$ and $\mathbf{D}_{\text{new}}$ are conditionally independent,

$$p(\boldsymbol{\theta}|\mathbf{D},\mathbf{D}_{\text{new}}) = \frac{p(\mathbf{D}_{\text{new}}|\boldsymbol{\theta})p(\mathbf{D}|\boldsymbol{\theta})p(\boldsymbol{\theta})}{p(\mathbf{D},\mathbf{D}_{\text{new}})} = \frac{p(\mathbf{D}_{\text{new}}|\boldsymbol{\theta})p(\boldsymbol{\theta}|\mathbf{D})}{\frac{p(\mathbf{D},\mathbf{D}_{\text{new}})}{p(\mathbf{D})}} \tag{H-2}$$

Then, we can apply the same technique in Appendix G, introducing a family of distribution, to update the model efficiently as:

$$p(\boldsymbol{\theta}|\mathbf{D},\mathbf{D}_{\text{new}},\gamma) \propto \pi_\gamma(\boldsymbol{\theta}) \coloneqq p(\mathbf{D}_{\text{new}}|\boldsymbol{\theta})^\gamma p(\boldsymbol{\theta}|\mathbf{D}) = p(\mathbf{D}_{\text{new}}|\boldsymbol{\theta})^\gamma \frac{p(\mathbf{D}|\boldsymbol{\theta})p(\boldsymbol{\theta})}{p(\mathbf{D})} \tag{H-3}$$

subject to $0 \le \gamma \le 1$. Here, $p(\mathbf{D})$ is the normalization constant which was calculated when we estimated $p(\boldsymbol{\theta}|\mathbf{D})$ with SMC. The particle approximation to the distribution is:

$$p(\boldsymbol{\theta}|\mathbf{D},\mathbf{D}_{\text{new}},\gamma) = \sum_{i=1}^{I} w_{r,i}\delta\left(\boldsymbol{\theta}_{\gamma,i} - \boldsymbol{\theta}\right) \tag{H-4}$$

where $\boldsymbol{\theta}_{\gamma,i}$ is a sample (particle) from $\pi_\gamma(\boldsymbol{\theta})$:

$$\boldsymbol{\theta}_{\gamma,i} \sim \pi_\gamma(\boldsymbol{\theta}) = p(\mathbf{D}_{\text{new}}|\boldsymbol{\theta})^\gamma p(\boldsymbol{\theta}|\mathbf{D}) \tag{H-5}$$

$$\sum_{i=1}^{I} w_{r,i} = 1 \tag{H-6}$$

Then, the particle approximation to the distribution of $\gamma = 0$ is:

$$p(\boldsymbol{\theta}|\mathbf{D},\mathbf{D}_{\text{new}},\gamma = 0) = \sum_{i=1}^{I} w_{0,i}\delta\left(\boldsymbol{\theta}_{0,i} - \boldsymbol{\theta}\right) \tag{H-7}$$

where

$$\boldsymbol{\theta}_{0,i} \sim \pi_0(\boldsymbol{\theta}) = p(\boldsymbol{\theta}|\mathbf{D}) \tag{H-8}$$

In other words, we start this sequential process with the posterior samples of $p(\boldsymbol{\theta}|\mathbf{D})$, and finally, get the posterior samples representing $p(\boldsymbol{\theta}|\mathbf{D}, \mathbf{D}_{\text{new}})$. In addition, we can get the $p(\mathbf{D}_{\text{new}}|\mathbf{D})$, which is used in Appendix I, and subsequently $p(\mathbf{D}, \mathbf{D}_{\text{new}})$ through the process.

APPENDIX I. COMPUTATION OF THE EXPECTED KULLBACK–LEIBLER DIVERGENCE

We want to compute

$$U(t_{\text{new}}, r_{\text{new}}) = \mathbb{E}_y\left[D_{KL}\left(p(\boldsymbol{\theta}|\mathbf{D}, \mathbf{d}_{\text{new}}) \parallel p(\boldsymbol{\theta}|\mathbf{D})\right)\right]$$

$$= \int \sum_{y_{\text{new}}=-1}^{2} p(\boldsymbol{\theta}|\mathbf{D}, \mathbf{d}_{\text{new}}) p(y_{\text{new}}|\mathbf{D}, t_{\text{new}}, r_{\text{new}}) \log \frac{p(\boldsymbol{\theta}|\mathbf{D}, \mathbf{d}_{\text{new}})}{p(\boldsymbol{\theta}|\mathbf{D})} d\boldsymbol{\theta} \tag{I-1}$$

We can rewrite the above equation as

$$U(t_{\text{new}}, r_{\text{new}}) = \int \sum_{y_{\text{new}}=-1}^{2} p(y_{\text{new}}|\boldsymbol{\theta}, t_{\text{new}}, r_{\text{new}}) p(\boldsymbol{\theta}|\mathbf{D}) \log \frac{p(y_{\text{new}}|\boldsymbol{\theta}, t_{\text{new}}, r_{\text{new}})}{p(y_{\text{new}}|\mathbf{D}, t_{\text{new}}, r_{\text{new}})} d\boldsymbol{\theta} \tag{I-2}$$

as

$$p(\boldsymbol{\theta}|\mathbf{D}, \mathbf{d}_{\text{new}}) = \frac{p(y_{\text{new}}|\boldsymbol{\theta}, t_{\text{new}}, r_{\text{new}}) p(\boldsymbol{\theta}|\mathbf{D})}{p(y_{\text{new}}|\mathbf{D}, t_{\text{new}}, r_{\text{new}})} \tag{I-3}$$

Since we have the samples representing $p(\boldsymbol{\theta}|\mathbf{D})$, we can calculate the quantity using Monte Carlo integration as,

$$\frac{1}{N} \sum_{i=1}^{N} \sum_{y_{\text{new}}=-1}^{2} p(y_{\text{new}}|\boldsymbol{\theta}_i, t_{\text{new}}, r_{\text{new}}) \log \frac{p(y_{\text{new}}|\boldsymbol{\theta}_i, t_{\text{new}}, r_{\text{new}})}{p(y_{\text{new}}|\mathbf{D}, t_{\text{new}}, r_{\text{new}})} \tag{I-4}$$

We can compute $p(y_{\text{new}}|\mathbf{D}, t_{\text{new}}, r_{\text{new}})$, which corresponds to $p(\mathbf{D}_{\text{new}}|\mathbf{D})$ in Appendix H, easily through the process of the Bayesian model update with sequential Monte Carlo.

REFERENCES

[1] P.O. Fanger, Thermal comfort-analysis and applications in environmental engineering, Danish Technical Press, Copenhagen, 1970.

[2] Z. Wang, R. de Dear, M. Luo, B. Lin, Y. He, A. Ghahramani, Y. Zhu, Individual difference in thermal comfort: A literature review, Build. Environ. 138 (2018) 181–193. doi:https://doi.org/10.1016/j.buildenv.2018.04.040.

[3] ASHRAE® Handbook - Fundamentals 2017 (SI Edition), American Society of Heating, Refrigerating and Air-Conditioning Engineers, Inc., n.d. https://app.knovel.com/hotlink/toc/id:kpASHRAEQ1/ashrae-handbook-fundamentals/ashrae-handbook-fundamentals.

[4] A.P. Gagge, A.P. Fobelets, L.G. Berglund, Standard Predictive Index of Human Response to the Thermal Environment, ASHRAE Trans. 92 (1986) 709–731.

[5] R.J. de Dear, G. Brager, D. Cooper, Developing an Adaptive Model of Thermal Comfort and Preference, ASHRAE, 1997.

[6] F. Nicol, M. Humphreys, Derivation of the adaptive equations for thermal comfort in free-running buildings in European standard EN15251, Build. Environ. 45 (2010) 11–17. doi:https://doi.org/10.1016/j.buildenv.2008.12.013.

[7] ASHRAE, ANSI/ASHRAE Standard 55-2013, Therm. Environ. Cond. Hum. Occup. (2013).

[8] ISO, ISO Standard 7730-2005, Ergon. Therm. Environ. Anal. Determ. Interpret. Therm. Comf. Using Calc. PMV PPD Indices Local Therm. Comf. Criteria. (2005).

[9] EN, CSN EN 15251, Indoor Environ. Input Parameters Des. Assess. Energy Perform. Build. Addressing Indoor Air Qual. Therm. Environ. Light. Acoust. (n.d.).

[10] G.S. Brager, R.J. de Dear, Thermal adaptation in the built environment: a literature review, Energy Build. 27 (1998) 83–96. doi:http://dx.doi.org/10.1016/S0378-7788(97)00053-4.

[11] R.J. de Dear, G.S. Brager, Developing an adaptive model of thermal comfort and preference, ASHRAE Trans. 104 (1998).

[12] P.O. Fanger, Calculation of thermal comfort: Introduction of a basic comfort equation, ASHRAE Trans. 73 (1967).

[13] R.-L. Hwang, M.-J. Cheng, T.-P. Lin, M.-C. Ho, Thermal perceptions, general adaptation methods and occupant's idea about the trade-off between thermal comfort and energy saving in hot–humid regions, Build. Environ. 44 (2009) 1128–1134. doi:http://dx.doi.org/10.1016/j.buildenv.2008.08.001.

[14] J.F. Nicol, M.A. Humphreys, New standards for comfort and energy use in buildings, Build. Res. Inf. 37 (2009) 68–73. doi:10.1080/09613210802611041.

[15] T. Hoyt, E. Arens, H. Zhang, Extending air temperature setpoints: Simulated energy savings and design considerations for new and retrofit buildings, Build. Environ. 88 (2015) 89–96. doi:https://doi.org/10.1016/j.buildenv.2014.09.010.

[16] M.L. Taub, Power to the people: personal control in offices for thermal comfort and energy savings, University of California, Berkeley, 2013.

[17] S. Shellenbarger, Let the Office Thermostat Wars Begin, Wall Str. J. (2016).

[18] Y. Murakami, M. Terano, K. Mizutani, M. Harada, S. Kuno, Field experiments on energy consumption and thermal comfort in the office environment controlled by occupants' requirements from PC terminal, Build. Environ. 42 (2007) 4022–4027. doi:http://dx.doi.org/10.1016/j.buildenv.2006.05.012.

[19] M. Feldmeier, J.A. Paradiso, Personalized HVAC control system, in: Internet Things (IOT), 2010, 2010: pp. 1–8. doi:10.1109/IOT.2010.5678444.

[20] V.L. Erickson, A.E. Cerpa, Thermovote: participatory sensing for efficient building hvac conditioning, in: Proc. Fourth ACMWorkshop Embed. Sens. Syst. Energy-Efficiency Build., ACM, New York, NY, USA, 2012: pp. 9–16.

[21] P.X. Gao, S. Keshav, Optimal Personal Comfort Management Using SPOT+, Proc. 5th ACM Work. Embed. Syst. Energy-Efficient Build. (2013) 1–8. doi:10.1145/2528282.2528297.

[22] P.X. Gao, S. Keshav, SPOT: a smart personalized office thermal control system, Proc. Fourth Int. Conf. Futur. Energy Syst. (e-Energy '13). (2013) 237–246. doi:10.1145/2487166.2487193.

[23] F. Jazizadeh, A. Ghahramani, B. Becerik-Gerber, T. Kichkaylo, M. Orosz, User-led decentralized thermal comfort driven HVAC operations for improved efficiency in office buildings, Energy Build. 70 (2014) 398–410. doi:http://dx.doi.org/10.1016/j.enbuild.2013.11.066.

[24] J. Kim, S. Schiavon, G. Brager, Personal comfort models – A new paradigm in thermal comfort for occupant-centric environmental control, Build. Environ. 132 (2018) 114–124. doi:https://doi.org/10.1016/j.buildenv.2018.01.023.

[25] J.L.M. Hensen, On the thermal interaction of building structure and heating and ventilating system, Technische Universiteitt Eindhoven, 1991.

[26] M. Frontczak, P. Wargocki, Literature survey on how different factors influence human comfort in indoor environments, Build. Environ. 46 (2011) 922–937. doi:https://doi.org/10.1016/j.buildenv.2010.10.021.

[27] W. Cui, G. Cao, J.H. Park, Q. Ouyang, Y. Zhu, Influence of indoor air temperature on human thermal comfort, motivation and performance, Build. Environ. 68 (2013) 114–122. doi:http://dx.doi.org/10.1016/j.buildenv.2013.06.012.

[28] P. Roelofsen, The impact of office environments on employee performance: The design of the workplace as a strategy for productivity enhancement, J. Facil. Manag. 1 (2002) 247–264. doi:10.1108/14725960310807944.

[29] R. Kosonen, F. Tan, Assessment of productivity loss in air-conditioned buildings using PMV index, Energy Build. 36 (2004) 987–993. doi:http://dx.doi.org/10.1016/j.enbuild.2004.06.021.

[30] O. Seppanen, W.J. Fisk, Q.H. Lei, Room temperature and productivity in office work, ; Ernest Orlando Lawrence Berkeley NationalLaboratory, Berkeley, CA (US), 2006. http://www.osti.gov/scitech/servlets/purl/903492.

[31] K.L. Jensen, J. Toftum, P. Friis-Hansen, A Bayesian Network approach to the evaluation of building design and its consequences for employee performance and operational costs, Build. Environ. 44 (2009) 456–462. doi:10.1016/J.BUILDENV.2008.04.008.

[32] L. Lan, P. Wargocki, Z. Lian, Quantitative measurement of productivity loss due to thermal discomfort, Energy Build. 43 (2011) 1057–1062. doi:http://dx.doi.org/10.1016/j.enbuild.2010.09.001.

[33] G. Jendritzky, R. de Dear, Adaptation and Thermal Environment, in: K.L. Ebi, I. Burton, G.R. McGregor (Eds.), Biometeorol. Adapt. to Clim. Var. Chang., Springer Netherlands, Dordrecht, 2009: pp. 9–32. doi:10.1007/978-1-4020-8921-3_2.

[34] A. Ghahramani, K. Zhang, K. Dutta, Z. Yang, B. Becerik-Gerber, Energy savings from temperature setpoints and deadband: Quantifying the influence of building and system properties on savings, Appl. Energy. 165 (2016) 930–942. doi:https://doi.org/10.1016/j.apenergy.2015.12.115.

[35] N. Djongyang, R. Tchinda, D. Njomo, Thermal comfort: A review paper, Renew. Sustain. Energy Rev. 14 (2010) 2626–2640. doi:https://doi.org/10.1016/j.rser.2010.07.040.

[36] Y. Cheng, J. Niu, N. Gao, Thermal comfort models: A review and numerical investigation, Build. Environ. 47 (2012) 13–22. doi:http://dx.doi.org/10.1016/j.buildenv.2011.05.011.

[37] R.F. Rupp, N.G. Vásquez, R. Lamberts, A review of human thermal comfort in the built environment, Energy Build. 105 (2015) 178–205. doi:https://doi.org/10.1016/j.enbuild.2015.07.047.

[38] F.H. Rohles Jr., R.G. Nevins, The Nature of Thermal Comfort for Sedentary man, ASHRAE Trans. 77 (1971) 239–246.

[39] ASHRAE, ASHRAE Handbook: Fundamentals, 2013.

[40] J.A. Wagner, S.M. Horvath, Cardiovascular reactions to cold exposures differ with age and gender, J. Appl. Physiol. 58 (1985) 187–192. https://www.scopus.com/inward/record.uri?eid=2-s2.0-0021796413&partnerID=40&md5=af9984172a4b95c71a267a7d682f1b1b.

[41] J.T. Liou, P.W. Lui, Y.L. Lo, L. Liou, S.S. Wang, H.B. Yuan, K.H. Chan, T.Y. Lee, Normative data of quantitative thermal and vibratory thresholds in normal subjects in Taiwan: Gender and age effect, Chinese Med. J. 62 (1999) 431–437. https://www.scopus.com/inward/record.uri?eid=2-s2.0-0032772959&partnerID=40&md5=e17aa695a753e8d274649c8e0742fb93.

[42] K. Tsuzuki, T. Ohfuku, Thermal sensation and thermoregulation in elderly compared to young people in Japanese winter season, Proc. Indoor Air. 2 (2002) 659–664.

[43] P. Golja, M.J. Tipton, I.B. Mekjavic, Cutaneous thermal thresholds—the reproducibility of their measurements and the effect of gender, J. Therm. Biol. 28 (2003) 341–346. doi:https://doi.org/10.1016/S0306-4565(03)00010-X.

[44] R.F. Rupp, J. Kim, R. de Dear, E. Ghisi, Associations of occupant demographics, thermal history and obesity variables with their thermal comfort in air-conditioned and mixed-mode ventilation office buildings, Build. Environ. 135 (2018) 1–9. doi:https://doi.org/10.1016/j.buildenv.2018.02.049.

[45] W. Liu, Z. Lian, B. Zhao, A neural network evaluation model for individual thermal comfort, Energy Build. 39 (2007) 1115–1122. doi:http://dx.doi.org/10.1016/j.enbuild.2006.12.005.

[46] D. Daum, F. Haldi, N. Morel, A personalized measure of thermal comfort for building controls, Build. Environ. 46 (2011) 3–11. doi:http://dx.doi.org/10.1016/j.buildenv.2010.06.011.

[47] F. Jazizadeh, A. Ghahramani, B. Becerik-Gerber, T. Kichkaylo, M. Orosz, Human-Building Interaction Framework for Personalized Thermal Comfort-Driven Systems in Office Buildings, J. Comput. Civ. Eng. 28 (2014) 2–16. doi:doi:10.1061/(ASCE)CP.1943-5487.0000300.

[48] Q. Zhao, Y. Zhao, F. Wang, J. Wang, Y. Jiang, F. Zhang, A data-driven method to describe the personalized dynamic thermal comfort in ordinary office environment: From model to application, Build. Environ. 72 (2014) 309–318. doi:http://dx.doi.org/10.1016/j.buildenv.2013.11.008.

[49] F. Auffenberg, S. Stein, A. Rogers, A personalised thermal comfort model using a Bayesian network, 24th Int. Conf. Artif. Intell. (2015) 2547–2553.

[50] X. Chen, Q. Wang, J. Srebric, A data-driven state-space model of indoor thermal sensation using occupant feedback for low-energy buildings, Energy Build. 91 (2015) 187–198. doi:http://dx.doi.org/10.1016/j.enbuild.2015.01.038.

[51] M.S. D. Fiala, K.J. Lomas, First principles modeling of thermal sensation responses in steady-state and transient conditions, ASHRAE Trans. (2003) 179–186.

[52] A. Ghahramani, C. Tang, B. Becerik-Gerber, An online learning approach for quantifying personalized thermal comfort via adaptive stochastic modeling, Build. Environ. 92 (2015) 86–96. doi:http://dx.doi.org/10.1016/j.buildenv.2015.04.017.

[53] C.-C. Hu, H.-L. Li, Deducing the classification rules for thermal comfort controls using optimal method, Build. Environ. 98 (2016) 107–120. doi:http://dx.doi.org/10.1016/j.buildenv.2015.12.025.

[54] L. Jiang, R. Yao, Modelling personal thermal sensations using C-Support Vector Classification (C-SVC) algorithm, Build. Environ. 99 (2016) 98–106. doi:https://doi.org/10.1016/j.buildenv.2016.01.022.

[55] C. Sarkar, A.U.N. SN, V.R. Prasad, iLTC: Achieving Individual Comfort in Shared Spaces, in: Int. Conf. Embed. Wirel. Syst. Networks (EWSN 2016)}, ACM}, 2016.

[56] D. Li, C.C. Menassa, V.R. Kamat, Personalized human comfort in indoor building environments under diverse conditioning modes, Build. Environ. 126 (2017) 304–317. doi:https://doi.org/10.1016/j.buildenv.2017.10.004.

[57] A. Ghahramani, G. Castro, S.A. Karvigh, B. Becerik-Gerber, Towards unsupervised learning of thermal comfort using infrared thermography, Appl. Energy. 211 (2018) 41–49. doi:https://doi.org/10.1016/j.apenergy.2017.11.021.

[58] J. Kim, Y. Zhou, S. Schiavon, P. Raftery, G. Brager, Personal comfort models: Predicting individuals' thermal preference using occupant heating and cooling behavior and machine learning, Build. Environ. 129 (2018) 96–106. doi:https://doi.org/10.1016/j.buildenv.2017.12.011.

[59] A. Ghahramani, G. Castro, B. Becerik-Gerber, X. Yu, Infrared thermography of human face for monitoring thermoregulation performance and estimating personal thermal comfort, Build. Environ. 109 (2016) 1–11. doi:http://dx.doi.org/10.1016/j.buildenv.2016.09.005.

[60] R. Rana, B. Kusy, R. Jurdak, J. Wall, W. Hu, Feasibility analysis of using humidex as an indoor thermal comfort predictor, Energy Build. 64 (2013) 17–25. doi:https://doi.org/10.1016/j.enbuild.2013.04.019.

[61] A. Sanguinetti, M. Pritoni, K. Salmon, A. Meier, J. Morejohn, Upscaling participatory thermal sensing: Lessons from an interdisciplinary case study at University of California for improving campus efficiency and comfort, Energy Res. Soc. Sci. 32 (2017) 44–54. doi:https://doi.org/10.1016/j.erss.2017.05.026.

[62] A. Ghahramani, F. Jazizadeh, B. Becerik-Gerber, A knowledge based approach for selecting energy-aware and comfort-driven HVAC temperature set points, Energy Build. 85 (2014) 536–548. doi:http://dx.doi.org/10.1016/j.enbuild.2014.09.055.

[63] S.K. Gupta, K. Kar, S. Mishra, J.T. Wen, Singular Perturbation Method for Smart Building Temperature Control Using Occupant Feedback, Asian J. Control. 20 (2018) 386–402. doi:doi:10.1002/asjc.1587.

[64] S.R. West, J.K. Ward, J. Wall, Trial results from a model predictive control and optimisation system for commercial building HVAC, Energy Build. 72 (2014) 271–279. doi:https://doi.org/10.1016/j.enbuild.2013.12.037.

[65] Y. Ma, A. Kelman, A. Daly, F. Borrelli, Predictive Control for Energy Efficient Buildings with Thermal Storage: Modeling, Stimulation, and Experiments, IEEE Control Syst. Mag. 32 (2012) 44–64. doi:10.1109/MCS.2011.2172532.

[66] S.C. Bengea, A.D. Kelman, F. Borrelli, R. Taylor, S. Narayanan, Implementation of model predictive control for an HVAC system in a mid-size commercial building, HVAC&R Res. 20 (2014) 121–135. doi:10.1080/10789669.2013.834781.

[67] F. Oldewurtel, A. Parisio, C.N. Jones, D. Gyalistras, M. Gwerder, V. Stauch, B. Lehmann, M. Morari, Use of model predictive control and weather forecasts for energy efficient building climate control, Energy Build. 45 (2012) 15–27. doi:https://doi.org/10.1016/j.enbuild.2011.09.022.

[68] C.D. Corbin, G.P. Henze, P. May-Ostendorp, A model predictive control optimization environment for real-time commercial building application, J. Build. Perform. Simul. 6 (2013) 159–174. doi:10.1080/19401493.2011.648343.

[69] J.E. Braun, K.W. Montgomery, N. Chaturvedi, Evaluating the Performance of Building Thermal Mass Control Strategies, HVAC&R Res. 7 (2001) 403–428. doi:10.1080/10789669.2001.10391283.

[70] A. Majumdar, J.L. Setter, J.R. Dobbs, B.M. Hencey, D.H. Albonesi, Energy-comfort optimization using discomfort history and probabilistic occupancy prediction, in: Int. Green Comput. Conf., 2014: pp. 1–10. doi:10.1109/IGCC.2014.7039173.

[71] J. Zhao, K.P. Lam, B.E. Ydstie, V. Loftness, Occupant-oriented mixed-mode EnergyPlus predictive control simulation, Energy Build. 117 (2016) 362–371. doi:https://doi.org/10.1016/j.enbuild.2015.09.027.

[72] X. Chen, Q. Wang, J. Srebric, Occupant feedback based model predictive control for thermal comfort and energy optimization: A chamber experimental evaluation, Appl. Energy. 164 (2016) 341–351. doi:https://doi.org/10.1016/j.apenergy.2015.11.065.

[73] S. Barlow, D. Fiala, Occupant comfort in UK offices—How adaptive comfort theories might influence future low energy office refurbishment strategies, Energy Build. 39 (2007) 837–846. doi:http://dx.doi.org/10.1016/j.enbuild.2007.02.002.

[74] S.P. Corgnati, M. Filippi, S. Viazzo, Perception of the thermal environment in high school and university classrooms: Subjective preferences and thermal comfort, Build. Environ. 42 (2007) 951–959. doi:http://dx.doi.org/10.1016/j.buildenv.2005.10.027.

[75] A. Wagner, E. Gossauer, C. Moosmann, T. Gropp, R. Leonhart, Thermal comfort and workplace occupant satisfaction—Results of field studies in German low energy office buildings, Energy Build. 39 (2007) 758–769. doi:http://dx.doi.org/10.1016/j.enbuild.2007.02.013.

[76] J. Langevin, J. Wen, P.L. Gurian, Modeling thermal comfort holistically: Bayesian estimation of thermal sensation, acceptability, and preference distributions for office building occupants, Build. Environ. 69 (2013) 206–226. doi:http://dx.doi.org/10.1016/j.buildenv.2013.07.017.

[77] K.P. Murphy, Machine learning: a probabilistic perspective, MIT press, 2012.

[78] C. Dai, H. Zhang, E. Arens, Z. Lian, Machine learning approaches to predict thermal demands using skin temperatures: Steady-state conditions, Build. Environ. 114 (2017) 1–10. doi:https://doi.org/10.1016/j.buildenv.2016.12.005.

[79] I. Bilionis, P.S. Koutsourelakis, Free energy computations by minimization of Kullback–Leibler divergence: An efficient adaptive biasing potential method for sparse representations, J. Comput. Phys. 231 (2012) 3849–3870. doi:http://dx.doi.org/10.1016/j.jcp.2012.01.033.

[80] I. Bilionis, PySMC, (2014). https://github.com/PredictiveScienceLab/pysmc.

[81] C. Fonnesbeck, A. Patil, D. Huard, J. Salvatier, PyMC, (2015). https://pymc-devs.github.io/pymc/.

[82] A. Jasra, C.C. Holmes, D.A. Stephens, Markov Chain Monte Carlo Methods and the Label Switching Problem in Bayesian Mixture Modeling, Stat. Sci. 20 (2005) 50–67. http://www.jstor.org/stable/20061160.

[83] C.M. Bishop, Pattern Recognition and Machine Learning, Springer New York, 2006.

[84] Y.W. Teh, Dirichlet processes: Tutorial and practical course, Gatsby Comput. Neurosci. Unit, Univ. Coll. London. (2007).

[85] D.M. Blei, M.I. Jordan, Variational inference for Dirichlet process mixtures, Bayesian Anal. 1 (2006) 121–144.

[86] T. Oden, R. Moser, O. Ghattas, Computer predictions with quantified uncertainty, Part I, SIAM News. 43 (2010) 1–3.

[87] M.H. Hasan, F. Alsaleem, M. Rafaie, Sensitivity study for the PMV thermal comfort model and the use of wearable devices biometric data for metabolic rate estimation, Build. Environ. 110 (2016) 173–183. doi:http://dx.doi.org/10.1016/j.buildenv.2016.10.007.

[88] G. Brager, M. Fountain, C. Benton, E.A. Arens, F. Bauman, A comparison of methods for assessing thermal sensation and acceptability in the field, in: Therm. Comf. Past, Present Futur., Building Research Establishment, Watford, United Kingdom, 1993.

[89] G. Havenith, I. Holmér, K. Parsons, Personal factors in thermal comfort assessment: clothing properties and metabolic heat production, Energy Build. 34 (2002) 581–591. doi:https://doi.org/10.1016/S0378-7788(02)00008-7.

[90] F.R. d'Ambrosio Alfano, B.I. Palella, G. Riccio, The role of measurement accuracy on the thermal environment assessment by means of PMV index, Build. Environ. 46 (2011) 1361–1369. doi:https://doi.org/10.1016/j.buildenv.2011.01.001.

[91] C. Ekici, Measurement Uncertainty Budget of the PMV Thermal Comfort Equation, Int. J. Thermophys. 37 (2016) 48. doi:10.1007/s10765-015-2011-3.

[92] R.J. Carroll, D. Ruppert, C.M. Crainiceanu, L.A. Stefanski, Measurement error in nonlinear models: a modern perspective, Chapman and Hall/CRC, 2006.

[93] Y.Y. Grace, Statistical Analysis with Measurement Error Or Misclassification, Springer, 2016.

[94] S. Muff, Errors and uncertainty in variables – When to worry and when to Bayes?, "Errors Var. Work. Work. Gr. Bayes Methodsof Int. Biometric Soc. Ger. Reg. (2016).

[95] A. Kucukelbir, D. Tran, R. Ranganath, A. Gelman, D.M. Blei, Automatic differentiation variational inference, J. Mach. Learn. Res. 18 (2017) 1–45.

[96] J. Salvatier, T. V. Wiecki, C. Fonnesbeck, Probabilistic programming in Python using PyMC3, PeerJ Comput. Sci. 2 (2016) e55. doi:10.7717/peerj-cs.55.

[97] S.A. Sadeghi, S. Lee, P. Karava, I. Bilionis, A. Tzempelikos, Bayesian classification and inference of occupant visual preferences in daylit perimeter private offices, Energy Build. 166 (2018) 505–524. doi:https://doi.org/10.1016/j.enbuild.2018.02.010.

[98] D. Kingma, J. Ba, Adam: A method for stochastic optimization, ArXiv Prepr. ArXiv1412.6980. (2014).

[99] W. Liu, D. Yang, X. Shen, P. Yang, Indoor clothing insulation and thermal history: A clothing model based on logistic function and running mean outdoor temperature, Build. Environ. 135 (2018) 142–152. doi:https://doi.org/10.1016/j.buildenv.2018.03.015.

[100] F. Pedregosa, G. Varoquaux, A. Gramfort, V. Michel, B. Thirion, O. Grisel, M. Blondel, P. Prettenhofer, R. Weiss, V. Dubourg, Scikit-learn: Machine learning in Python, J. Mach. Learn. Res. 12 (2011) 2825–2830.

[101] J. Xiong, A. Tzempelikos, I. Bilionis, N.M. Awalgaonkar, S. Lee, I. Konstantzos, S.A. Sadeghi, P. Karava, Inferring personalized visual satisfaction profiles in daylit offices from comparative preferences using a Bayesian approach, Build. Environ. 138 (2018) 74–88. doi:https://doi.org/10.1016/j.buildenv.2018.04.022.

[102] J. Hernández-Orallo, P. Flach, C. Ferri, A unified view of performance metrics: translating threshold choice into expected classification loss, J. Mach. Learn. Res. 13 (2012) 2813–2869.

[103] S. Lee, P. Karava, A. Tzempelikos, I. Bilionis, Inference of thermal preference profiles for personalized thermal environments with actual building occupants, Build. Environ. 148 (2019) 714–729. doi:https://doi.org/10.1016/j.buildenv.2018.10.027.

[104] S. Lee, I. Bilionis, P. Karava, A. Tzempelikos, A Bayesian approach for probabilistic classification and inference of occupant thermal preferences in office buildings, Build. Environ. 118 (2017) 323–343. doi:https://doi.org/10.1016/j.buildenv.2017.03.009.

[105] J. Joe, P. Karava, Agent-based system identification for control-oriented building models, J. Build. Perform. Simul. 10 (2017) 183–204. doi:10.1080/19401493.2016.1212272.

[106] J. Joe, P. Karava, X. Hou, Y. Xiao, J. Hu, A distributed approach to model-predictive control of radiant comfort delivery systems in office spaces with localized thermal environments, Energy Build. 175 (2018) 173–188. doi:https://doi.org/10.1016/j.enbuild.2018.06.068.

[107] M. Krajčík, R. Tomasi, A. Simone, B.W. Olesen, Experimental study including subjective evaluations of mixing and displacement ventilation combined with radiant floor heating/cooling system, HVAC&R Res. 19 (2013) 1063–1072. doi:10.1080/10789669.2013.806173.

[108] M. Krajčík, R. Tomasi, A. Simone, B.W. Olesen, Thermal comfort and ventilation effectiveness in an office room with radiant floor cooling and displacement ventilation, Sci. Technol. Built Environ. 22 (2016) 317–327. doi:10.1080/23744731.2016.1131568.

[109] Z. Wang, H. Zhang, E. Arens, D. Lehrer, C. Huizenga, T. Yu, S. Hoffman, Modeling thermal comfort with radiant floors and ceilings, in: 4th Int. Build. Phys. Conf. 2009, Istanbul, 2009.

[110] W.E. Becker, P.E. Kennedy, A Graphical Exposition of the Ordered Probit, Econom. Theory. 8 (1992) 127–131.

[111] K. Chaloner, I. Verdinelli, Bayesian experimental design: a review, Stat. Sci. 10 (1995) 273–304.

[112] S. Kullback, R.A. Leibler, On information and sufficiency, Ann. Math. Stat. 22 (1951) 79–86.

[113] X. Huan, Y.M. Marzouk, Sequential Bayesian optimal experimental design via approximate dynamic programming, (2016). https://arxiv.org/abs/1604.08320 (accessed November 10, 2019).

[114] M. Abramowitz, I. Stegun, Handbook of Mathematical Functions, 1964.

[115] J.S. Liu, Monte Carlo Strategies in Scientific Computing, Springer Series in Statistics, 2001.

VITA

SEUNGJAE LEE

Ph.D., Lyles School of Civil Engineering, Purdue University (2014 – 2019)

M.S., Department of Architectural Engineering, Yonsei University (2011)

B.S., Department of Architectural Engineering, Yonsei University (2009)

PUBLICATIONS

In Refereed Journals

1. **S. Lee**, J. Joe, P. Karava, I. Bilionis, A. Tzempelikos. "Implementation of a self-tuned HVAC controller to satisfy occupant thermal preferences and optimize energy use." Energy and Buildings, 2019, 194:301-316.
2. **S. Lee,** P. Karava, A. Tzempelikos, I. Bilionis. "Inference of thermal preference profiles for personalized thermal environments with actual building occupants." Building and Environment, 2019, 148:714-729.
3. J. Xiong, A. Tzempelikos, I. Bilionis, N. Awalgaonkar, **S. Lee,** I. Konstantzos, A. Sadeghi, P. Karava. "Inferring personalized visual satisfaction profiles in daylit offices from comparative preferences using a Bayesian approach." Building and Environment, 2018, 138:74-88.
4. A. Sadeghi, **S. Lee,** P. Karava, I. Bilionis, A. Tzempelikos. "Bayesian classification and inference of occupant visual preferences in daylit perimeter private offices." Energy and Buildings, 2018, 166:505-524.
5. **S. Lee,** I. Bilionis, P. Karava, A. Tzempelikos. "A Bayesian approach for probabilistic classification and inference of occupant thermal preferences in office buildings." Building and Environment, 2017, 118:323-343.

In Refereed Conference Proceedings

1. **S. Lee,** P. Karava, A. Tzempelikos, I. Bilionis. "Integrating occupants' voluntary thermal preference responses into personalized thermal control in office buildings." Proceedings of CISBAT 2019 International Conference, Sep 2019, Lausanne, Switzerland.
2. **S. Lee,** J. Joe, P. Karava, I. Bilionis, A. Tzempelikos. "Simulation and implementation of a self-tuned HVAC controller." Proceedings of 16th IBPSA International Conference Building Simulation 2019, Sep 2019, Rome, Italy.
3. D. Lee, **S. Lee,** P. Karava, J. Hu. "Simulation-based policy gradient and its building control application." Proceedings of IEEE American Control Conference (IEEE ACC2018), Jun 2018, Milwaukee.

4. D. Lee, **S. Lee,** P. Karava, J. Hu. "Approximate dynamic programming for building control problems with occupant Interactions." Proceedings of IEEE American Control Conference (IEEE ACC2018), Jun 2018, Milwaukee.
5. **S. Lee,** P. Karava, I. Bilionis, A. Tzempelikos. "Inference of thermal preference profiles for personalized thermal environments." Proceedings of ASHRAE Winter Conference, Jan 2018, Chicago.
6. J. Xiong, **S. Lee,** P. Karava, A. Tzempelikos. "The influence of lighting conditions, shading patterns and weather on occupant visual preferences in building perimeter zones." Proceedings of ASHRAE Winter Conference, Jan 2018, Chicago.
7. J. Xiong, **S. Lee,** P. Karava, A. Tzempelikos. "Personalized visual satisfaction profiles from comparative preferences using Bayesian inference." Proceedings of CISBAT17 Conference, Sep 2017, Lausanne, Switzerland.

In Non-Refereed Conference Proceedings

1. **S. Lee,** P. Karava, A. Tzempelikos, I. Bilionis. "An efficient method for learning personalized thermal preference profiles in office spaces." Proceedings of 5th High Performance Buildings Conference at Purdue, Jul 2018.
2. **S. Lee,** I. Bilionis, P. Karava, A. Tzempelikos. "A Bayesian approach for learning and predicting personal thermal preference." Proceedings of 4th High Performance Buildings Conference at Purdue, Jul 2016.
3. J. Xiong, **S. Lee,** A. Tzempelikos, P. Karava. "Adaptive personalized shading control strategies to maximize occupant satisfaction while reducing lighting energy use in buildings." Proceedings of 4th High Performance Buildings Conference at Purdue, Jul 2016.

Posters

1. **S. Lee,** P. Karava, A. Tzempelikos, I. Bilionis. "Smart and Less Intrusive User-Interface for Self-Tuned HVAC Systems." Poster presented at the Herrick Industrial Advisory Committee (IAC) meeting, Oct 2019.

2. **S. Lee,** J. Joe, P. Karava, A. Tzempelikos, I. Bilionis. “Demonstration of a self-tuned HVAC system.” Poster presented at the Herrick Industrial Advisory Committee (IAC) meeting, Oct 2018.
3. **S. Lee,** P. Karava, A. Tzempelikos, I. Bilionis. "Inference of thermal preference profiles for personalized thermal environments.” Poster presented at the Herrick Industrial Advisory Committee (IAC) meeting, Oct 2017.
4. J. Xiong, **S. Lee,** A. Tzempelikos, P. Karava. "Personalized visual satisfaction profiles from comparative preferences using Bayesian inference." Poster presented at the Herrick Industrial Advisory Committee (IAC) meeting, Oct 2017.
5. S. A. Sadeghi, **S. Lee,** P. Karava, I. Bilionis, A. Tzempelikos. “Bayesian classification and inference of occupant visual preferences in private offices of perimeter building zones.” Poster presented at the Herrick Industrial Advisory Committee (IAC) meeting, Oct 2017.
6. **S. Lee,** P. Karava, A. Tzempelikos, I. Bilionis. "A Bayesian modelling approach for learning occupant thermal preferences in office buildings.” Poster presented at the Herrick Industrial Advisory Committee (IAC) meeting, Oct 2016.
7. J. Xiong, **S. Lee,** A. Tzempelikos. “Personalized shading control to max satisfaction while min lighting energy use by multi-objective optimization.” Poster presented at the Herrick Industrial Advisory Committee (IAC) meeting, Oct 2016.
8. **S. Lee,** A. Sadeghi, P. Karava, A. Tzempelikos. “Inference of thermal and visual comfort profiles for personalized control of buildings.” Poster presented at the Herrick Industrial Advisory Committee (IAC) meeting, Oct 2015.